A quantitative interaction screen for neurodegenerative disease proteins

D i s s e r t a t i o n

zur Erlangung des akademischen Grades

d o c t o r r e r u m n a t u r a l i u m

(Dr. rer. nat.)

im Fach Biologie

eingereicht an der

Mathematisch-Naturwissenschaftlichen Fakultät I

der Humboldt-Universität zu Berlin

von

Dipl.-Biol. Fabian Hosp

Präsident der Humboldt-Universität zu Berlin

Prof. Dr. Jan-Hendrik Olbertz

Dekan der Mathematisch-Naturwissenschaftlichen Fakultät I

Prof. Stefan Hecht, Ph.D.

Gutachter/innen:

1. Prof. Dr. Thomas Sommer
2. Prof. Dr. Matthias Selbach
3. Prof. Dr. Christian Schmitz-Linneweber

Tag der mündlichen Prüfung: 23.01.2013

im Andenken an Nadine

“The important thing in science is not so much to obtain new facts as to discover new ways of thinking about them.“

Sir William Henry Bragg
(1915 Nobel Prize laureate in physics)

“That’s the whole problem with science. You’ve got a bunch of empiricists trying to describe things of unimaginable wonder.”

William “Bill” Boyd Watterson II
(syndicated cartoonist)

Table of contents

Abstract

One of the biggest challenges for personalized medicine is to link genetic information of disease-causative genes to disease mechanisms. This requires functional characterization of the respective gene products. Since proteins are the key players in most biological processes, elucidation of protein-protein interactions (PPI) of disease-associated proteins can provide important insights into disease mechanisms. The first part of the present thesis describes the development of a quantitative protein-protein interaction screen with a focus on proteins involved in four common neurodegenerative diseases (NDDs): Alzheimer's disease (AD), Parkinson's disease (PD), Huntington's disease (HD) and spinocerebellar ataxia type 1 (SCA1). The interaction screen combines stable-isotope labeling by amino acids in cell culture (SILAC) with affinity purification and high-resolution mass spectrometry. This approach aims to systematically identify and quantify interaction partners of normal and known disease-associated variants of proteins involved in NDDs. Moreover, the quantitative interaction screen was employed to study how PPIs are affected by disease-associated mutations, which lead to the identification of so-called differential interactors with potential direct implications in disease pathogenesis or progression. Along with validation of possible off-target effects and comparison of the data with literature-reported PPIs, a subset of identified interactors was validated by additional co-immunoprecipitation experiments in two different cell lines. Utilizing NDD *Drosophila* models for SCA1 in combination with RNAi-mediated silencing of identified interactors, a large fraction of candidates was observed to also affect neurodegeneration *in vivo*. In addition, AD-specific PPI data was mapped to large-scale patient cohort data obtained from genome-wide associations studies. Notably, single-nucleotide polymorphisms in the genes of interactors of the disease-associated protein variants were more likely associated with susceptibility to AD than randomly selected genes. Finally, functional follow-ups for two selected interaction partners provided evidence for a yet unreported role of *N*-linked glycosylation in AD, and a novel link to mitochondrial dysfunction in AD by means of the RNA-binding protein LRPPRC. In summary, the findings of the present thesis show that quantitative interaction proteomics provides novel insights into mechanisms of neurodegenerative diseases, particularly for early-onset Alzheimer's disease. The present dataset also represents a valuable resource for the neurodegenerative disease community.

Zusammenfassung

Eine der größten Herausforderungen der individualisierten Medizin ist die Verknüpfung genetischer Information ursächlicher Gene mit Erkrankungsmechanismen, welche eine eine funktionelle Charakterisierung der jeweiligen Genprodukte voraussetzt. Da Proteine in der Prozessierung zellulärer Informationen eine Schlüsselrolle einnehmen, bietet die Aufklärung von Protein-Protein-Interaktionen (PPI) krankheitsassoziierter Proteine eingehende Erkenntnisse in Erkrankungsmechanismen. Der erste Teil dieser Arbeit beschreibt die Durchführung eines quantitativen Ansatzes zur Detektion von Protein-Protein-Interaktionen mit einem Schwerpunkt für Proteine, welche in vier häufigen neurodegenerativen Erkrankungen eine Rolle spielen: die Alzheimer-, Parkinson- und Huntington-Krankheit, sowie die spinozerebelläre Ataxie Typ 1 (SCA1). Die Interaktionsstudie kombiniert die stabile Isotopen-Markierung von Aminosäuren in der Zellkultur mit der Affinitätsaufreinigung von Proteinen und hochauflösender Massenspektrometrie. Dieser Ansatz zielt darauf ab, systematisch die Interaktionspartner von gesunden und krankheitsassoziierten Proteinvarianten zu identifizieren und zu quantifizieren. Darüber hinaus wurde das quantitative Interaktionsverfahren genutzt, um zu prüfen ob PPI durch krankheitsassoziierte Mutationen beeinträchtigt werden. Dies führte zur Identifizierung sogenannter differenzieller Interaktoren, welche potenziell einen direkten Einfluss auf die Entstehung oder das Fortschreiten der Erkrankung haben. Neben der Validierung möglicher Nebeneffekte sowie dem Vergleich der Daten mit Informationen über PPI aus der Literatur, wurde ein Teil der identifizierten Interaktoren durch zusätzliche Koimmunopräzipitations-Experimente in zwei verschiedenen Zelllinien bestätigt. Mit Hilfe von SCA1-Erkrankungsmodellen in der Fruchtfliege *Drosophila* und in Kombination mit RNA-Interferenz-basierter Stummschaltung identifizierter Interaktoren wurde festgestellt, dass ein großer Teil der Kandidaten neurodegenerative Prozesse *in vivo* beeinflusst. Um zu bestimmen, ob ein weiterer Teil der identifizierten Interaktoren möglicherweise an der ursächlichen Entstehung der Alzheimer-Erkrankung beteiligt ist, wurden die PPI-Daten auf umfassende genomweite Assoziationsstudien übertragen. Bemerkenswerterweise waren Polymorphismen in einzelnen Nukleotiden in den Genen zugehöriger Interaktoren wahrscheinlicher mit solchen Genen assoziiert, die eine Prädisposition für die Alzheimer-Krankheit haben, als mit zufällig ausgewählten Genen. Schlussendlich konnten Folgeexperimente für zwei ausgewählte Interaktionspartner den Nachweis für eine bislang unbekannte Rolle der *N*-Glykosylierung in der Alzheimer-Krankheit vorlegen, sowie einen neuen Zusammenhang zwischen dem RNA-bindenden Protein LRPPRC und mitochondrialer Dysfunktion in der Alzheimer-Krankheit. Die Erkenntnisse der vorliegenden Doktorarbeit zeigen zusammenfassend auf, dass quantitative Interaktionsproteomik neue Einblicke in die Wirkungsweise neurodegenerativer Erkrankungen ermöglicht, insbesondere für Alzheimer-Erkrankungen mit frühzeitigem Ausbruch. Der bestehende Datensatz repräsentiert außerdem eine wertvolle Bezugsquelle für die neurodegenerative Forschungsgemeinschaft.

Abbreviations

A	ampere
ABC	ammonium bicarbonate
cf.	confer
cfu	colony formig units
CID	collision induced dissociation
ConA	Concanavalin A
dFCS	dialyzed fetal calf serum
DMEM	Dulbecco's Modified Eagle Medium
DNA	deoxyribonucleic acid
DTT	dithiothreitol
EDTA	ethylene diamine tetraacetic acid
ER	endoplasmatic reticulum
ESI	electrospray ionization
EtOH	ethanol
FDR	false discovery rate
GC-MS/MS	gas chromatography-tandem mass spectrometry
GO	gene ontology
GST	glutathione S-transferase
GWAS	genome-wide association study
HEK cells	human embryonic kidney cells
hrs	hours
HCD	higher-energy collisional dissociation
HPLC	high performance liquid chromatography
IP	immunoprecipitation
kDa	kilo-Dalton
LB medium	lysogeny broth medium
LC-MS/MS	liquid chromatography-tandem mass spectrometry
LTQ	linear trap quadrupole
LysC	lysl endopeptidase
MES	2-N-morpholinoethanesulfonic acid
min	minutes
MOPS	4-morpholinepropanesulfonic acid
m/z	mass-to-charge ratio
mRNA	messenger ribonucleic acid
MS	mass spectrometry
nanoLC	nanoflow liquid chromatography
OD_{600}	optical density at 600 nanometer
Orbitrap	orbital ion trap mass analyzer
PBS	phosphate buffered saline
PPI	protein-protein interaction

ppm	parts per million
PTM	post-translational modification
q-AP-MS	quantitative affinity purification followed by mass spectrometry
qRT-PCR	quantitative reverse transcription polymerase chain reaction
RP-HPLC	reversed-phase high performance liquid chromatography
RIPA	radioimmunoprecipitation assay
RNAi	ribonucleic acid interference
rpm	revolutions per minute
RT	room temperature
SDS-PAGE	sodium dodecyl sulfate-polyacrylamide gel electrophoresis
SILAC	stable isotope labeling by amino acids in cell culture
shRNA	short hairpin ribonucleic acid
siRNA	small interfering ribonucleic acid
STAGE tips	stop-and-go extraction tips
TFA	trifluoroacetic acid
Tris	tris(hydroxymethyl)aminomethane
UAS	upstream activating sequence
V	volt
XIC	extracted ion chromatogram
Important gene products and diseases	
Aβ peptide	amyloid-beta peptide
AD	Alzheimer's disease
APP	amyloid precursor protein (amyloid beta A4 protein)
ATXN1	ataxin-1
COX1	cytochrome c oxidase subunit 1
FTD	frontotemporal dementia
HD	Huntington's disease
Hsp	heat shock protein
HTT	huntingtin
LRPPRC	leucine-rich pentatricopeptide repeat motif-containing protein
LSFC	Leigh syndrome French-Canadian type
MAPT	microtubule-associated protein Tau
NDD	neurodegenerative disease
OST complex	oligosaccharyltransferase complex
PARK2	parkin
PD	Parkinson's disease
PSEN1	presenilin-1
SCA1	spinocerebellar ataxia type 1
SNCA	alpha-synuclein
Ub	ubiquitin
UPS	ubiquitin proteasome system

I Introduction

I.1 Neurodegenerative diseases (NDDs)

Decoding disease concepts is central to an effective cure of human patients. Technological developments and innovations have profoundly driven our understanding of many diseases over the last centuries. While improved antibiotics, vaccines and drugs have helped to successfully treat or even eradicate plenty of infectious diseases, disorders with a hereditary component or a genetic disposition are, with some few exceptions, mostly remediless and can be treated only symptomatically, if at all. Within the last decades, the genomic revolution has dramatically improved our ability to reveal the genetic basis of hereditary diseases. Given the enormous increase in sequencing speed at dramatically reduced costs, next generation sequencing approaches and large-scale genome-wide association studies (GWAS) are now able to identify disease-associated alleles at an unprecedented pace. Yet, compared to the speed of their discovery, functional characterization of disease-causative genes is still lagging behind. One possible explanation for this is the current lack of straightforward methods to study gene function with a sufficiently high throughput. Besides, the hereditary component of many complex diseases is often distributed over many genes, thus known associations might explain only a small fraction of the disease burden within the population (Gandhi and Wood, 2010). Translation of genetic information into functional mechanisms most relevant to disease pathogenesis remains one of the largest challenges for personalized medicine.

This challenge is in particular important for neurodegenerative diseases (NDDs), a heterogeneous group of disorders characterized by a progressive loss of neuronal cells. While disease-causing mutations have been identified for most NDDs, the mechanistic details of pathogenesis for almost all of them remain largely elusive. It is assumed that progression of NDDs is largely mediated at the protein level, thus investigating NDD-related proteins and their behavior seems to be a promising approach to decipher disease mechanisms. An important aspect of protein function is characterization of protein-protein interactions (PPIs). PPIs are an immediate lead to biological function and can provide valuable insights into cell signaling (Scott and Pawson, 2009; Walhout and Vidal, 2001). Mass spectrometry, especially combined with quantitative information, has become an attractive approach to elucidate PPI formation and even more importantly, dynamic changes in protein complex composition (Gingras et al., 2007; Kocher and Superti-Furga, 2007; Vermeulen et al., 2008).

In this thesis, quantitative mass-spectrometry was used to systematically identify and quantify protein-protein interactions across several different NDDs. Subsequent validation experiments have been carried out to assess the quality of the PPI dataset and to establish links to

disease phenotypes *in vivo*. Finally, functional characterization of selected PPI targets was performed, thereby identifying novel mechanistic details for an early-onset forms of Alzheimer's disease. The following introduction will first focus on the commonalities of several different NDDs and the cause-effect principle of imbalanced protein aggregation with a special emphasis on Alzheimer's disease. Second, the introduction will describe quantitative mass spectrometry as the major technology used in this study.

I.1.1 Commonalities of NDDs and the role of protein aggregation

Neurodegenerative diseases such as Alzheimer's disease (AD), Huntington's disease (HD), Parkinson's disease (PD) or different types of spinocerebellar ataxias (SCAs) are devastating multifactorial disorders with a clear genetic background (Martin, 1999). However, while for some diseases the genetic causality is now fully disclosed, other diseases seem to be caused by many disease causing genes and additional risk factors. On one hand, expansion of CAG repeats in the ataxin-1 or huntingtin gene over a certain threshold leads to pathogenic proteins with abnormally long polyglutamine (polyQ) tracts that irrevocably cause SCA1 or HD with full penetrance (Chung et al., 1993; Orr et al., 1993; Rubinsztein et al., 1996). On the other hand, AD and PD are genetically complex and more heterogeneous diseases with no single mode of inheritance. Rare early-onset forms are caused by a handful of genes while frequent late-onset forms show less obvious or no apparent familial inheritance at all. These so-called 'sporadic' forms of disease are likely to be affected by a cohort of risk alleles across a number of different genes (Bertram and Tanzi, 2008). In spite of the diverging genetic causalities, NDDs show a considerable overlap of clinical phenotypes characterized by a selective loss of neurons in cognitive and motor systems, suggesting common pathogenic features at the molecular level. One such feature is protein misfolding and formation of insoluble protein aggregates – a key event during molecular pathogenesis of NDDs (Ross and Poirier, 2004, 2005; Taylor et al., 2002). As the name implies, NDDs most severely affect neuronal cells. Neurons, being post-mitotic cells, are in particular vulnerable to the deleterious effects of misfolded proteins, since they cannot dilute toxic protein species through normal cell division. To understand the impact of protein misfolding events during initiation of neurodegenerative diseases, it is crucial to realize why especially NDD-related proteins are prone to aggregation and how they bypass the numerous mechanisms which cells have evolved to protect themselves from detrimental misfolding effects.

Proteins are synthesized as linear chains of amino acids in a specific order. In order to function properly, it is necessary for the nascent chains to fold into the native three-dimensional structure that is unique for each protein. Hence, polypeptide chains undergo a highly complicated and energy-consuming assembly process which is referred to as protein folding (Dobson

et al., 1998). All the information that is necessary to achieve a functional three-dimensional structure of a given protein is contained in the amino acid sequence of the polypeptide chain, a premise that is known as the Anfinsen postulate (Anfinsen, 1973). However, already in 1968 the famous Levinthal paradox (Levinthal, 1968) proclaimed the inconsistency that an unfolded polypeptide chain would have an astronomical number of possible conformation states, thus will never find its native structure. In an attempt to solve this paradox, Levinthal himself proposed 'folding pathways' that would speed up the folding process significantly. Indeed, partially folded transition states and folding intermediates were experimentally detected later on, suggesting a concept of funnel-like energy landscapes, where the native structure of protein is the thermodynamically most stable and thus most desirable structure to achieve in terms of thermodynamic properties (Dill et al., 2008; Dobson et al., 1998).

In addition, some proteins do also need the help of specific assistance molecules termed molecular chaperones to fold properly. Chaperones recognize and bind to nascent polypeptide chains and folded intermediate states, assisting proper protein folding assembly. There are numerous classes of chaperones with distinct functions: for instance, the HSP70/HSP40 families and others seem to be primarily involved in remodeling already misfolded polypeptide chains and minimizing further aggregation. In contrast, the HSP60 family and others rather actively support and facilitate the intrinsic folding process (Fink, 1999). The ability of cellular proteins to assemble with high precision and high fidelity is therefore strongly facilitated by chaperones, making them the first line of defense to prevent aggregation of protein molecules before their actual folding process is finished. Even though a multitude of chaperone species is constantly expressed and active, the folding process is not always accurate and misfolding of nascent proteins is a common event within a healthy cell. It is estimated that roughly 30 % of all newly synthesized proteins are not folded correctly and thus are either subjected to refolding or undergo degradation via the ubiquitin-proteasome system (UPS) for recycling of amino acids (Schubert et al., 2000). As the failure of proper protein folding is a major threat to cell function and overall viability, additional elaborate quality control mechanisms have evolved over time to constantly monitor protein folding within the cell and to countermeasure deleterious effects of misfolded proteins (Berke and Paulson, 2003; Taylor et al., 2002).

The cellular quality control is composed of different mechanistic pathways, including (i) the already introduced molecular chaperones, (ii) the ubiquitin-proteasome system (UPS), (iii) unfolded protein response in the ER (UPR), (iv) endoplasmatic reticulum-associated protein degradation (ERAD) and finally (v) autophagy clearance of protein aggregates.

The proteasome is large multi-protein complex of about 2.5 MDa, which is responsible for degradation of mainly nuclear and cytoplasmic proteins, as well as secretory and membrane proteins that have been retrotranslocated from the ER to the cytoplasm via the ERAD pathway

(Coux et al., 1996; Glickman and Ciechanover, 2002). Briefly, recognition of proteasome targets is achieved through covalent modification of proteins with small protein modifiers, most commonly by ubiquitin. The ubiquitin-substrate conjugation system is highly complex, giving rise to an ubiquitination code with a wide variety of downstream signaling and processing effects (Glickman and Ciechanover, 2002; Hershko and Ciechanover, 1998). Besides the cytoplasm, the ER represents the second major environment for protein folding. Proteins entering the secretory pathway are specifically folded in the ER and rise of unfolded proteins in the ER is coped by the UPR and ERAD in both overlapping and compensatory means in order to eliminate misfolded proteins under normal conditions (Buchberger et al., 2010; Friedlander et al., 2000; Travers et al., 2000). However, under stress conditions, such as constant expression of an aggregation-prone gene product, the continuous flux of misfolded protein species usually overcomes the capabilities of the cellular protein quality control (Morimoto, 2008). In addition, substrates of the 26S proteasome need to be unfolded prior to their degradation, an assignment that usually precludes insoluble protein aggregate species. Thus, when aggregation-prone protein substrates cannot be sufficiently cleared by the proteasome system, subsequent resistance seems to be mediated via autophagy clearance of aggregates (Rubinsztein, 2006; Williams et al., 2006). Though, as the drastic increase in aggregation-propensity of NDDs-associated proteins presumably overcharges the cellular capacity of handling protein misfolding stress, definite aggregate species can then mediate their neurotoxic effects. Collateral stress, for instance mitochondrial dysfunction, likely contributes to failure of aggregation clearance as well (Martinez-Vicente and Cuervo, 2007).

Similar to native protein folding, progressive protein aggregation is also a complex process, including several transition steps which give rise to a multiplicity of soluble oligomers or intermediate aggregate species (FIG. I.1). Structural properties and pathogenic impact of these intermediates differ quite substantially within the range of NDD-related proteins (Chiti and Dobson, 2006; Ross and Poirier, 2004). Ultimately, the final stage of protein aggregation is the sequestration of intermediate aggregates into so-called aggresomes or inclusion bodies by microtubule-mediated transport. Aggresomes are then translocated near the nucleus where the cell attempts to clear them by macroautophagy (Johnston et al., 1998; Ross and Poirier, 2005).

One of the major unsolved questions in the neurodegeneration field deals with the identification of the genuine intermediate aggregate species that is mainly responsible for neurotoxic effects within the cell. Whether monomers, soluble oligomers or even larger aggregate structures are the most neurotoxic species is still the subject of debate (Ross and Poirier, 2005). Historically, final aggregate deposits have been the prime suspect for a long time as they were identified as pathological hallmarks of the corresponding diseases in autopsy material from af-

fected patient brains. However, this view changed over the last decades towards the more soluble oligomers being the toxic species (Ross and Poirier, 2004). There is some evidence that this proposition might hold true at least for Aβ oligomers (Gandy et al., 2010; Walsh et al., 2002), although others propose a more complex view of Aβ-mediated neurotoxicity (Benilova et al., 2012). For further disease-associated proteins involved in different NDDs, however, the nature of the toxic species remains largely elusive to date.

Although it has not yet been possible to pinpoint the essence of the true toxic species, the even more important question is how the toxic aggregates actually induce neurotoxicity. Within the last ten years, the scientific community focused most extensively on the interference with protein quality control (Bence et al., 2001; Cuervo et al., 2004; Tanaka et al., 2001), albeit many other direct toxicity-effects have been observed as well (Song et al., 2011; Zhu et al., 2003); this has been extensively studied for Aβ-mediated neurotoxicity (described later, cf. I.1.2). Most notably, many proteins that are natively not prone to aggregate are sequestered to already formed intermediate stages or final aggregates and are thus deposited in these inclusion bodies as well. These differential protein interactions also contribute to neurotoxicity as uninvolved proteins are intercepted and hence not available any more to fulfill their normal tasks within the cell (described later in more detail, cf. I.1.3). The final inclusion bodies, full of misfolded and sequestrated proteins, are nowadays suspected to have a more protective than toxic function – a last-ditch attempt of the cell to corral irrevocably damaged proteins in order to prevent them from sequestering additional proteins and getting more detrimental.

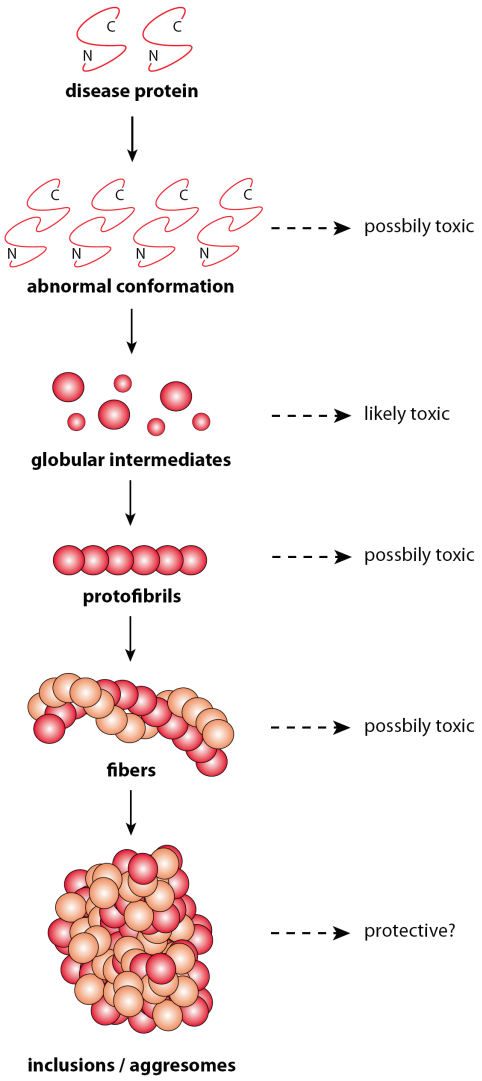

FIG I.1 | Hypothetical several-step pathway of protein aggregation. An initiative event converts a native disease protein into an abnormal form. Globular (oligomeric) intermediates may subsequently form, and then protofibrilliar structures are assembled. Fibers form possibly through association of protofibrils, resulting in aggresome or inclusion formation visible in the light microscope. The intermediate species are considered to be the more toxic ones, rather than precursors or final aggregates (Illustration adapted from Ross and Poirier, 2004).

While it now has become clear that accumulation of misfolded proteins is a common feature of many neurodegenerative diseases, less is known about the actual initiation of aggregation *in vivo*. Initiation of protein misfolding may be a stochastic event, with a constant risk over the lifetime of the individual (Clarke et al., 2000). Aggregate formation may then proceed and accelerate via a 'seeded polymerization' effect (Dobson, 2003; Lansbury, 1997; Soto, 2003). More tangible effects that increase the likelihood of aggregation are: (i) increased protein concentration, (ii) protein-coding mutations or (iii) covalent modifications of proteins. Evidence for increased protein concentrations as cause for aggregation initiation has come from genetic dosage alterations in familial PD patients with triplication of the alpha-synuclein gene locus (Singleton et al., 2003) or early Aβ plaque load in individuals with Down's syndrome, who carry an extra copy of the Alzheimer-causing gene APP on chromosome 21 (Schupf and Sergievsky, 2002; Tanzi et al., 1988). Protein-coding mutations are a common cause for protein aggregation and exert their effects in two ways: either the mutation directly alters the primary structure of the affected protein and thus makes it more prone to aggregation, e.g. polyglutamine expansion in the huntingtin gene (Scherzinger et al., 1997; The Huntington's Disease Collaborative Research Group, 1993), or the mutation affects the processing of other disease proteins, e.g. the PSEN1-A431E mutation modulates γ-secretase activity hence altering the Aβ isoform pattern (Portelius et al., 2010). Finally, covalent modification of proteins can also initiate the aggregation of several protein species, most importantly via phosphorylation, e.g. hyperphosphorylation of Tau protein (Grundke-Iqbal et al., 1986) or the disease-critical phosphorylation of Ataxin-1 on position Serine776 (Emamian et al., 2003). Additionally, misfolding and aggregation can also proceed via transmission of infectious protein species. However, this has so far only been experimentally validated for prion particles that are not within the focus of this work. Earlier indications, whether or not Aβ isoforms can be transmitted in a prion-like fashion *in vivo*, are still inconclusive. Although inoculation of postmortem AD brain extracts can accelerate deposition of Aβ fibrils when directly injected to either the brain or the peritoneal cavity of transgenic AD mice (Eisele et al., 2010; Kane et al., 2000; Meyer-Luehmann et al., 2006), all host animals utilized so far were predisposed to develop AD pathology as they overexpressed mutant amyloid precursor protein already. The extra inoculation with AD brain extracts thus might be an additional amyloid enhancer only.

In a nutshell, disease-associated mutations provoke erroneous protein folding, commuting native gene products into aggregation-prone protein species responsible for the formation of NDDs. Despite the evolution of numerous cellular countermeasures to prevent toxic effects of those pathogenic protein species, the disease-causing mutation and thus the primordial causality of the disorder is not restored. As a result, the cell is not able to cope with the continuous

flux of mutated gene products and the protein homeostasis is imbalanced over time. This process is, however, rather slow and can take decades until full penetration of clear clinical symptoms, hence the vast majority of all NDD cases are late-onset forms with an age of onset greater than 65 years. Given the fact that population ageing has emerged as a major demographic trend in most countries worldwide, the frequency of NDD cases is considered to increase dramatically over the next decades. For example, prevalence for dementia patients only is estimated to triple worldwide from around 36 million nowadays to 115 million by 2050 (World Alzheimer Report, 2011).

Conclusively, substantial progress has been made over the last 30 years in discovering the disease-causing mutations for several different NDDs, however, functional characterization is still lagging behind. The drastic increase in NDD-affected patients and the lack of therapeutic strategies will therefore have an enormously high socio-economic impact on the health care systems and affiliated societies, reflecting the urgent need for further substantial research on NDDs to elucidate disease mechanisms in more detail.

I.1.2 Alzheimer's disease: competing hypotheses and causative agents

Alzheimer's disease (AD) is the most common neurodegenerative disease, currently affecting approximately 30 million people worldwide. It is named after the German psychiatrist and neuropathologist Alois Alzheimer who defined the 'first' Alzheimer's disease case (Alzheimer, 1907), even though there is evidence that at least six other physicians have described the disease prior to Alois Alzheimer (Berrios, 1990), going along with Stiegler's law of eponymy.

Clinically, Alzheimer's disease is characterized by a progressive impairment of short-term memory, judgment, orientation and language toward a state of profound dementia. Pathological hallmarks of the disease are neuronal loss, particularly in the frontotemporal cortex and the hippocampus, and aggregation of two proteinaceous species, Aβ and tau. Protein aggregates are found as intracellular neurofibrillary tangles (NFTs), mainly composed of hyperphosphorylated forms of the microtubule-associated protein tau (MAPT), and extracellular senile plaques containing mainly different isoforms of the beta-amyloid peptide Aβ. The Aβ peptide is derived from the amyloid precursor protein (APP) through sequential cleavage by two transmembrane proteases: the β-secretase and the γ-secretase (Bertram and Tanzi, 2008; Selkoe, 2001).

AD can be classified into early-onset cases with familial inheritance (onset of disease before 60 years) and late-onset cases (onset after 60 years). So far, all mutations that are known to cause early-onset AD are located either in the APP gene itself or in genes of presenilin-1 (PSEN1) or presenilin-2 (PSEN2), both catalytic subunits of the γ-secretase complex (Bertram and Tanzi, 2008). However, the vast majority of all Alzheimer's disease cases (>90-98%) presents as late-onset forms with no single mode of inheritance, thus often called sporadic AD. As mentioned

earlier, sporadic forms of AD are probably modulated by a several risk alleles with relatively low penetrance but high prevalence (Bertram et al., 2007). So far, hundreds of gene polymorphisms have been claimed to be implicated in the origin of AD. The AlzGene database (www.alzgene.org) currently lists ~3,000 polymorphisms in ~700 different genes as risk factors for AD, although, with the exception of the ε4 allele of the apolipoprotein E gene (APOE), none of these purported candidates has been proven to consistently influence disease risk or onset in more than a handful of samples or restricted populations of patients (Bertram et al., 2007; Bu, 2009). Consequently, as the genetic basis for most AD cases remains largely elusive, it is not surprising that no unifying mechanism has been posted to date that would explain all varieties of causal AD formation. Nonetheless, many different hypotheses have been proposed over the last 20 years, trying to better understand general disease concepts and pathogenic pathways of AD. In the following, I will focus on the two most prominent hypotheses: the amyloid cascade hypothesis and the mitochondrial cascade hypothesis.

The amyloid cascade hypothesis has dominated AD research over the last two decades (Hardy and Selkoe, 2002; Hardy and Higgins, 1992; Selkoe, 1991), as the evidence for a central role of Aβ in AD pathogenesis is indisputable. The main proposition of the amyloid cascade hypothesis is that sufficient accumulation of toxic Aβ species induces all biochemical and histological changes in AD-affected neurons. Aβ is a proteolytic fragment of the APP protein and is generated mainly in neurons by sequential scission of APP by β- and γ-secretase enzymes (Selkoe, 2001). An alternative processing of APP via α-secretase followed by γ-secretase generates shorter hydrophobic peptide species, termed p3, whose role in AD are yet unclear. The processing of APP via the α-secretase prevents formation of Aβ, as the α-cleaving site is located within the Aβ sequence domain. Hence, p3 was initially claimed to have a non-amyloidogenic function, although it has later been found as constituent of both Aβ plaques in AD patients and cerebellar preamyloids in Down's syndrome (Higgins et al., 1996; Lalowski et al., 1996).

It is important to realize that Aβ is actually present in several isoforms, thus representing a heterogeneous mixture of several Aβ species of different lengths and modifications. Due to variations in γ-secretase sequence specificity, the C-terminal part of APP is cleaved at different positions giving rise to $Aβ_{37-43}$ (digits indicate the number of amino acids comprising the peptide, with residue 1 being the amino acid residue aspartyl-1 of the Aβ sequence in APP, FIG. I.2). So far, only $Aβ_{37}$, $Aβ_{38}$, $Aβ_{40}$, $Aβ_{42}$ and $Aβ_{43}$ have been detected in cell culture and body fluids. Additional heterogeneity is produced by aminopeptidases, glutaminyl-isomerases and kinases, which can modify Aβ peptides even further (Benilova et al., 2012; Selkoe, 2004). This mélange of Aβ species contributes to different extents to putative Aβ functions in both healthy and AD-afflicted neurons. While earlier publications focused mainly on the role of selected Aβ isoforms only, the view has now shifted to a more holistic perception of the whole Aβ family. It now

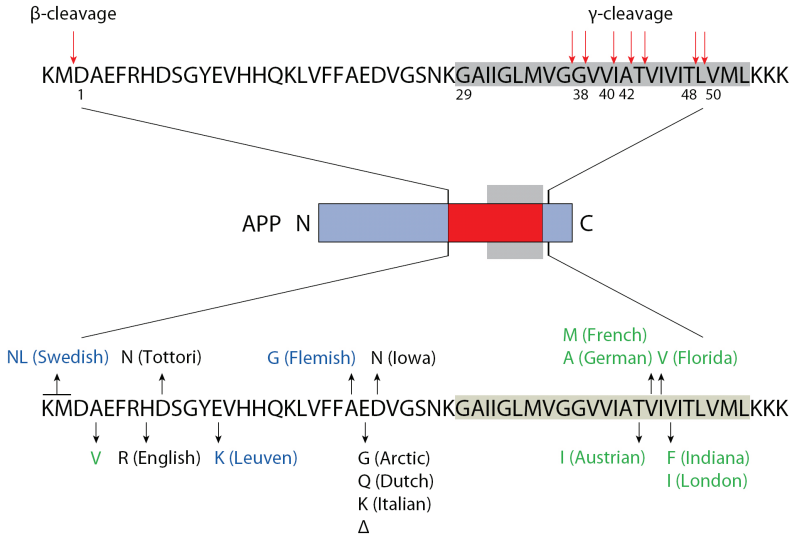

FIG I.2 | Generation of Aβ from amyloid precursor protein APP. The transmembrane region of APP is displayed in grey, red arrows indicate the sites of β- and γ-secretase-mediated cleavage sites (upper panel). Familial Alzheimer's disease-associated mutations (illustrated in the lower panel) either increase the total net production of Aβ (blue), alter biophysical properties of Aβ (black) or affect the Aβ peptide spectrum in both quantitative and qualitative ways (green) (Illustration adapted from Benilova et al., 2012).

becomes evident that the different Aβ isoforms influence each other in a complex process. Accordingly, equilibrium alterations within the scope of different Aβ peptides are more likely to change biophysical properties of Aβ with regard to toxicity and aggregation propensity, rather than quantitative increases of individual Aβ peptide species alone (Benilova et al., 2012). Owing to their inherent cross-β-sheet structure, Aβ monomers can arrange into soluble Aβ oligomers giving rise to many different Aβ assemblies (up to 36-mers) with a wide biological effector spectrum (Benilova et al., 2012). For instance, known toxic effects of Aβ oligomers are direct inhibition of several receptors (Giuffrida et al., 2010; Thathiah and De Strooper, 2009; Yamin, 2009), microtubule loss (King et al., 2006) or membrane bilayer permeabilization, either indirect or through amyloid pore formation, thus strongly affecting mitochondrial function through Ca^{2+} overload and direct interference with the respiratory chain (Manczak et al., 2006; Smith et al., 2000). Additionally, Aβ assemblies seem to derogate synaptic functionality of neurons, leading to restraints in long-term potentiation (Cleary et al., 2005; Walsh et al., 2002). Most importantly, Aβ oligomerization is associated with tau pathology, probably by ultimately triggering the hyperphosphorylation and other post-translational modifications of tau (Cohen et al., 2011; Iqbal et al., 2010), hence allowing NFT formation. Genetics of AD suggest that Aβ acts upstream of tau, as mutations in APP lead to AD with amyloid plaques and NFTs (Bertram et al., 2010), whereas MAPT mutations alone cause NFTs but never lead to amyloid plaque formation or development of AD. MAPT gene polymorphisms cause frontotemporal lobar degeneration (FTLD), a neurodegenerative disease closely connected to AD (Ballatore et al., 2007). Adverse effects of Aβ are, at least partly, dependent on tau but not vice versa, making Aβ the primary causative agent of familial AD cases according to the amyloid cascade hypothesis (Huang and Mucke, 2012). In summary, it is most likely that neurotoxicity in early-onset AD-afflicted neurons is primary due to the accumulation of Aβ oligomers, triggering a fatal cascade of downstream effectors and copathogens, which contribute to or potentiate pathological conditions even further.

Although the amyloid cascade hypothesis is of help to understand familial AD cases in more detail, numerous open questions are still remaining in order to completely decode AD mechanisms. For instance, the amyloid cascade hypothesis has been extrapolated to sporadic cases of AD, albeit these patients do not have mutations in APP or the PSEN genes but still show elevated levels of Aβ species. The cause for this phenomenon is still unclear, although, presumably other AD-associated gene polymorphisms may alter the processing of APP and thus the generation of Aβ isoforms as well. Another frequently voiced concern has been the poor correlation of insoluble Aβ levels with the progression of the disease or amyloid plaque load (McLean et al., 1999; Terry et al., 1991). Even many non-demented elderly individuals have amyloid plaques and NFTs (Savva et al., 2009). Conversely, significant correlation has been observed between soluble Aβ levels and cognitive decline (Hsiao et al., 1996; Naslund et al., 2000). These and many other observations suggest that plaque amyloids *per se* are a weak indicator to describe cognitive status in AD.

In order to account for AD cases which do not seem to meet the amyloid cascade hypothesis, Swerdlow and Khan formulated the mitochondrial cascade hypothesis (Swerdlow and Khan, 2004). It posits that defects in mitochondrial activity within AD-afflicted neurons are the primary cause of AD, actually driving Aβ production and subsequent neurodegeneration (Khan et al., 2000; Markesbery, 1997; Yao et al., 2009).

One of the major strengths of the mitochondrial cascade hypothesis is the implementation of ageing phenomena. It proclaims that both, inherited and age-driven acquired mtDNA mutations predispose the pathological features toward late-onset sporadic AD. It is commonly accepted that mitochondrial function is declining with age and one of the greatest risk factors for NDDs is increased age. Mitochondria are thought to contribute to ageing, mainly through accumulation of mutations within the mitochondrial DNA (mtDNA). This has been experimentally shown utilizing mtDNA-mutator mice with proofreading-deficient mitochondrial DNA-Polymerase, which exhibited an almost twofold decrease in average lifespan (Trifunovic et al., 2004). Another important contributing factor to ageing is the net production of reactive oxygen species (ROS). Gene expression studies of human postmortem cortex samples have revealed that oxidative damage contributes to ageing-accompanied cognitive decline (Lu et al., 2004). Extensive support from the literature emphasizes the role of mitochondrial dysfunction and oxidative damage in AD, even before onset of significant plaque pathology (Lin and Beal, 2006; Nunomura et al., 2001; Pratico et al., 2001). Among the earliest detectable defects in AD are altered cytochrome C (COX) activity (Parker, 1991) and a general decrease in the cellular energy metabolism levels. For instance, these manifestations include loss of body weight, peak oxygen consumption or altered insulin levels (Burns et al., 2008; Craft et al., 1998; John-

son et al., 2006). Evidence supporting inherited mtDNA polymorphisms as drivers of sporadic AD has come from findings on amplified mtDNA deletion mutations found in several late-onset AD patients when compared to healthy controls (Bosetti et al., 2002; Castellani et al., 2002; Corral-Debrinski et al., 1994; Coskun et al., 2004). Caught in a vicious circle, somatic mtDNA mutations would cause increased ROS production, which in turn inhibit mitochondrial activity and can, through accumulation, cause more mutations in the mtDNA and ultimately lead to mitochondrial dysfunction.

However, the mitochondrial cascade hypothesis, similar to the amyloid cascade hypothesis, cannot account for all AD variations observed so far. Especially, it only focuses on late-onset, sporadic AD cases, whereas early-onset AD cases are regarded as primary amyloidoses only. In addition, the mitochondrial cascade hypothesis claims that Aβ production and plaque deposition is a secondary event in sporadic AD, actually mediated by primary defects in mitochondrial function. However, early APP processing events and accumulation of soluble or insoluble Aβ species might fall below the current limit of detection, thus defining mitochondrial dysfunction as cause or consequence of Aβ-mediated toxicity becomes extremely challenging.

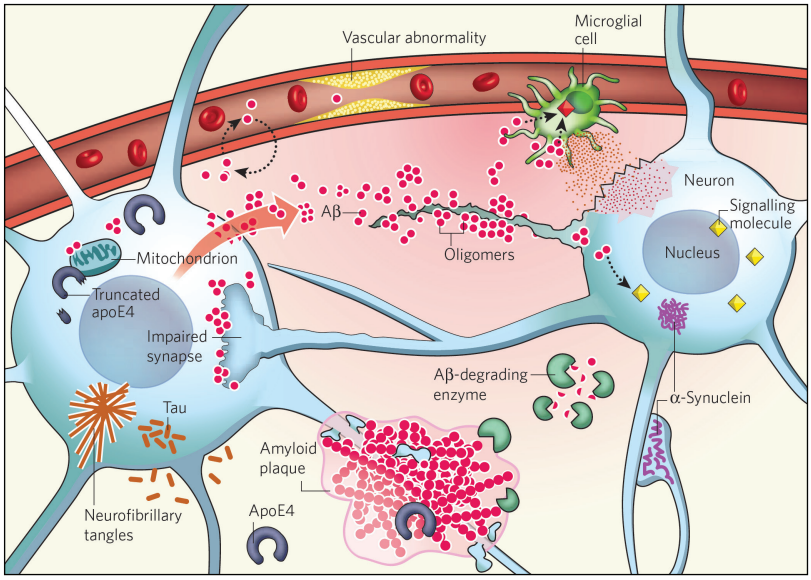

FIG I.3 | Multifactorial basis of Alzheimer's disease pathogenesis. Aggregation and accumulation of amyloid-β (Aβ) in the brain may result from increased neuronal production of Aβ, decreased activity of Aβ-degrading enzymes, or alterations in transport processes that shuttle Aβ across the blood–brain barrier. Aβ oligomers impair synaptic functions, whereas fibrillar amyloid plaques displace and distort neuronal processes. Aβ oligomers interact with cell-surface membranes and receptors, altering signal-transduction cascades, changing neuronal activities and triggering the release of neurotoxic mediators by microglia (resident immune cells). Vascular abnormalities impair the supply of nutrients and removal of metabolic by-products, cause microinfarcts and promote the activation of astrocytes (not shown) and microglia. The lipid-carrier protein apoE4 increases Aβ production and impairs Aβ clearance. When produced within stressed neurons, apoE4 is cleaved into neurotoxic fragments that destabilize the cytoskeleton and, like intracellular Aβ, impair mitochondrial functions. The proteins tau and α-synuclein can also self-assemble into pathogenic oligomers and can form larger intra-neuronal aggregates, displacing vital intracellular organelles.

The amyloid and the mitochondrial cascade hypothesis have both provided unique perspectives on AD, contributing to our understanding of AD-based neurodegeneration (FIG. I.3). Nonetheless, many more factors are likely to be involved in AD awaiting further elucidation. By way of example, the most important risk factor for late-onset AD to date is APOE (Corder et al., 1993; Strittmatter et al., 1993), it is the only risk allele that has been validated in numerous genome wide association studies across different populations around the world (it ranks number one in the AlzGene database). The APOE ε4 allele frequency is about 15% in general populations but about 40% in patients with AD (Bu, 2009). The mechanis-

tic details of ApoE4 in AD are not yet completely understood but ApoE4 probably acts in both Aβ-dependent and Aβ-independent pathways. On the one hand, ApoE4 impairs Aβ clearance and elevates Aβ deposition thus promoting Aβ-related effects in AD patients. On the other hand, proteolysis of ApoE4 under stress or injury conditions can mediate downstream Tau pathology and mitochondrial energy impairment, hence promoting mitochondrial neurotoxicity (Bu, 2009; Huang and Mucke, 2012).

Figure I.4 summarizes the heterogeneity of different effectors that have been proposed so far to contribute to AD. As evident from the multiplicity of involved factors, it becomes clear that there is probably no single linear chain of disease-driving events but initiation and progression of late-onset AD may be a complicated conglomerate of pathways with mutual interplay (Querfurth and LaFerla, 2010). It is likely that future findings enable a more detailed view on AD mechanisms allowing classification of AD subtypes with heterogeneous origins – thus potentially unifying diverging hypotheses.

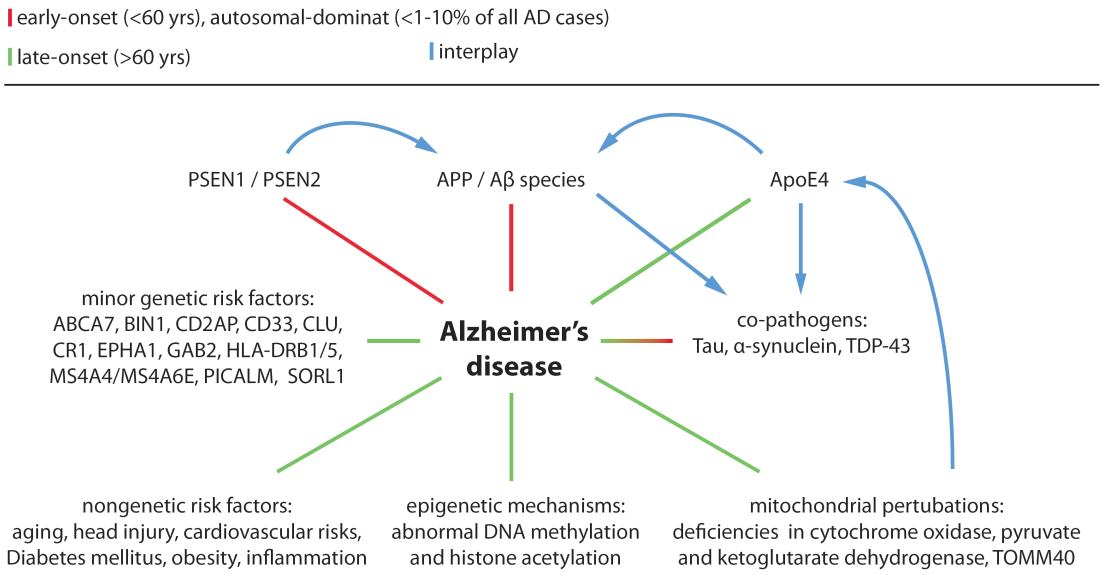

FIG I.4 | Heterogeneity of Alzheimer's disease-associated risk factors. Early-onset AD cases are caused by mutations in either PSEN1/2 or APP genes. Late-onset AD cases are most likely modulated by a several risk alleles, for instance ApoE4 or other minor genetic risk factors. Important co-pathogens are considered to influence both early- and late-onset variants of AD and can act synergistically with each other and/or with Aβ. Further mechanistic effects which can influence onset and progression of AD include mitochondrial pertubations, epigentic events or further nongenetic risk factors. Mutual interplay between most effectors additionally increases the complexity of AD-causing pathways.

I.1.3 Protein-protein interactions and their impact on neurodegeneration

Biomolecular interactions are central to all biological processes. A key aim in the postgenomic era is to systematically understand the roles of protein-protein interactions (PPIs) on a global scale, as signal information cascades are transmitted and processed throughout the cell mainly via protein interaction networks (Scott and Pawson, 2009). Proteins very rarely act isolated, in fact, the cellular environment is densely packed and rich in interfaces of a plethora of biomolecules, which are mostly dynamic and move around to fulfill their biological function. Thus, already the precise definition of a PPI becomes challenging since some PPIs are stable across almost the whole lifetime of a cell, while others are more transient and happen within a nanosecond timescale. For instance, the assembly of the histone octamer arises from extremely stable PPIs, whereas the binding of most kinases towards their substrates is rather temporary.

Given the importance of PPIs in biological systems, numerous techniques have been developed over the last decades to systematically map PPIs, nonetheless, most of them are limited in either throughput or reproducibility. For instance, low-throughput methods such as isothermal titration calorimetry, ITC, (Pierce et al., 1999), Förster resonance energy transfer, FRET, (Kenworthy, 2001) or classical co-immunoprecipitation are accompanied by high-throughput methods such as yeast-two-hybrid, Y2H, (Fields and Song, 1989) or protein fragment complementation assays (Tarassov et al., 2008). Most of the aforementioned assays focus on binary interactions and have specific advantages and disadvantages. An alternative approach is mass spectrometry (MS)-based identification of PPIs, which relies on affinity purification of a bait molecule followed by mass spectrometry, AP-MS (Rigaut et al., 1999). AP-MS can be performed in high-throughput and is currently the most powerful and unbiased experimental tool to identify the constituents of whole protein complexes (Ewing et al., 2007; Malovannaya et al., 2011). In addition, AP-MS retains posttranslational modifications (PTMs) of target proteins and is therefore able to detect PTM-dependent PPIs as well, which are often crucial for complex formation (Seet et al., 2006). Also, AP-MS can be performed under near physiological conditions and in the relevant organism and subcellular compartment (Gingras et al., 2007). Over the years, several advances have been made, which now allow researchers to choose between plenty of different experimental variations of the original AP-MS approach. Technical developments primarily focused on either (i) optimizing the expression level of the bait protein, (ii) improvements of the tag system, (iii) advances in mass spectrometry-based identification of proteins and (iv) assessment of data quality via bioinformatic filtering (Gavin et al., 2011; Gingras et al., 2007).

Almost all biochemical approaches for identification of PPI suffer from the trade-off between sensitivity and specificity. Affinity matrices used in AP-MS are composed of an antibody target-

ed against the bait protein (or directed against a fused purification tag) coupled to a matrix. Both components, matrix and antibodies, are subject to extensive interaction with non-specific binders, which will give rise to false-positive identifications. On the one hand, stringent washing procedures are required to eliminate these non-specific binders. On the other hand, transient interactors of the bait protein can be lost due to excessive washing steps (false-negatives). In order to circumvent this problem, sophisticated bioinformatic tools have been developed, which try to extract background noise from AP-MS experiments. This can be addressed either through accentuation of potential genuine interactors or by exclusion of potential spurious interactors. The latter approach has been systematically assessed by comparing the 'bead proteome' of routinely used affinity matrices such as Sepharose, agarose and magnetic beads (Trinkle-Mulcahy et al., 2008). The reported bead proteome filters provide a useful resource, however, they are restricted to certain baits and cell lines so far and indicated contaminants might readily have a genuine function under different experimental conditions or in different cell extracts. Highlighting true interactors from biochemical purifications is much more challenging. More elaborate software approaches have been designed, trying to implement scoring systems utilizing socio-affinity scores (Gavin et al., 2006), semi-quantitative information (Sardiu et al., 2008; Sowa et al., 2009) or probability distributions (Choi et al., 2010). However, software tools do not get to the root of the true problem and face the background discrimination dilemma after the actual experiment has been carried out. Thus, implementation of quantitative information prior to the data analysis provides an attractive alternative to minimize false-positive interactions arisen from unspecific protein binding. Quantitative proteomics is a smart tool, which allows distinguishing true interaction partners from background binders by differentially labeling the specific and the control pull-down (Paul et al., 2011; Vermeulen et al., 2008). In addition to background discrimination, quantitative proteomic approaches can also uncover dynamic changes in the composition of PPIs. This becomes of particular interest when focusing on signaling networks upon activation with a certain effector (Blagoev et al., 2003), dynamic changes of PTM-mediated PPIs (Olsen et al., 2006), cellular differentiation processes (Brand et al., 2004), and many more biological questions (Mousson et al., 2008; Pflieger et al., 2008; Vermeulen et al., 2008).

Progression of many human diseases commonly involves abnormal protein-protein interactions, thus knowledge of PPIs is crucial to understand disease mechanisms in general (Schuster-Bockler and Bateman, 2008; Vidal et al., 2011). It has been observed that proteins causative for several disease phenotypes frequently interact with each other (Ideker and Sharan, 2008). Loss of binding partners can abolish the 'normal' function of the protein, depriving the cell of certain vital capacities. Contrary, gain of protein binding partners can trigger toxic secondary actions, as for instance activation of additional pathways or sequestration of other un-

related proteins. Thus, not surprisingly, several reports have linked differential PPIs to pathogenic effects strongly mediating NDD progression. For instance, wild-type ataxin-1 associates with at least two distinct protein complexes: one containing the transcriptional repressor Capicua (CIC) and another one containing the splicing factor RBM17. Disease-associated polyglutamine expansion of ataxin-1 now strongly enhances the formation of the ataxin-1/RBM17 complex, whereas the formation of the ataxin-1/CIC complex is reduced, resulting in a partial loss of ataxin-1 function and worsening of SCA1 neuropathology (Lim et al., 2008). Another observation is the interaction of polyglutamine expanded huntingtin with a wide range of transcription factors, such as CBP, TAFII130, SF1, TBP, N-CoR, Sin3A and many other factors of the basal transcription machinery (Harjes and Wanker, 2003). Hence, transcriptional dysfunction is an early event observed in Huntington's disease (Cha, 2000; Sugars and Rubinsztein, 2003). Prospective studies on deciphering protein interactions in NDDs should enable a more detailed view on disease-related dysfunction of cellular information processing and overall fidelity. Applying quantitative AP-MS to resolve both dynamic and differential PPIs in the context of NDDs presumably seems to be the most promising approach to address this issue.

I.2 Mass spectrometry-based quantitative proteomics

The term "proteomics" expresses the ambition to obtain a systematic survey of all proteins in a sample such as a single cell or an individual organism, ultimately in a tempo-spatial manner (Wilkins et al., 1996). Proteomics encompasses many different techniques including yeast-two-hybrid assays, protein microarrays or high-throughput protein production and crystallization. Among the various proteomic approaches, mass-spectrometry (MS)-based proteomics is particular popular. A major breakthrough in MS-based proteomic research was accomplished by the development of soft ionization methods such as matrix-assisted laser desorption/ionization (MALDI) and electrospray ionization (ESI), which made large biological molecules amenable to mass spectrometry – an advance recognized by the 2002 Nobel prize in Chemistry.

Over the last ten years many technological improvements, both on the hardware and the software side, made MS-based proteomics the dominant technique for most proteomic purposes. Ongoing developments on novel types of mass spectrometers, fragmentation techniques, more sophisticated data analysis tools but also improved pre-fractionation approaches for sample preparation have pushed the limits of MS-based applications even further. Currently, MS-based proteomics is routinely applied to study global protein composition of complete cell lines or whole organisms, changes in protein characteristics upon perturbation, biomarker discovery, for detection of a magnitude of post-translational modifications (PTMs) and protein-protein interactions (Aebersold and Mann, 2003; Cox and Mann, 2011; Cravatt et al., 2007; Domon and Aebersold, 2006; Mallick and Kuster, 2010).

I.2.1 Instrumentation and workflow of mass spectrometry

Mass spectrometers determine the mass-to-charge (m/z) ratio of chemical and biological entities, such as peptides and proteins. Thus, they can either be used to measure simply the plain molecular mass of a polypeptide species or to infer the exact amino acid sequence and other more structural features such as PTMs and their respective positional site on the polypeptide chain. Identification of proteins can be performed in two ways, either “top-down” by measuring the mass of intact proteins or “bottom-up” through peptide analysis of digested proteins. While the first approach is attractive and valuable for certain kinds of biological questions, it is technically more feasible to analyze peptides and not whole proteins by MS. Separation and solubility issues can be solved easier at the peptide level, furthermore, combinatorial effects of ubiquitous protein modifications complicate the exact m/z determination of intact proteins (Steen and Mann, 2004).

A typical bottom-up experimental design for MS-based proteomics is depicted in FIG. I.5. As this workflow is central to all MS-related experiments in the present thesis, it will be described in more detail. Following the isolation of a protein sample from any biological source, proteins are subjected to proteolytic digestion by sequence-specific proteases. Depending on the complexity, samples can be further fractionated at the peptide or the protein level. Most commonly, this is achieved by SDS-PAGE, electrostatic exchange procedures (strong anion/cation exchange) or isoelectric focusing of peptides or proteins. The generated peptide mixture usually comprises thousands of peptides of various length and sequence composition. Mass spectrometers yet cannot handle the massive sample complexity, since the peptide stoichiometry spans additionally several orders of magnitude in abundance. In order to resolve the complexity issue, it is necessary to interpose amendatory separation techniques within the proteomic workflow. Most commonly, various combinations of sequential electrophoretic or chromatographic separation methods are used to gain satisfying separation efficiency. One of the highest resolving powers can be achieved via reversed-phased liquid chromatography (rpLC). Peptides are injected onto microscale capillary columns filled with reversed-phase material, which are directly coupled to the mass spectrometer thus allowing “on-line” examination of analytes. Eventual, solvent gradients with an increasing fraction of organic content are applied to elute peptides from the column in order of their hydrophobicity. As mass spectrometric measurements are carried out in the gas phase, LC-separated peptides are directly ionized by electrostatic dispersion. While the peptide-solvent mixture is nebulized to highly charged droplets at the needle tip by the action of high voltage applied to the column, peptides subsequently ionize and the solvent vaporizes completely (Steen and Mann, 2004). This electrospray ionization allows peptide ions to enter the orifice of the MS, whereas uncharged background molecules do not reach the instrument’s transfer capillary. ESI-generated peptides within the vacuum system of the MS are then guided and further manipulated by electrostatic fields.

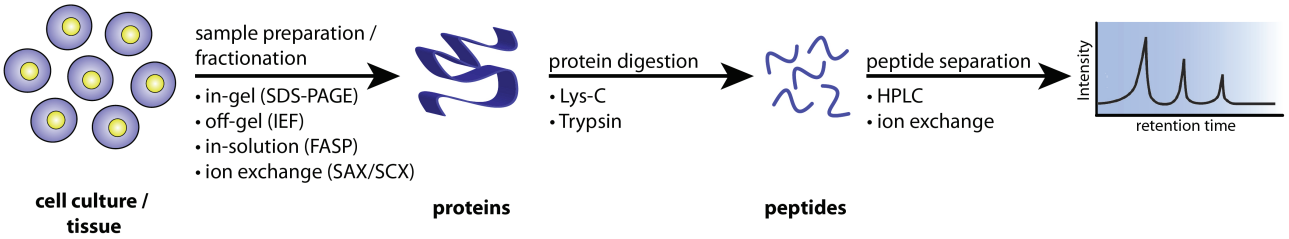

By definition, mass spectrometers consist of three components: an ion source, a mass analyzer which determines the m/z ratio of ionized analytes and a detector that records the ion count at each m/z value (Aebersold and Mann, 2003). There are many different types of mass spectrometers available, however, as all described experiments in the present thesis were exclusively analyzed using either LTQ-Orbitrap or Q-Exactive systems, all further remarks refer to these types of instruments. The LTQ-Orbitrap is a hybrid mass spectrometer, which combines the unique advantages of a linear trap quadrupole (LTQ) system and an Orbitrap mass analyzer. It became the first fundamentally new mass analyzer for more than 20 years and since its introduction in 2005, the LTQ-Orbitrap is the instrument of choice for many applications in the proteomic field. The major breakthrough feature of the Orbitrap is its name-giving orbital-shaped ion trap, where ions move around a central electrode trapped by an electrostatic field. Although already theoretically anticipated in the 1920s (Kingdon, 1923), technical limitations hindered a successful adaption for mass spectrometry until 2000 (Makarov, 2000). The Q-Exactive system is the state-of-the art MS device for large-scale identification of proteins derived from complex samples. It combines the Orbitrap mass analyzer with an upstream, high-precision quadrupole mass filter (Michalski et al., 2011). Though conceptually distinct, both types of instruments follow the general principle of mass spectra acquisition in a similar way.

Ionized peptides trapped in the Orbitrap circle around the central electrode with distinct frequencies, which are inversely proportional to the m/z value of each individual peptide. The frequency oscillation induces a current which can be constituted in a frequency spectrum and, by help of Fourier transformation, can be mathematically converted into a mass spectrum. Oscillations frequencies from individual peptides with different masses are used to compute the respective m/z value of a given peptide, whereas the amplitude of the oscillation is utilized to infer the signal intensity of the analyzed peptide. Recording all peptide masses present in the Orbitrap mass analyzer at a specific point in time results in the so called precursor scan.

Having determined the initial mass and intensity information, the MS then proceeds to acquire structural information on the peptide sequence by selecting specific peptide ions and subjecting them to fragmentation through collision (Steen and Mann, 2004). This approach is called tandem MS (MS/MS). While in the LTQ-Orbitrap system inert gas molecules such as helium are used to fragment the precursor peptide (referred to as collision-induced dissociation, CID),

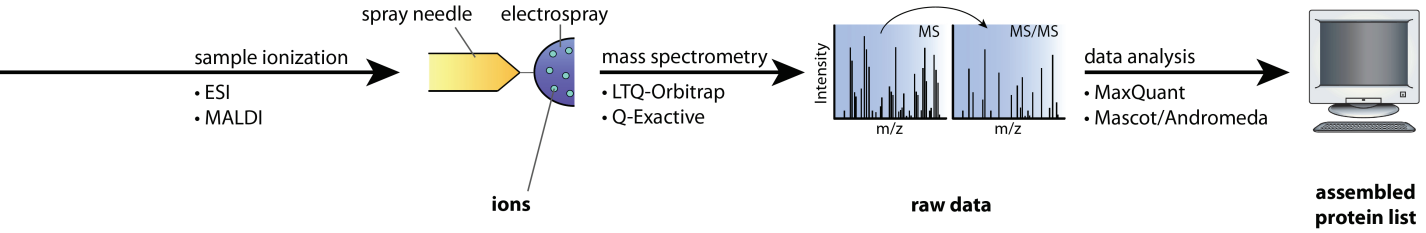

FIG I.5 | Common workflow for mass spectrometry-based proteomics. Proteins derived from a biological source are fractionated by various techniques in order to reduce sample complexity, and are subsequently subjected to enzymatic digestion. The generated peptide mixture is then further separated by reversed phase high performance liquid chromatography (rpHPLC) directly coupled to electrospray ionization (ESI). Alternatively, peptides can also be ionized via matrix-assisted laser desorption/ionization (MALDI). Thereupon, ionized peptides are subjected to the orifice of a mass spectrometer and further manipulated by electrostatic fields within various types of mass spectrometers in order to determine the accurate mass of ionized peptides (MS spectra) or to obtain sequence information from the fragmented peptides (MS/MS spectra). Finally, the peptide-sequencing data deduced from the acquired mass spectra are searched against protein databases using different analysis software tools, e.g. the MaxQuant platform. (Illustration adapted from Steen and Mann, 2004).

the Q-Exactive uses higher-energy collisional dissociation (HCD) to break the selected ion into smaller structural pieces. Similar to CID, HCD also uses collision gas such as nitrogen for fragmentation, but the radiofrequency voltage in the collision cell is increased by 60% to generate high-energy collisions of precursor ions (Olsen et al., 2007). During the precursor scan in the Orbitrap, the top N most abundant precursor ions are selected for fragmentation in either the LTQ or the quadrupole filter, depending on the system. As a result, the precursor ion produces fragment ions of specific m/z values, from which the amino acid sequence of the selected precursor can be deduced. The mass spectrometer will cycle between a sequence of generated MS and MS/MS spectra, resulting in a specific cycle time for data acquisition.

As described earlier, hybrid mass spectrometers combine the strengths of different mass analyzers. Each system has unique performance parameters, which can be outlined in generic terms such as resolution, speed, sensitivity and dynamic range. The resolution of a MS resembles its ability to sufficiently resolve peptide peaks with minimal variations in m/z value. For instance, high resolution instruments can itemize distinct isotopes of a specific peptide. This is an important consideration as peptide peaks are not displayed as single peak lines but as isotope clusters reflecting their natural isotopic distribution. Speed constitutes the number of spectra that can be acquired per unit of time, thus is mainly dependent on the instrument's cycle time. The sensitivity represents the ability of an MS instrument to detect the smallest possible quantity of an analyte, which is currently in the lower attomolar range. Finally, the dynamic range describes the range between the most intense and the least intense analyte signal observed in a survey. At present, MS-based identification of proteins is mainly limited by the dynamic range of protein expression within a cell. The dynamic range of proteins spans seven orders of magnitude in most human cell types (Geiger et al., 2012), human plasma is even estimated to have a concentration range that exceeds ten orders of magnitude (Anderson and Anderson, 2002). State-of-the art mass spectrometers can nowadays cover a dynamic range of 10^3-10^5 in single shot experiments (Makarov et al., 2006a,b), still, complete proteome

coverage can be achieved through more extensive pre-fractionation and oversampling, i.e. repeated mass spectrometric measurements of the very same sample, at least for most standard cell lines (Geiger et al., 2012). Conclusively, the temporal and spatial separated acquisition of MS and MS/MS spectra enable hybrid MS instruments to develop their full potential through exploitation of their distinct analytical systems.

In a final step of the proteomic workflow, the acquired mass spectra information needs to be converted into peptide and subsequent protein identification events. A probability-based matching algorithm is applied which compares the acquired spectra to theoretical spectra obtained from *in silico* digestion and fragmentation with the very same parametric prerequisites as given from the experimental analysis. The algorithm selects the best matching MS/MS spectra and subjects them to a database search of the particular organism under investigation. Given the tremendous amount of high-resolution mass spectra that are acquired on state-of-the-art mass spectrometers nowadays, it is no surprise that all the data analysis regarding peptide and protein assignment are performed automatically using sophisticated bioinformatic tools.

As a concluding remark, it is important to mention that all proteomic experiments in the present thesis have been performed conducting “shotgun” or “discovery” proteomics. This method attempts to sequence all proteins present in a particular sample, thus always means *de novo* discovery of a given protein set. The main strength of the shotgun approach is its experimental simplicity and the high proteomic coverage. However, it suffers from the yet limited dynamic range of modern mass spectrometers and bioinformatic challenges related to inferring protein information from peptide information (Domon and Aebersold, 2006). Hence, if only a subset of proteins is under investigation, for instance a particular signaling pathway, “targeted” proteomics might be preferable. Such an approach exclusively targets a well defined set of proteins; nonetheless, it inherently requires *a priori* information on the peptide sequence for the target selection, which has to be compiled by previous discovery proteomic experiments.

I.2.2 Stable isotope labeling by amino acids in cell culture (SILAC)

Recent progress in MS-based proteomics has enabled the routine and robust identification of peptides. However, maybe the even more interesting biological questions remain unaddressed without adding a quantitative dimension, thus quantification of proteins is of central importance. Mass spectrometry is not inherently quantitative, therefore, several quantitative techniques have been developed by the MS community to enable accurate assessments of quantitative differences between cellular conditions.

Relative quantification allows comparing proteins derived from different cell populations relative to each other. Several methods have been employed in recent years but a thorough review of all quantification strategies is beyond the scope of the present thesis, thus they will be de-

scribed only very briefly. The easiest way to quantify proteins from distinct conditions is the so-called label-free approach. High abundant proteins are more likely to be detected within the mass spectrometer. Therefore, most label-free approaches apply either counting of fragment spectra (termed spectral counting) or raw MS signal intensities of peptides derived from the very same protein (termed extracted ion current, XIC). Label-free approaches are easy to implement within the proteomic workflow and do not cause extra costs as quantification of peptides and proteins is done bioinformatically. However, label-free approaches inherently compare peptide abundances across independent LC-MS runs, thus several limitations accompany label-free strategies. Mainly, differences in sample preparation, ionization efficiency, flyability of ionized peptides and minimal shifts in chromatographic retention times may affect the precision of label-free quantification approaches.

More accurate quantification can be achieved by stable isotopes. The isotopes can be introduced into biological systems either via chemical modification of proteins or peptides or via metabolic labeling of living cells. Frequently used chemical modification approaches are, for instance, the transfer of heavy oxygen (^{18}O) during the enzymatic protein digestion (Yao et al., 2001), chemical tagging of peptides (called isotope-coded affinity tag, ICAT) (Gygi et al., 1999) or proteins (termed isobaric tags for relative and absolute quantification, iTRAQ) (Ross et al., 2004). Like chemical modification strategies, metabolic labeling approaches also require the incorporation of heavy stable isotopes, which is based on supplementing growth media of living cells with stable isotopes. The basic concept of stable isotope labeling to elucidate cellular functions has been pioneered by the work of Rudolf Schoenheimer already in the 1930s essentially to study intermediary metabolism (Schoenheimer and Rittenberg, 1938). Application of metabolic labeling to quantitative proteomics was adapted by ^{15}N labeling and has been applied to a wide range of biological questions (Gouw et al., 2011). However, it is only since 2002 that another metabolic labeling approach, called SILAC, has received a lot of attention and has now become the most widely used metabolic labeling approach in quantitative MS. SILAC stands for stable isotope labeling by amino acids in cell culture and has been developed by Shao-En Ong in the lab of Matthias Mann (Ong et al., 2002). As all quantitative MS experiments in this present thesis were accomplished using SILAC, the SILAC strategy will be discussed in more detail.

SILAC entails the cultivation of cells in different growth media, supplemented with either normal light or heavy stable isotope versions of essential amino acids containing a distinct number of ^{13}C, ^{15}N or ^{2}H atoms (Ong et al., 2002). Hence, heavy amino acids are incorporated into all newly synthesized proteins. For particular reasons, arginine and lysine are most commonly employed as heavy amino acid carriers: lysine is an essential amino acid, which cannot be synthesized by cells and thus has to be taken up from exogenous sources to maintain cell viabil-

ity. Arginine is an conditionally essential amino acid and is mostly gained through the normal diet of cells. In addition, both arginine and lysine have a rather uniform distribution throughout the proteome of most organisms, ensuring a high labeling saturation of most peptides. Finally, in most cases trypsin is used as proteolytic enzyme to digest proteins to peptides within the proteomic workflow. As trypsin usually cleaves carboxyl-terminally after each arginine and lysine, its sequence specificity generates tryptic peptides carrying only one labeled amino acid, which facilitates the bioinformatic data analysis. Furthermore, labeling by SILAC is very fast: after at least five cell doublings the incorporation rate of the heavy isotopes is about ~97% (1- $(0.5)^5$) (Ong and Mann, 2006) and given the fast cell division rates of most immortalized cell lines, a proper labeling is usually achieved within less than 10 days. The biggest advantage of SILAC, however, is the sample combination at a very early stage right after the actual experiment, which minimizes potential errors introduced by sample handling and processing compared to label-free and other common chemical labeling strategies. Although stable isotope labeling affects chromatographic characteristics of peptides, co-eluting pairs of chemically equivalent peptides (referred to as "SILAC pairs") can still be distinguished from each other due to the constant mass differential introduced by the heavy isotopes. Noteworthy, ^{13}C and ^{15}N-labeled peptides disclose less retention time shifts compared to ^{2}H-labeled peptides, thus most researchers use amino acids carrying ^{13}C and ^{15}N atoms in SILAC-based quantitative mass spectrometry. As a result, signal intensities derived from the either the light or the heavy peptide peak can be compared reliably and allow an accurate quantification of several thousands of proteins in a single experiment, relative to their distinct abundance in the conditions under investigation.

In addition, SILAC is not restricted to cultivated cell lines. Over the last years, the scientific community has successfully adapted the once *in vitro*-technique to living organisms such as yeast (Gruhler et al., 2005), flies (Sury et al., 2010), nematodes (Larance et al., 2011), newts (Looso et al., 2010), mice (Kruger et al., 2008) and others. Even proteins derived from human tissue, which is not applicable to metabolic labeling itself, can be quantified via a so called Super-SILAC approach: here, unlabeled human tissue is compared against a Super-SILAC mixture of several stable isotope labeled human cell lines, which most closely resembles the tissue's protein expression profile (Geiger et al., 2010). In principle, SILAC is amenable to every living organism if a sufficient heavy stable isotope containing diet can be assured and if the organism does not dilute the introduced stable isotopes via conversion to other than the desired amino acids. Interestingly, SILAC can also be utilized to distinguish non-cell autonomous proteins in human cells derived from infectious pathogens, referred to as trans-SILAC (Rechavi et al., 2010).

The overall simplicity has made the SILAC strategy one of the most commonly used quantitative labeling approaches; however, SILAC does have some drawbacks and limitations. First of all, SILAC is not easily applicable to primary cell lines, which are potentially the most interesting *in vitro* system being closest to *in vivo* conditions in a Petri dish. Secondly, SILAC requires proper labeling which can be time-consuming when working with cells exhibiting extremely slow cell division rates, such as many neuronal cell lines. Thirdly, SILAC can only be used to distinguish up to five different conditions at once (Molina et al., 2009), thus other labeling strategies have to be employed if even more conditions are under investigation. Fourthly, extreme care is required when handling the growth medium: fetal calf serum (FCS) is required as supplemental for most cell lines but it is a potential source of light amino acids. Consequently, dialyzed FCS (dFCS) has to be used that is, however, not compatible with all cell lines, as some rare ones do need certain growth factors lost by dialysis. In addition, trypsin can be a common source of light amino acids as it is necessary to dissociate adherent cells during passaging. Therefore, cells have to be centrifuged after each trypsinization step in order to remove remaining trypsin. Fifthly, certain cell lines convert excessive arginine towards proline. Though, this problem can be circumvented by either titrating the amount of arginine in the media (Ong and Mann, 2006) or by computationally setting off the heavy proline peaks against the heavy arginine peak leftovers (Park et al., 2009). Finally, the utilized heavy stable isotopes are expensive, making *in vitro* SILAC and especially *in vivo* SILAC-based quantitative proteomics rather expensive compared to other labeling strategies.

I.3 Outline and objectives of the thesis

Neurodegenerative diseases are devastating disorders with a clear proteopathic impact, causing millions of deaths worldwide each year. Currently, no therapeutic treatment option is available for any of the described NDDs that substantially cures the disease.

Given the shared pathogenic commonalities of many NDDs at the protein level, a comprehensive PPI screening approach across several NDD-causative bait proteins might have a great potential to pinpoint disease-critical proteins. Although several studies have been performed to elucidate PPI networks for one particular NDD alone (Bai et al., 2008; Goehler et al., 2004; Jin et al., 2007; Soler-Lopez et al., 2011), there is only very limited data available for a comparative PPI analysis of several different NDDs altogether (Lim et al., 2006; Limviphuvadh et al., 2007) clearly pointing out the need for systematic and in-depth PPI analysis across distinct NDDs. The aim of the present thesis was thus to systematically identify and quantify PPIs of the major disease proteins involved in the most common NDDs, utilizing SILAC-based quantitative mass spectrometry.

The q-AP-MS approach is ideally suited for studying quantitative PPIs. On one hand, it allows unambiguous discrimination of unspecific binders and thus excludes many spurious interactors from the dataset. On the other hand, it enables the detection of preferential binders, hence shows how PPIs might be affected by NDD-associated mutations.

To this end, the q-AP-MS strategy is applied to highlight both total and differential interactors of wild-type and disease-associated variants implicated in neurodegeneration, resulting in a global PPI network for NDDs. The generated quantitative PPI data should provide a highly valuable resource for the neurodegenerative disease community. Functional follow-up experiments of either wild-type or mutant bait variants will most likely gain novel insights into molecular mechanisms involved in progression and potential crosstalk of distinct neurological diseases.

II Material and Methods

II.1 General suppliers

All chemicals were purchased from the laboratory suppliers Merck (Darmstadt, Germany), Roth (Karlsruhe, Germany) or Sigma-Aldrich (Steinheim, Germany), if not stated otherwise.

II.2 General buffers and solutions

Solutions and buffers for bacterial handling

LB (lysogeny broth) medium

10 g Bacto tryptone (BD, Franklin Lakes, NJ, USA), 5 g Bacto yeast extract (BD), 5 g NaCl, ad 1 L with dH_2O adjusted to pH 7.4; for plates 1.5% (w/v) agar was added.

Ampicillin

100 mg/µl stock solution in dH_2O, sterilized by filtration, aliquots were stored at -20°C. Working concentration was 100 µg/µl.

IPTG (Isopropyl β-D-1-thiogalactopyranoside)

1 M stock solution in dH_2O, sterilized by filtration, aliquots were stored at -20°C. Working concentration was 1 mM.

Solutions and buffers for DNA manipulation and electrophoresis

PEI (polyethylenimine) transfection reagent

10 mg of linear PEI Max (nominally MW 40,000; PolySciences, Eppelheim, Germany) was dissolved in 10 ml dH_2O, neutralized to pH 7.5 with approximately 100 µl 1 M NaOH and sterilized by filtration. Aliquots were stored at -20°C.

1x TE buffer

10 mM Tris-HCl pH 7.4, 1 mM EDTA

1x TAE running buffer

40 mM Tris-HCl (pH 8.5), 40 mM acetic acid, 1 mM EDTA

5x DNA loading buffer

63 mM Tris-HCl (pH 6.8), 2% [w/v] SDS, 10% [v/v] glycerol, 0.01% [w/v] bromphenol blue

Solutions and buffers for protein electrophoresis and protein purification

Radioimmunoprecipitation assay (RIPA) buffer for cell lysis

50 mM Tris-HCl pH 7.4, 150 mM NaCl, 1mM EDTA, 1% [v/v] Triton-X 100, 1% [w/v] Na-Deoxycholate, 0.1% [w/v] SDS. Complete Protease Inhibitor Cocktail (Roche) (1:25) and Phosphatase Inhibitor Mix 1 (Sigma) (1:100) were added right before use.

SDS running buffer MES

40 ml 20x NuPAGE MES SDS running buffer for Bis/Tris gels (Invitrogen, Karlsruhe, Germany) in 760 ml dH_2O.

Transfer buffer

25 mM Tris-HCl pH 8.5, 190 mM glycine, 10% [v/v] methanol, 0.1% [w/v] SDS

Stripping buffer

68 mM Tris-HCl pH 7.5, 2% [w/v] SDS, 0.8% [v/v] β-mercaptoethanol

10x TBS

200 mM Tris base, 1.4 M NaCl, adjusted to pH 7.4

1x TBST

0.1 % [v/v] Tween-20 in 1x TBS

Blocking solution

1x TBST supplemented with 5% [w/v] non-fat dry milk powder

ConA buffer

100 mM sodium acetate pH 7.0, 0.1 M NaCl, 5 mM $MgCl_2$, 5 mM $MnCl_2$, 5 mM $CaCl_2$

Solutions and buffers for LC-MS sample preparation and instrumentation

ABC buffer

50 mM ammonium bicarbonate (NH_4HCO_3) in water (pH 8.0)

Destaining buffer

25 mM ammonium bicarbonate / 50% [v/v] ethanol (EtOH). Equal volumes of 50 mM ABC buffer and 100% [v/v] EtOH were combined.

Reduction buffer

10 mM dithiothreitol (DTT) in 50 mM ABC buffer. Stored in small aliquots at -20°C.

Alkylation buffer

55 mM iodoacetamide in 50 mM ABC buffer. Stored in small aliquots at -20°C and kept in the dark.

Extraction buffer

3% [v/v] trifluoroacetic acid (TFA) / 30% [v/v] acetonitrile (ACN). Stored at RT.

Denaturation buffer

6 M urea / 2 M thiourea in 10 mM HEPES (pH 8.0). Stored in small aliquots at -80°C.

Buffer A

5% [v/v] acetonitrile, 0.1% [v/v] formic acid in water. Stored at RT.

Buffer A*

5% [v/v] acetonitrile, 0.1% [v/v] formic acid in water, 3% [v/v] trifluoroacetic acid. Stored at RT.

Buffer B

0.1% formic acid, 80% acetonitrile in water. Stored at RT.

All solutions with direct application for LC-MS/MS analysis were made with LiChrosolv grade water or acetonitrile. Further fine chemicals were conform to the standard laboratory equipment.

II.3 CONSUMABLES

DNA cloning and purification

- LR Clonase II Enzyme Mix, including LR Clonase II and Proteinase K (Invitrogen)
- Plasmid purification Mini and Midi kits (Qiagen, Hilden, Germany)

SDS-PAGE & Western blotting

- NuPAGE Novex Bis-Tris gels 4-12% (Invitrogen)
- NuPAGE MES SDS running buffer (Invitrogen)
- 4x LDS sample buffer (Invitrogen)
- PVDF blotting membrane Millipore Immobilon-P, 0.45µm pore size (Roth)
- Western Lightning Chemilumincescence Reagent Plus Enhanced Luminol (PerkinElmer, Rodgau, Germany)
- Amersham Hyperfilm ECL (GE Healthcare, München, Germany)

Immunoprecipitation

- µMACS c-myc isolation kit, MACS MultiStand, OctoMACS separation unit, µ and M columns (Miltenyi Biotec, Bergisch Gladbach, Germany)
- NHS-activated Sepharose 4 FastFlow (GE Healthcare)
- ConcanavalinA Sepharose 4B beads (Sigma-Aldrich)

Mitochondria isolation and Aconitase activity test

- Mitochondria isolation kit (human), QuadroMACS separation unit, LC columns (Miltenyi Biotec, Bergisch Gladbach, Germany)
- Aconitase activity assay kit (Novagen, Merck)

II.4 BIOLOGICALS

***Escherichia coli* strains**

- OneShot Mach1 T1R for chemocompetent transformation of bacteria, genotype: F- ϕ80(lacZ)ΔM15 ΔlacX74 hsdR(rK-mK+) ΔrecA1398 endA1 tonA (Invitrogen)
- OneShot TOP10 for chemocompetent transformation of bacteria, genotype: F- mcrA Δ(mrr-hsdRMS-mcrBC) ϕ80(lacZ)ΔM15 ΔlacX74 recA1 araD139 Δ(ara-leu) 7697 galU galK rpsL StrR endA1 nupG λ- (Invitrogen)

***Drosophila melanogaster* strains**

Transgenic flies and housing conditions

All fly-related work was accomplished by Hannes Vossfeldt (University Clinics, RWTH Aachen, Aaron Voigt lab). Fly stocks were maintained on standard cornmeal-agar-yeast-molasses-based food at 18 °C. Standard crossbreeding of adult Drosophila were conducted at 25 °C. RNAi fly strains comprising the human homolog sublibrary were purchased from the Vienna Drosophila RNAi Center (VDRC) where they have been generated by random integration of shRNA-transcribing inverted repeats under UAS-GAL4 control into the Drosophila genome (UAS-shRNA). Screening for eye changes by shRNA expression itself was conducted using the GMR-GAL4 line as a control (TAB.II.1). GMR-GAL4 and UAS-ATXN1-Q30/82 strains were recombined in order to generate the screening stock for the polyQ modifier screen (GMR_ATXN1-Q30/Q82). For the screening of polyQ specificity of RNAi candidates, flies overexpressing the mutant tau transgene in the eye were utilized (UAS_Tau[R406W] > GMR_Tau[R406W]). For screening purposes, GMR driver stocks were crossbred with UAS-shRNA lines from the VDRC. Screening for eye changes by shRNA expression itself was conducted using the GMR-GAL4 line as a control. GMR-ATXN1-Q82 virgins were crossed to males carrying UAS-RNAi constructs. F1 females (GMR-ATXN1 in combination with the respective UAS-RNAi expression) were selected for REP evaluation 1-5 days post eclosion. The 29 RNAi lines for the human homologue sublibrary used in this study were selected by the VDRC considering known or predicted human homologues to the fly genes (Supplementary TAB. VII.1).

Table II.1 | Utilized *Drosophila melanogaster* strains

Transgenic line	Genotype[1]	Source
Oregon-R-C	wild-type	Bloomington #5
GMR-GAL4	w[*];P{w[+mC]=GAL4-ninaE.GMR}12	Bloomington #1104
UAS-lacZ	P{w[+mC]=UAS-lacZ.Exel}2	Bloomington #8529
UAS-ATXN1-Q30	y[1]w[118] P{[+]=UAS-SCA1.30Q}[F7]	gift of Juan Botas
UAS-ATXN1-Q82	y[1]w[118] P{[+]=UAS-SCA1.82Q}[F7]	gift of Juan Botas
GMR_ATXN1-Q30	y[1]w[118]P{[+]=UAS-SCA1.30Q}[F7]/ FM7c; w[*]; P{w[+mC]=long GMR-GAL4}/CyO	created by Hannes Voss-feldt
GMR_ATXN1-Q82	y[1]w[118]P{[+]=UAS-SCA1.82Q}[F7]/ FM7c; w[*]; P{w[+mC]=long GMR-GAL4}/CyO	created by Hannes Voss-feldt
UAS-Tau[R406W]	w[*];;P{w[+mC]=UAS-hTau[R406W]}	gift of Mel Feany
GMR_Tau[R406W]	w[*];P{w[+mC]=GAL4-ninaE.GMR}12/ CyO;P{w[+]=UAS-Tau[R406W]}/TM3,S	created in the Aaron Voigt lab

[1] genotype as suggested by Flybase

Evaluation of rough eye phenotype (REP) modification

For assessment of REP modulation, at least five female flies were analysed for changes in the severity of eye degeneration. Modifications by the induction of RNAi in polyQ and tau models were categorized as follows: wild type-like phenotype (---), obvious REP suppression (--), subtle REP suppression (-), no change of REP (0), subtle enhancement of REP (+), obvious enhancement of REP (++) and lethal (+++). For the GMR-GAL4 screening only the “no change” and enhancement terms apply. RNAi lines exhibiting such effects in the GMR-GAL4 control flies were excluded from subsequent experiments due to impact unconnected to expression of elongated polyQ. Designation of an RNAi line as polyQ modifier candidate required no change in control flies and an at least obvious enhancement/suppression of the REP in three independent experiments. Candidate lines were tested for polyQ specificity by rescreening with Tau[R406W] screening stock. RNAi lines exhibiting similar effects in both models were excluded from the polyQ candidate set and remainder strains were subjected to more detailed analysis. Drosophila compound eyes were pictured using an Olympus zoom stereo microscope at 6.3x magnification and Cell A software.

***Homo sapiens* cell lines**

- HEK293TN: adherent human embryonic kidney cells, carrying a plasmid containing the temperature sensitive mutant of SV-40 large T-antigen and a neomycin resistance cassette. Obtained from System Biosciences, Mountain View, CA, USA
- SH-SY5Y: adherent human neuroblastoma cells. Obtained from the Erich Wanker lab (MDC, Berlin)

***Mus musculus* brain samples**

Freshly prepared mice brains (female BL/6 mice, 12 weeks old) were obtained from the Ibanez-Tallon lab (MDC, Berlin). Mice brains were dissected by making a sagittal cut and each cerebral hemisphere was lysed completely with 500 µl brain lysis buffer (50 mM Tris pH 7.4, 150 mM NaCl, 1% [v/v] Triton X-100, 1 mM EDTA, 1 mM EGTA, Complete Protease Inhibitor Cocktail 1:25) in a glass dounce tissue grinder with approximately 50 strokes on ice. Fully grinded brain lysate was immediately snap frozen in liquid nitrogen and stored at -80°C until further usage.

Table II.2 | Antibodies

Name (clone)	Host species	working dilution 1st antibody	working dilution 2nd antibody	Supplier
αAPP (B-4)	mouse monoclonal	1:500	1:20,000	Santa Cruz
αATXN1 (L-19)	goat polyclonal	1:500	1:30,000	Santa Cruz
αc-Myc (9E10)	mouse monoclonal	1:500	1:20,000	Santa Cruz
αCOX1 (1D6E1A8)	mouse monoclonal	1:1,000	1:20,000	MitoSciences
αDHCR24 (H-300)	rabbit polyclonal	1:500	1:20,000	Santa Cruz
αLRPPRC (H-300)	rabbit polyclonal	1:500	1:20,000	Santa Cruz
αPSEN1 (N-19)	goat polyclonal	1:500	1:30,000	Santa Cruz
αRPN1 (E-7)	mouse monoclonal	1:500	1:20,000	Santa Cruz
αSKP1 (H-6)	mouse monoclonal	1:500	1:20,000	Santa Cruz
αSNCA (211)	mouse monoclonal	1:500	1:20,000	Santa Cruz
αTBL1XR1 (L-08)	mouse monoclonal	1:500	1:20,000	Santa Cruz
αBeta-actin	mouse monoclonal	1:50,000	1:20,000	Sigma
HRP conjugated anti-mouse	sheep	-	as indicated above	GE Healthcare
HRP conjugated anti-rabbit	donkey	-	as indicated above	GE Healthcare
HRP conjugated anti-goat	donkey	-	as indicated above	Santa Cruz

Working dilutions used for Western blotting experiments.

II.5 Cell culture and medium preparation

II.5.1 Cell culture

All cells were cultivated at 37°C with 5% CO_2 and split every second or third day. To generate cell stocks ~10^6 confluent cells were briefly washed with 1x PBS, trypsinized (Invitrogen) and centrifuged at RT and 1,200 rpm for 5 min, the supernatant was discarded. Next, the cells were resuspended in cell freezing medium (Gibco) and gradually frozen using a 5100 cryo 1°C freezing container (VWR, Darmstadt, Germany) filled with isoproanol at -80°C. After two days the cell stocks were transferred to the liquid nitrogen storage and kept at -160°C.

II.5.2 Standard media for cell culture

Dulbecco's Modified Eagle's Medium GlutaMAX (DMEM GlutaMAX, High Glucose 4.5 g/l, Gibco) was supplemented with fetal calf serum (FCS, Invitrogen). Media were filtered sterile through 0.22 µM vacuum filtration systems (TPP, Trasadingen, Switzerland). For metabolic pulse labeling experiments the glucose concentration was lowered to 2.5 g/l.

II.5.3 SILAC media for cell culture

For the preparation of SILAC media for mammalian cells, Dulbecco's Modified Eagle's Medium (DMEM, High Glucose 4.5 g/l) lacking arginine and lysine (a custom preparation from Invitrogen) was supplemented with dialyzed fetal calf serum (dFCS, Invitrogen) and 4 mM glutamine (Invitrogen). "Heavy" and "medium-heavy" SILAC media were prepared by adding 28 mg/l $^{13}C_6{}^{15}N_4$ L-arginine plus 49 mg/l $^{13}C_6{}^{15}N_2$ L-lysine or by adding 28 mg/l $^{13}C_6$-L-arginine plus 49 mg/l D_4-L-lysine, respectively. Labeled amino acids were obtained from Sigma Isotec ($^{13}C_6$-L-arginine, $^{13}C_6{}^{15}N_4$ L-arginine and $^{13}C_6{}^{15}N_2$ L-lysine) and Cambridge Isotope Laboratories (D_4-L-lysine). To prepare "light" SILAC medium, the corresponding non-labeled amino acids (Sigma) were added. All SILAC media were filtered sterile through 0.22 µM vacuum filtration systems (TPP, Trasadingen, Switzerland).

Table II.3 | Media composition (standard and SILAC media)

Cell line	Medium	Serum	Glutamine source	Antibiotics
HEK293TN	DMEM	10 % [v/v] FCS	GlutaMAX	100 U/ml penicillin, 100 µg/ml streptavidin
HEK293TN	SILAC-DMEM	10 % [v/v] dFCS	4 mM glutamine	100 U/ml penicillin, 100 µg/ml streptavidin
SH-SY5Y	DMEM	15 % [v/v] FCS	GlutaMAX	100 U/ml penicillin, 100 µg/ml streptavidin
SH-SY5Y	SILAC-DMEM	15 % [v/v] dFCS	4 mM glutamine	100 U/ml penicillin, 100 µg/ml streptavidin

II.6 Nucleic Acid Work

II.6.1 Cloning utilizing the GATEWAY system

Genes of interest for the protein-protein interaction assay were provided in pDONR201, pDONR221 or pDONR223 entry clone plasmids by Katja Muehlenberg (PostDoc in the group of Erich Wanker, MDC, Berlin). To shuttle the inserts into the pcDNA5/FRT/TO::1xc-myc destination vector used for immunoprecipitation, a LR reaction via the GATEWAY system (Invitrogen) was performed. 50 ng of entry clone was mixed with 150 ng of destination vector and filled up to 8 µl with TE buffer (pH 8.0). After adding of 2 µl LR Clonase II the reaction was incubated at

25°C for one hour before the shuttling was terminated using 1 µl Proteinase K to degrade the LR Clonase II at 37°C for 10 minutes. Destination vectors carrying the shuttled gene of interest were subsequently transformed into *E.coli* Mach1 cells.

II.6.2 Preparation of plasmid DNA

For isolation of plasmid DNA from bacteria a Mini or Midi prep kit (Qiagen) was used according to the manufacturer's instructions. The DNA concentration was measured spectrometrically using a NanoDrop ND-1000 device (Peqlab, Erlangen, Germany).

II.6.3 Agarose gel electrophoresis

Preparative analysis of shuttled plasmid vectors was achieved by DNA restriction reaction and subsequent agarose gel electrophoresis. 1 µg plasmid DNA was incubated with 1 µl (10 U) BsrGI (NEB, Frankfurt a.M., Germany) restriction enzyme, 3 µl Buffer 2 (NEB), 0.3 µl 100x BSA (NEB) and 23.7 µl dH_2O. The restriction reaction was incubated for 1 hour at 37°C and stopped by incubation at 80°C for 20 minutes. Restricted probes were mixed with DNA loading buffer. Separation and detection of DNA fragments in the gel was performed with 0.6-1.0% [w/v] of agarose in 0.5x TAE buffer supplemented with 1 µg/ml ethidiumbromide and applying 80-120 V for the aspired time. Visualization of DNA was achieved using an Gel iX imager (Intas, Göttingen) thereby detecting the fluorescence of the DNA-intercalating dye ethidiumbromide. To identify the size of nucleic acids, a standard marker (DNA ladder 1kb, NEB) was used.

II.6.4 Sequencing of plasmid DNA

To guaranty sequence quality of isolated plasmid DNA, all DNA samples were send to an external DNA sequencing facility (SMB Services in Molecular Biology, Berlin). Obtained DNA sequence chromatograph data were carefully checked for quality and mutations using DNA Chromatogram Explorer (HeracleSoftware).

II.6.5 qRT-PCR

Expression changes at the transcript level were analyzed by qRT-PCR (quantitative reverse transcription polymerase chain reaction) performed by Emanuel Wyler (Markus Landthaler lab, MDC Berlin). Total RNA from cells were isolated using the miRNeasy kit (Qiagen) according to the manufacturer's protocol. RNA concentration was measured using a NanoDrop system (Thermo Scientific, Wilmington, DE, USA). Reverse transcription was performed using 2.2 µg total RNA, except for RIP (cf. II.6.6) precipitates where isolated RNA was used completely. After DNaseI (Invitrogen) digestion for 15 minutes at 25 °C, the sample was split in 2x20 µl reactions and one of them was reversed transcribed using SuperScript III (Invitrogen) and an oligo-dT18 primer for 1 hour at 50 °C. For quantitative PCR, the 2x SYBR green PCR Mastermix (Applied Biosciences, Carlsbad, CA, USA) was used in a 20 µl reaction with 400 nM of each primer and 0.4 µl of the RT reaction. The amplification was measured and quantified using the StepOne system from applied biosciences using relative quantification for all primer pairs.

Table II.4 | Primer sequences

Gene	Sequence
COX1 (forward)	CAGCAGTCCTACTTCTCCTATCTCT
COX1 (reverse)	GGGTCGAAGAAGGTGGTGTT
LRPPRC (forward)	GAAGATGCCTTGAACTTGAAAGA
LRPPRC (reverse)	GCCTACATACTTGCCGGTGT
Vinculin (forward)	CTCGTCCGGGTTGGAAAAGAG
Vinculin (reverse)	AGTAAGGGTCTGACTGAAGCAT

Primers are taken from PrimerBank (http://pga.mgh.harvard.edu/primerbank/citation.html) (Vinculin) and from the Roche Universal ProbeLibrary (COX1 and LRPPRC).

II.6.6 RIP (RNA-immunoprecipitation)

In order to test whether a distinct protein binds to certain RNA molecules, the protein of interest was immunoprecipiated (cf. II.9.3). Total RNA from lysates used for RIP experiments was extracted using Trizol (Invitrogen) followed by ethanol precipitation. RIP precipitates were treated with Proteinase K, extracted using Phenol/Chloroform and RNA was isolated using ethanol precipitation. Isolated RNA was then subjected to qRT-PCR analysis (cf. II.6.5).

II.7 Bacterial work

II.7.1 Transformation of chemocompetent bacteria

For the transformation of DNA into bacterial cells the heat shock transformation technique was used. Chemocompetent *E.coli* cells were thawed on ice, 200 ng plasmid DNA was added to the cells and incubated for 30 min on ice to guarantee an efficient attachment of the plasmid DNA to the bacterial membrane. The bacteria/DNA mixture was heat shocked for 30 sec at 42°C in a waterbath and immediately put on ice afterwards for 1 min. Next, 250 µl SOC medium (Invitrogen; warmed to 37°C) was added to the cells, followed by a 1 hour incubation at 37°C and 220 rpm. An adequate dilution of transformed cells was plated on LB agar plates. Obtained efficiency was 10^8-10^9 cfu/µg plasmid DNA.

II.8 Working with mammalian cells

II.8.1 Transient transfection of mammalian cells

Plasmid DNA and polyethylenimine (PEI) transfection reagent were mixed together (ratio DNA:PEI 1:2) with serum-free cell culture medium (DMEM) and incubated for 15 min at RT to ensure an efficient binding of the negatively charged DNA to the polycation PEI. The transfection setup was then applied directly to the adherent cells and harvested 24-72 hrs after transfection. Cells were transfected at 60% confluency.

Table II.5 | Setup for PEI-mediated transient transfection of mammalian cells

dish size	DNA	PEI	serum-free medium	final medium volume on plate
6well	2 µg	4 µg	0.2 ml	2 ml
10cm	10 µg	20 µg	1.0 ml	10 ml
15cm	15 µg	30 µg	1.5 ml	15 ml

II.8.2 Transfection of siRNAs for RNAi-mediated knockdown

For the transfection of 6well plates 2.5 µg siRNA was mixed with 5 µl Dharmafect transfection reagent (Thermo Scientific) and 285 µl serum-free cell culture medium (DMEM). The transfection setup was incubated for 20 min at RT and then applied directly to the adherent cells and harvested 72-96 hrs after transfection. Cells were transfected at 60% confluency.

II.8.3 Harvesting of mammalian cells

Adherent mammalian cells were washed with ice-cold PBS buffer. Next, ice-cold RIPA lysis buffer was added (300 µl RIPA buffer/15 cm cell culture dish) and the cells were scraped off the plate using cell scrapers (Corning Inc., Amsterdam, The Netherlands). Depending on the cell line, 2-10 U of Benzonase endonuclease (Merck) were added and incubated on ice for 30 min to degrade DNA. Cell debris was cleared by centrifugation at 4°C and 13,000 rpm for 15 min.

II.9 Protein analytics

II.9.1 SDS-PAGE

Molecular weight separation of proteins according to their electrophoretic mobility was achieved by SDS-PAGE (sodium dodecyl sulfate polyacrylamide gel electrophoresis). To ensure equal loading of all lanes on the gel the protein concentration was determined spectrometrically upfront using a NanoDrop ND-1000. Protein probes were mixed with SDS loading buffer and heated up to 95°C for 5 min. Separation was achieved using discontinous 4-12% Bis-Tris gels (NuPAGE, Invitrogen) and applying 200 V (100 mA, 30 Watt) for the desired time. Visualization of proteins was achieved by Coomassie blue staining. Therefore, the gel was incubated for 10 min in fixing solution (40% [v/v] methanol, 10% [v/v] acetic acid and 40% [v/v] dH_2O), another 10 min in pre-staining solution (30% [v/v] methanol, 30% [v/v] NuPAGE Stainer A and 40% [v/v] dH_2O) and 1 hour in colloidal Coomassie blue. After 1 hour, the staining solution was replaced with water.

II.9.2 Western blotting

One-dimensional separation of protein samples was performed by SDS-PAGE (cf. II.9.1). Gels were then blotted onto PVDF membranes via wet (tank) blotting using the XCell II Blot Module (Invitrogen) according to the manufacturer's instructions, applying 1 mA of current per cm^2 of membrane for 2 h. The membrane was activated prior to use with 100% [v/v] methanol and washed once in transfer buffer. Unspecific binding sites were blocked with 5% [w/v]

dry milk powder in 1x TBST at 4°C for 60 min. In order to visualize specific protein bands, the membrane was incubated with the respective primary antibody (TAB. II.2) in blocking solution at 4°C overnight with shaking. Blots were washed three times in TBST and incubated either with the appropriate secondary antibody (TAB. II.2) conjugated to horseradish peroxidase for 1 h at RT. After three more washing steps in TBST for 10 min the signals of the bound secondary antibodies were detected by applying Western Blot Chemiluminescence Reagent Plus for ECL immunostaining (PerkinElmer) to the membrane followed by exposition to X-ray films (GE Healthcare). For sequential detection of different proteins on the same membrane, the PVDF membrane was stripped in stripping buffer (37°C, 20 min, 200 rpm shaking) and washed thoroughly with distilled water. Subsequently, the membrane was blocked again and treated as described above.

II.9.3 Immunoprecipitation

Immunoprecipitations of c-myc-tagged bait proteins were performed using the µMACS c-myc Isolation Kit (Miltenyi Biotec) according to the manufacturer's instructions. Cell lysates with overexpressed c-myc::bait fusion proteins (from $2x10^7$ cells) were lysed (cf. II.8.3.) and incubated with 75 µl of anti-c-myc µMACS beads for 30 min on ice. Next, the beads were transferred to a µMACS M column placed in the magnetic field of the OctoMACS separator. Before, M columns were equilibrated with 100 µl RIPA lysis buffer. The on-column beads were washed three times with wash buffer 1 and once with wash buffer 2 that are both part of the Miltenyi µMACS kit. Proteins bound to the beads were eluted by applying three times 100 µl elution buffer (100 mM glycine pH 2.5). The collected eluates were combined in a fresh 2 ml Eppendorf tube and set to protein precipitation (cf. II.9.7).

II.9.4 Co-immunoprecipitation

For one pull-down experiment 50 µl of NHS-Sepharose (N-Hydroxysuccinimide-Sepharose) slurry was transferred into a 1.5 ml Eppendorf tube and centrifuged (1,000 g for 2 min) to remove the isopropanol conservation covering. Subsequently, the beads were washed once with 500 µl 1 mM hydrochloric acid and centrifuged again (1,000 g for 2 min), the supernatant was discarded. The beads were now washed twice with 200 µl coupling buffer (0.2 M sodium borate pH 9.0) by centrifugation (1,000 g for 2 min) and removing of the supernatant. Next, 5 -10 µg of the anti-bait antibody was crosslinked to the NHS-activated beads by incubating for 2 hrs at RT on a spinning wheel. Afterwards the beads were centrifuged (1,000 g for 2 min), supernatant was discarded, and free binding sites on the beads were quenched with 150 µl quenching buffer (0.2 M ethanolamine pH 8.0) for 30 min at RT on a spinning wheel. After quenching, the beads were centrifuged (1,000 g for 2 min), supernatant was removed, and the beads were washed three times each with 200 µl alternating washing buffers (wash buffer 1: 0.1 M acetate, 0.5 M NaCl, pH 5.0; wash buffer 2: 0.1 M Tris-HCl pH 8.0) to remove non-covalently coupled anti-bait antibody. Finally, the beads were washed with 200 µl RIPA lysis buffer to equilibrate for the following pull-down from cell lysate. For the actual pull-down the beads were

incubated overnight at 4°C on a spinning wheel and washed three times on the next day with 200 µl stringency washing buffer (20 mM Tris pH 7.6, 300 mM NaCl, 5 mM MgCl2) by centrifugation (1,000 g for 2 min), supernatant was discarded. To elute proteins bound to the NHS-Sepharose beads, 50 µl of SDS-loading buffer was added and the beads were boiled at 95°C for 5 min. After centrifugation (2,000 g for 5 min), the supernatant was transferred into a fresh tube and was set to SDS-PAGE and Western blotting (cf. II.9.1 and II.9.2).

II.9.5 Pull-down of *N*-glycosylated proteins

To enrich *N*-glycosylated proteins, Concanavalin A-Sepharose 4B (Sigma-Aldrich) was used as affinity matrix for pull-down experiments. Since Concanavalin A requires Mn^{2+} and Ca^{2+} ions for carbohydrate binding, all necessary buffers were supplemented with 5 mM $MnCl_2$ and 5 mM $CaCl_2$. For one pull-down experiment 50 µl of Concanavalin A-Sepharose slurry was transferred into a 1.5 ml Eppendorf tube and centrifuged (1,000 g for 2 min) to remove the isopropanol conservation covering. Subsequently, the beads were washed three times with 200 µl ConA buffer by centrifugation (1,000 g for 2 min each) and the supernatant was discarded. Afterwards, the Concanavalin A-Sepharose beads were incubated with the cell lysate overnight on a spinning wheel at 4°C. The next day, the beads were centrifuged (1,000 g for 2 min) and the supernatant was removed, followed by a triple washing step with ConA buffer. To elute the target proteins, the beads were incubated three times with 100 µl 1 M glucose solution for 5 min on a spinning wheel, followed by centrifugation (1,000 g for 2 min) after each elution step. The resulting supernatant was combined in a fresh 2 ml Eppendorf tube and set to protein precipitation (cf. II.9.7).

II.9.6 ELISA detection of secreted $A\beta_{1\text{-}40}$ peptides

Detection of secreted $A\beta_{1\text{-}40}$ was performed using the 96-well Multi-Array Human/Rodent (4G8)-Abeta 40 Ultra-Sensitive ELISA (enzyme-linked immunosrobent assay) (MSD, Gaithersburg, MD, USA). The assay was carried out according to the manufacturer's instructions under the supervision of Vanessa Schmidt (PostDoc in the group of Thomas Willnow, MDC Berlin). For all experiments, SH-SY5Y cells were conditioned for 24 hrs and the conditioned medium was used directly for the ELISA.

II.9.7 Protein precipitation

The sample volume (not more than 300 µl) from a pull-down experiment was transferred to a 2 ml dust-free Eppendorf tube. Next, 70 µl 2.5 M sodium acetate and 2 µl Glycoblue (Ambion) was added to improve precipitation. The mixture was filled up to 2 ml with 100% [v/v] ethanol and mixed briefly. The precipitation solution was incubated overnight at room temperature and centrifuged the next day with 20,000 g at 4°C for 60 min. The supernatant was removed carefully and the protein pellet was air dried. Precipitated protein pellets were stored at 4°C until use (cf. II.11.1.2).

II.10 Assessment of oxidative stress in mitochondria

II.10.1 Isolation of mitochondria

Mitochondria were isolated from HEK293TN cells using the Mitochondria Isolation kit (Miltenyi Biotec) according to the manufacturer's instructions. Mitochondria were prepared from 10^4-10^5 HEK293TN cells. The mitochondrial protein concentration was measured spectrometrically using a NanoDrop ND-1000 device (Peqlab).

II.10.2 Enzymatic assay of mitochondrial aconitase activity

Measurement of oxidative stress in isolated mitochondria from HEK293TN cells was determined by mitochondrial aconitase activity (Aconitase Acitvity Assay Kit, Merck) according to the manufacturer's instructions.

II.11 Liquid-chromatography mass spectrometry (LC-MS)

II.11.1 Sample preparation for mass spectrometry

II.11.1.1 In-gel digestion

To decrease sample complexity, proteins were separated based on their molecular weight by 1-D discontinuous SDS-PAGE prior to digestion (Shevchenko et al., 2006). SDS-PAGE was performed with harvested whole-cell lysates (cf. II.8.3 and II.9.1) using NuPAGE Novex 4 to 12% gradient gels (Invitrogen) under reducing conditions according to the manufacturer's instructions. Proteins were fixed in fixative solution and stained afterwards with the Colloidal Blue staining Kit (Invitrogen). Whole gel lanes were cut into several gel slices (up to 15 slices) and washed three times with ABC buffer to remove Coomassie staining and detergents (SDS). Afterwards, reduction buffer was applied to each slice for 30 min at 56°C for reduction of disulfide bonds followed by alkylation with iodoacetamide (IAA) for 30 min at 37°C in the dark. After another washing step, the gel pieces were dehydrated in 100% [v/v] ethanol. The gel slices were rehydrated with sequence grade modified trypsin (Promega, Madison, WI, USA; protein:enzyme ratio of 50:1) resolved in ABC buffer and incubated overnight at 37°C. Protease activity was quenched by adding trifluoroacetic acid to adjust the pH to < 2. Peptide extraction from the gel matrix was performed by incubating the gel pieces twice with extraction buffer for 20 min each followed by complete dehydration of the gel pieces with 100% [v/v] acetonitrile. After each incubation step, the gel pieces were spun down, supernatants were recovered and finally combined. Lastly, samples were dried in a vacuum concentrator (Eppendorf) until 10-20% original volume to remove the acetonitrile and applied to StageTips (cf. II.11.2) for desalting and further sample concentration.

II.11.1.2 In-solution digestion

Precipitated protein pellets from immunoprecipitation experiments were set to in-solution digestion. 40 µl of denaturation buffer was added to precipitated pellets to solubilize the pro-

teins. To reduce disulfide bonds 10 mM DTT was added and incubated at 56°C and 1,400 rpm in an orbital shaker. Next, 55 mM iodoacetamide was added and incubated at RT and 1,400 rpm in the dark to alkylate free cysteine moieties, resulting in carbamidomethylation of all free cysteine residues. Proteins were then digested by Lys-C endoprotease (Wako, Osaka, Japan; total protein:LysC ratio of 50:1) for at least three hours. The in-solution digestion was finally diluted four times with ABC buffer to reduce the urea/thiourea concentration to 2 M before adding sequence grade modified trypsin (total protein:trypsin ratio of 50:1) and incubating the digestion over night at RT and 300 rpm in an orbital shaker. The digestion was stopped the next day by adding 10 µl 10% [v/v] trifluoroacetic acid.

II.11.2. Stop and Go Extraction Tip (StageTip) purification

StageTips (Rappsilber et al., 2003) were assembled by punching out small discs of C18 Empore (3M) filter using a 22 G syringe and ejecting the discs into 200 µl pipet tips. The resulting C18 Empore columns were conditioned by methanol and equilibrated with buffer A. Peptide solutions from in-solution or in-gel digests were adjusted to pH <2.5 and forced through the C18 Empore column by centrifugation at a maximum speed of 5,000 rpm. The columns were washed once with buffer A*. Peptides were eluted from the StageTips by applying 60 µl of buffer B to the microcolumns. Peptides were directly eluted into an HPLC autosampler plate and concentrated in a vacuum concentrator (Eppendorf, Hamburg, Germany) down to 2-3 µl. After mixing the peptide solutions with an equal amount of buffer A the samples were ready for LC-MS/MS analysis.

II.11.3. HPLC and mass spectrometry

For a single measurement, 5 µl of peptide mixture was injected by an autosampler (LC PAL; CTC Analytics, Zwingen, Switzerland) onto a 15 cm silica microcolumn (inner diameter: 75 µm) packed in-house with ReproSil-Pur C18-AQ 3-µm resin (Dr. Maisch GmbH, Ammerbuch, Germany). Peptides were eluted by an Eksigent NanoLC-1D Plus liquid chromatography system (Eksigent, Dublin, CA, USA) on a 8-59% acetonitrile gradient (200 min) with 0.5% formic acid at a nanoflow rate of 200 nl/min. Eluted peptides were sprayed via an electrospray ion source (Thermo Scientific, Bremen, Germany) into an LTQ-Orbitrap or LTQ-Orbitrap XL hybrid mass spectrometer (Thermo Scientific). Data dependent mode was used for the LTQ-Orbitrap instrument. For one scan cycle, one precusor ion scan was performed in the Orbitrap (m/z range = 300-1,700; R = 60,000; target value = 10^6), followed by five most intense ions selected for fragmentation by collision induced dissociation (target value: 3,000; monoisotopic precursor selection enabled; wideband activation enabled) and MS/MS scans in the LTQ (linear trap quadrupole) part of the machine. Ions were rejected if their charge state was unassigned or if they were singly charged. The dynamic exclusion duration for precursor ions selected for MS/MS scans was set to 60 s.

Whole proteome experiments were mesured on Q Exactive systems (Thermo Scientific). For this purpose, peptide mixtures were separated by reversed phase chromatography using the EASY-nLC system (Thermo Scientific) on in-house manufactured 20 cm fritless silica microcolumns with an inner diameter of 75 µm. Columns were packed with ReproSil-Pur C18-AQ 3 µm resin (Dr. Maisch GmbH). Peptides were separated on a 8-60% acetonitrile gradient (108 min) with 0.5% formic acid at a nanoflow rate of 200 nl/min. Eluting peptides were directly ionized by electrospray ionization and transferred into a Q Exactive mass spectrometer (Thermo Scientific). Mass spectrometry was performed in the data dependent positive mode with one full scan (m/z range = 300-1,700; R = 70,000; target value: 3×10^6; maximum injection time = 120 ms). The 10 most intense ions with a charge state greater than one were selected (R = 35,000, target value = 5×10^5; isolation window = 4 m/z; maximum injection time = 120 ms). Dynamic exclusion for selected precursor ions was set to 30 s (Kelstrup et al., 2012).

II.11.4. Processing of raw LC-mass spectrometry data

The generated raw files from the immunoprecipitation experiments, containing the acquired MS and MS/MS spectra, were processed using the MaxQuant platform version 1.0.13.13 (Cox and Mann, 2008; Cox, et al., 2009). SILAC pairs were assembled from detected isotope patterns, recalibrated and quantified in the Quant module (heavy labels: Lys-8; maximum of 3 labeled amino acids per peptide; maximum peptide charge of 6; top 6 MS/MS peaks per 100 Da; polymer detection enabled). The derived peak lists were searched using the MASCOT search engine (version 2.2, MatrixScience, Boston, MA, USA) against an in-house concatenated target-decoy database (Nesvizhskii and Aebersold, 2005) combining forward and reversed protein sequences from the *Homo sapiens* IPI protein database (release 3.72) and 31 common contaminants. LysC specificity, cleaving peptide bonds at the C-terminal side of lysine residues, was required. Carbamidomethylation of cysteine was used as fixed modification; oxidation of methionine and acetylation of the protein N-terminus were set as variable modifications. A maximum of 2 missed cleavages were allowed, and the mass tolerance for fragment ions was set at 0.5 Da. In the Identify module, the MASCOT-generated results were further filtered. For protein identification, a minimum peptide length of 6 amino acids was required. At least one peptide was required to be a unique peptide in a protein group, and a minimum peptide count required for a protein group was set to one. Maximum false discovery rate was set at 1% for both peptide and protein identifications, estimated based on the reverse hits matched in the target-decoy database. Protein quantification was based on unique peptides and non-unique peptides assigned to the protein group with highest number of peptides (razor peptides). At least one peptide SILAC ratio count was required for quantification of a protein group. Protein tables were finally filtered to eliminate the identifications from the reverse database and common contaminants.

Raw files derived from whole proteome experiments were processed using MaxQuant version 1.2.2.5. Here, MS/MS spectra were searched by the internal Andromeda search engine (Cox et al., 2011a) against the decoy *Homo sapiens* IPI protein database (release 3.84) containing for-

ward and reverse sequences. Additionally the database included 248 common contaminants. MaxQuant analysis included an initial search with a precursor mass tolerance of 20 ppm the results of which were used for mass recalibration (Cox et al., 2011b). In the main Andromeda search precursor mass and fragment mass had an initial mass tolerance of 6 ppm and 20 ppm, respectively. The search included variable modifications of methionine oxidation, N-terminal acetylation and fixed modification of carbamidomethylated cysteine. Minimal peptide length was set to six amino acids and a maximum of two miscleavages was allowed. The false discovery rate (FDR) was set to 0.01 for peptide and protein identifications. In the case of identified peptides that are all shared between two proteins, these are combined and reported as one protein group. Protein quantification was based on unique peptides and non-unique peptides assigned to the protein group with highest number of peptides (razor peptides). At least three peptide SILAC ratio counts were required for quantification of a protein group. Protein tables were finally filtered to eliminate the identifications from the reverse database and common contaminants.

II.12 Genome-wide association studies (GWAS)

All GWAS-related work was conducted by Matthias Heinig (MDC Berlin, Norbert Huebner lab).

II.12.1 Cohort data acquisition

Cohort data was acquired from two large genome wide wide association studies (GWAS) with 753/736 cases/controls (GenADA; Li et al, 2008) and 3,941/7,848 cases/controls (GERAD; Harold et al., 2009).

II.12.2 GWAS data analysis

Genomic coordinates of all genes were obtained from biomart (Ensembl release 54). SNP coordinates (NCBI36 assembly) and association summary statistics of the GenADA study were obtained from dbGAP (accession number phs000219v1). The same data structure for the GERAD study was kindly provided by the authors. For each bait protein SNP sets were defined which comprise all SNPs that are located within a distance of 100 kb of any gene whose protein interacts with the corresponding bait protein. One-sided Wilcoxon-Mann-Whitney test was applied in order to detect differences of the means of the distribution of GWAS P-values within a SNP set compared to the global distribution of P-values. (Heinig et al., 2010). Combined P-values were computed using Fisher's method.

II.13 BIOINFORMATIC ANALYSES

II.13.1 Statistical data analysis

Statistical analysis was done using R statistical environment (version 2.11; Team RDC, 2009) or Prism 5 (GraphPad Software, Inc.).

II.13.2 Construction of protein-protein interaction networks

Interaction data was loaded to Biolayout 3D Express (version 2.0, open source software, The Roslin Institute, University of Edinburgh, UK) and then manipulated using standard settings (Theocharidis et al., 2009).

II.13.3 Cluster analysis of gene ontology (GO) terms

In order to test whether identified PPIs are enriched for certain Gene Ontology (GO) terms, an enrichment analysis was performed using the online DAVID bioninformatics resource (http://david.abcc.ncifcrf.gov/) (Huang et al., 2009). Calculation of over-represented GO terms was done by comparing the entire list of identified PPIs per bait proteins to the background, i.e. all human proteins. Significant count treshold was set at 1 and the EASE score (modified Fisher's exact test probability) cutoff was set to be 1. Terms with a p-value <0.01 were selected, log- and z-transformed, hierarchically clustered and plotted as heatmap using in-house Perl and R scripts.

III Results

III.1 A quantitative proteomic screen for PPIs of neurodegenerative disease proteins

A fundamental challenge in affinity purification-based protein interaction screens is the discrimination of specific from background interactors, as all biochemical purification procedures suffer from the trade-off between sensitivity and specificity. On the one hand, mild purification procedures achieve high sensitivity as they preserve weak protein-protein interactions (PPIs), however, at the same time they give rise to a larger number of unspecific binders. Conversely, more stringent washing conditions can reduce the number of unspecific binders but also result in loss of more transient PPIs (Gingras et al., 2007). In order to circumvent this issue, quantitative affinity purification followed by mass spectrometry (q-AP-MS) was employed (Paul et al., 2011; Vermeulen et al., 2008). The q-AP-MS strategy uses the information of the quantitative labeling technique to compare the abundance of proteins co-purifying with the bait molecule relatively to proteins co-purifying within a control pull-down. In the present thesis, stable isotope labeling with amino acids in cell culture (SILAC) was utilized to differentially label two populations of HEK293TN cells. Heavy-labeled cells were transiently transfected to express a single N-terminal c-myc-tagged fusion protein, while light-labeled control cells were transfected with a corresponding empty vector control (FIG. III.1A). After overexpression of the vector constructs for 24 hours, an immunoprecipitation directed against the c-myc-tag was performed and the eluates from both pull-down conditions were combined in a 1:1 fashion. Finally, the proteins in the combined pull-down eluates were ethanol-precipitated and subjected to LC-MS/MS analysis. Comparison of SILAC ratios obtained from the MS analysis now allowed discrimination of specific from unspecific binders. Specific interaction partners were expected to show an increased abundance in the heavy form while non-specific contaminants should have a 1:1 ratio. To increase the specificity, additional control experiments were carried out with swapped isotope labels (termed ‘crossover’ or ‘reverse’ experiments, in contrast to initial ‘forward’ experiments), in which protein ratios were expected to be inverted. Proteins were considered as specific interaction partners when they were enriched at least twofold on average and showed an inverted ratio in the crossover experiment (FIG. III.2).

As a proof-of-principle, the results from the ataxin-1 pull-downs are discussed in the following. Ataxin-1 is the disease-causing protein for spinocerebellar ataxia type 1 (SCA1), an autosomal dominant NDD caused by expansions of the CAG repeat tract in the corresponding gene sequence, leading to expanded polyglutamine (polyQ) stretches in the protein sequence. Healthy individuals carry up to 39 CAG repeats in the ataxin-1 gene sequence, while expanded tracts with 40 or more CAG repeats irrevocably cause SCA1 (Gatchel and Zoghbi, 2005). Furthermore, the length of the CAG repeat expansion is inversely correlated to the age of disease onset (Zoghbi and Orr, 2000). Ataxin-1 is expressed in various types of neurons but most abun-

dantly in Purkinje cells of the cerebellum. Disease-associated ataxin-1 with extended polyQ tract accumulates in the nucleus and induces neurodegeneration (Kang and Hong, 2009).

First, proteins that specifically co-purify with the wild-type variant of ataxin-1 with a normal polyQ track length (ATXN1-Q30) relatively to the empty vector control were investigated (FIG. III.1B). In total, 968 proteins were identified in the ATXN1-Q30 pull-down experiments; though, most of these proteins had a heavy-to-light (H/L) SILAC ratio around 1 in both the forward and reverse experiments. Thus, these proteins are considered to represent unspecific binders. As an important control, the bait protein ATXN1-Q30 itself was found to have a high H/L ratio in the forward and an inverse ratio in the crossover experiment, indicating an efficient enrichment of the bait protein during the affinity purification process. In addition, 50 proteins were found to specifically co-purify with ATXN1-Q30 in both forward and crossover experiments when compared to the empty vector control. Among these, the transcriptional repressor Capi-

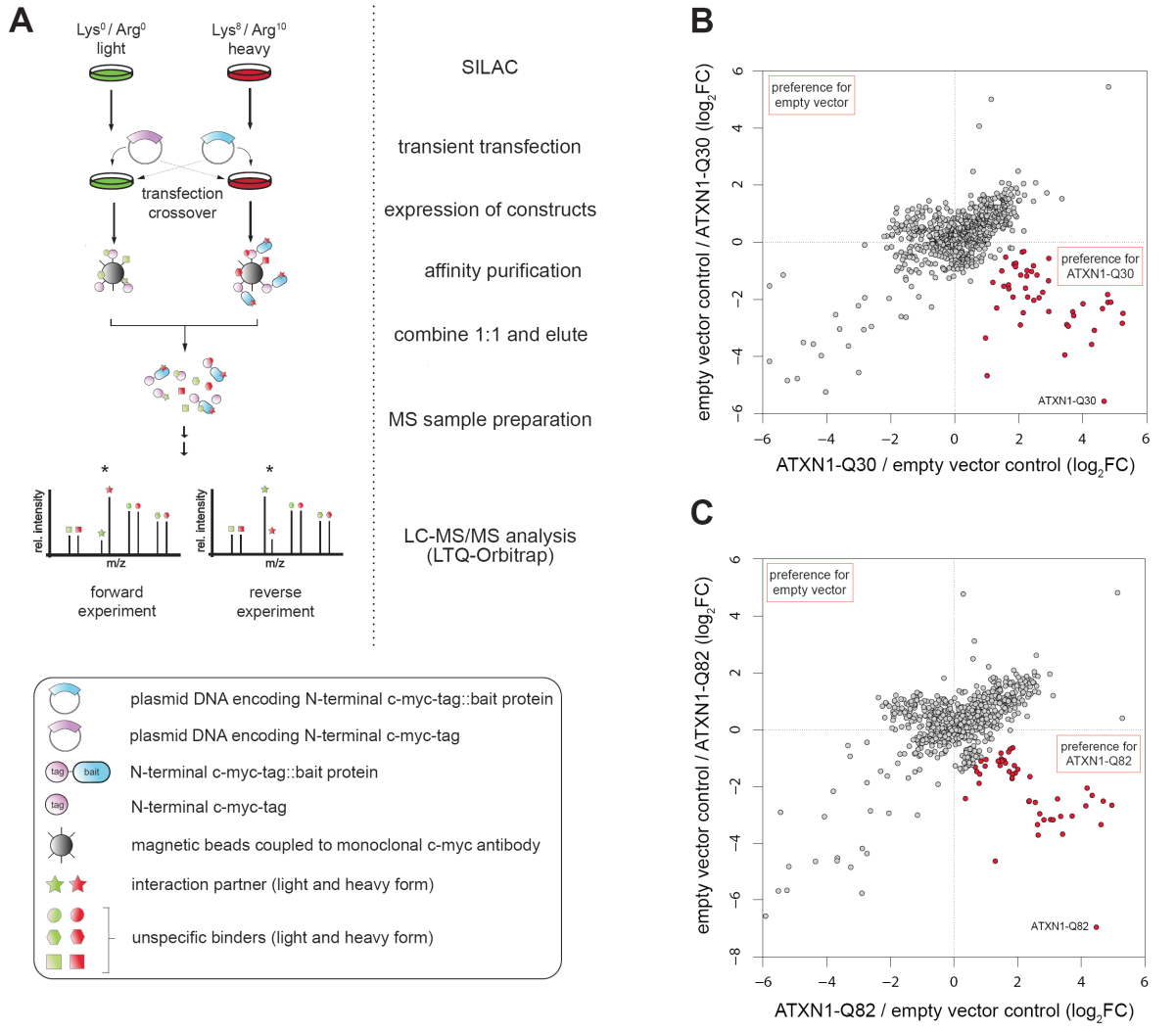

FIG. III.1 | Experimental design for the q-AP-MS screen. (A) Stable istotope-labeled HEK293TN cells are transiently transfected with expression plasmids encoding a bait or control protein with a single c-myc-tag. After protein expression, the tagged constructs are immunoprecipitated and the eluates are combined before subsequent MS sample preparation and LC-MS/MS analysis. Crossover experiments are performed by swapping the transfected plasmid constructs. Specific interaction partners are observed by high heavy-to-light ratios in the forward and low heavy-to-light-ratios in the reverse experiments (highlighted by asterisks), whereas non-specific binders have 1:1 heavy-to-light ratio in both experimental conditions. (B+C) Protein-protein interaction screen for empty vector control pull-down against (B) ATXN1-Q30 (wild-type) and (C) ATXN1-Q82 (mutant), including reverse experiments. Specific interactors of ATXN1-Q30 and ATXN1-Q82, repectively, are marked in red. The position of the bait protein is indicated.

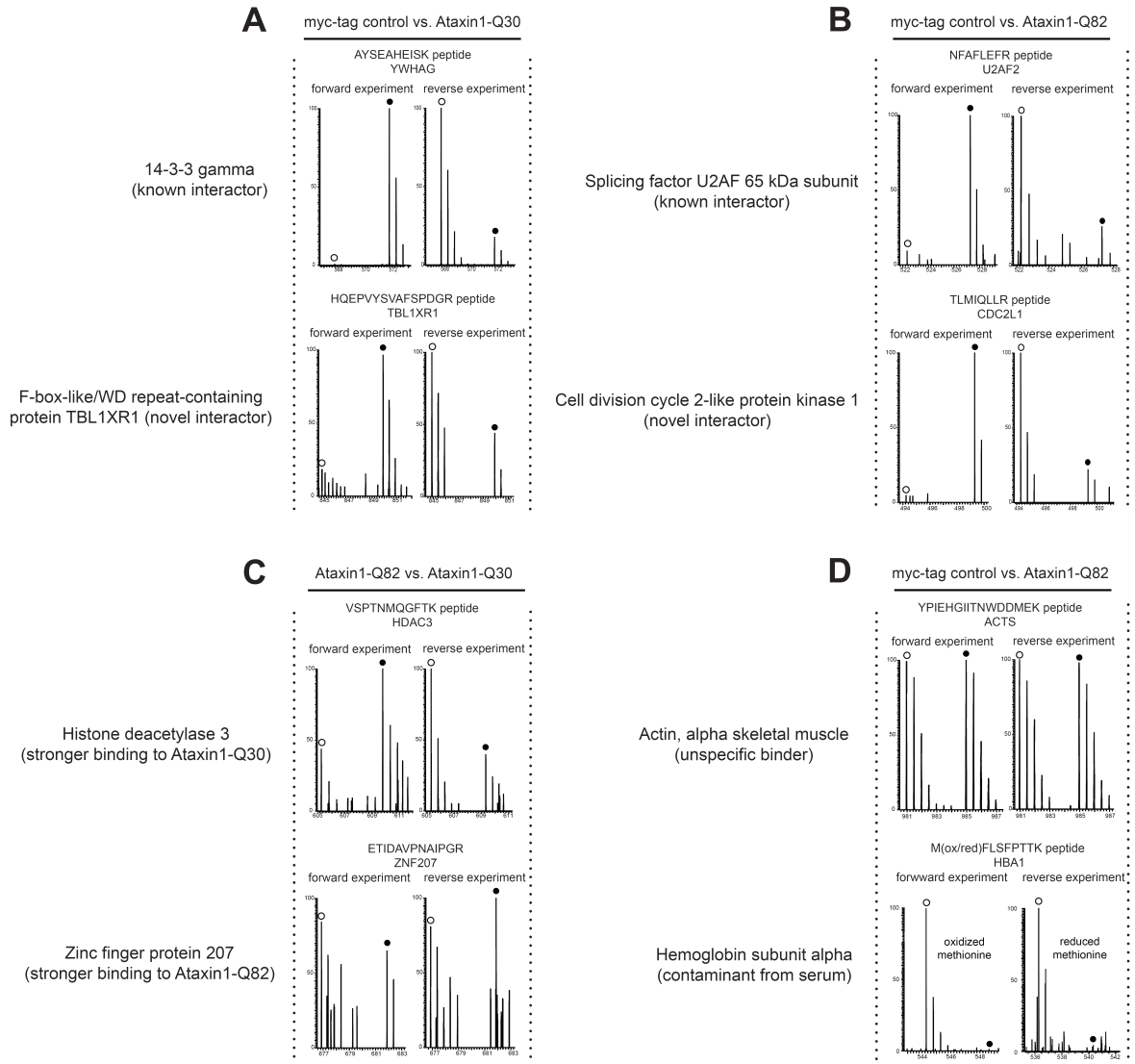

FIG. III.2 | Exemplary MS/MS spectra of identified peptides from the q-AP-MS screen. SILAC pairs of the forward and the corresponding reverse experiment are depicted next to each other. Selected peptides contain one labeled amino acid, resulting in a mass difference of 8 Da (Lysine-8 label) or 10 Da (Arginine-10 label) between the light (white circle) and the corresponding heavy (black circle) peptide peaks. Note that the heavy-to-light ratios swap between forward and reverse experiments, indicating a specific interaction (A-C). Contaminations and unspecific binders do not show a label-swap behavior (D).

(A) Wild-type Ataxin1-Q30 interacts with YWHAG (known interaction) and TBL1XR1 (novel interaction), compared to empty empty-vector control. (B) Disease-associated Ataxin1-Q82 interacts with U2AF2 (known interaction) and CDC2L1 (novel interaction), compared to empty vector control. (C) When both wild-type and mutant Ataxin1 variants are used as baits in an immunoprecipitation experiment, HDAC3 preferentially binds to Ataxin1-Q30, whereas ZNF207 preferentially binds to Ataxin1-Q82. (D) Actin exhibits ~1:1 ratios in both forward and reverse experiments, indicating an unspecific interaction. The unlabeled serum protein hemoglobin shows very low heavy-to-light ratios in both experimental conditions, indicating an non-specific contamination derived from serum.

cua (CIC) was identified as interaction partner of ataxin-1. CIC is known to interact with ataxin-1 in mouse cerebellum to cause SCA1 neuropathology (Lam et al., 2006), which indicates that the q-AP-MS approach can in addition identify functionally relevant *in vivo* interaction partners. Moreover, six 14-3-3 protein isoforms (beta/alpha, gamma, zeta/delta, epsilon, eta and theta) out of seven encoded in the genome, were identified to specifically co-purify with ATXN1-Q30. 14-3-3 proteins are considered to be scaffold proteins vital to many different cellular functions; they are known protein interaction partners of both wild-type and mutant ataxin-1 and play a critical role in mediating the neurotoxicity in SCA1 (Chen et al., 2003). The association of 14-3-3 with ataxin-1 requires the phosphorylation of the ataxin-1 protein on ser-

ine residue 776 by Akt kinase. Indeed, phosphorylation of ATXN1-S776 was identified in the mass spectrometry data (Supplementary FIG. VII.1), indicating that the q-AP-MS approach can identify phosphorylation-dependent protein-protein interactions.

Most of the 50 specific interaction partners have not yet been reported to interact with ataxin-1, however, a large fraction of the interactors is involved in either splicing (CDC2L1, ELAVL1, MBNL1, SF1, U2AF1) or transcriptional regulation (KDM1A, MED27, TBL1XR1, TLE4), which is consistent with the proposed function of ataxin-1 in the nucleus (Klement et al., 1998; Zoghbi and Orr, 2000). Furthermore, other identified interactors were associated with the ubiquitin-proteasome system (PSMA4, PSMB1, SQSTM1, SKP1, SUMO2, UBC), which has been reported as well (Gatchel and Zoghbi, 2005; Zoghbi and Orr, 2000). A yet unanticipated finding was the discovery of several interactors related to mitotic checkpoint control (BUB3, CDC2, CDC2L1, CDK2, GSPT1), suggesting a putative role of ataxin-1 in cell cycle regulation.

When performing the same pull-downs experiments with the polyQ-expanded mutant ataxin-1 protein (FIG. III.1C), 49 specific interactors were identified in total. Remarkably, ~80% of the interactors were shared between the wild-type and the mutant ataxin-1 variants. Interestingly, these results suggest that the expansion of the polyQ tract does not dramatically change the global protein interactome set of ataxin-1. This is consistent with the observation that the polyQ length *per se* does not influence PPIs in the absence of aggregated protein species (Davranche et al., 2011). It is more likely that the polyQ expansion of ATXN1 shifts the quantitative rather than the qualitative balance of certain protein complexes between wild-type and disease-associated variants, thus contributing to SCA1 pathology (Lim et al., 2008; Zoghbi and Orr, 2009).

III.1.1 Global analysis of q-AP-MS target identifications

In order to characterize protein-protein interactions of the most common disease-associated gene products involved in neurodegenerative diseases, six bait proteins involved in four different disorders were selected and q-AP-MS screens as described above were carried out. For each protein both wild-type and disease-associated variants were selected, resulting in 17 different bait candidates (TAB. III.1). Including crossover experiments, 34 pull-downs were performed in total, giving rise to 468 specific protein-protein interactions between 308 unique proteins identifications (Supplementary TAB. VII.1). The generated interaction data was assembled into a combined network and grouped for the four NDDs of interest (FIG. III.3A).

Of note, only two proteins, BAG family molecular chaperone regulator 2 (BAG2) and ubiquitin (UBC), were detected as interaction partners in all four diseases (FIG. III.3B). Eight further proteins, including five proteasomal subunits (PSMA4, PSMA5, PSMA6, PSMB1, PSMD2), two heat shock proteins (HSPA8 and HSPB1) and the ubiquitin ligase SKP1 were identified as interaction partners shared between at least three of the four diseases. These shared interactors are significantly enriched in gene ontology terms protein folding ($p < 0.02$) and regulators of proteolysis ($p < 4.0E-05$, Benjamini-Hochberg correction applied), which is consistent with the current hypothesis that protein misfolding is a common theme in several NDDs and cellular

countermeasures include the UPS and molecular chaperones (Muchowski and Wacker, 2005). However, the vast majority of PPIs were unique for the individual diseases. These results reflect not only the considerable differences between the native cellular functions of the respective disease proteins, but also suggest distinct pathogenic processes in the NDDs under investigation.

TAB III.1 | Bait protein variants utilized for the q-AP-MS screen. Six disease-driving proteins in neurodegeneration, covering the four most common neurodegenerative diseases were selected for the protein-protein interaction screen. For each of the six bait proteins, wild-type and disease-associated sequence variants were selected. Mutant baits are known to trigger the particular disease in either human patients or animal models of disease. In total, 17 different bait variants were utilized for the q-AP-MS screen.

Neurodegenerative disease	Gene	Name	Variant	#
Alzheimer's disease (AD)	APP	Amyloid beta A4 protein (amyloid precursor protein)	wild-type	1
			K670N/M671L	2
			V717I	3
	PSEN1	Presenilin-1	wild-type	4
			A431E	5
Huntington's disease (HD)	Htt506	Huntingtin (N-term 506 aa)	Q23 (wild-type)	6
			Q145 (mutant)	7
	HttEx1	Huntingtin (Exon 1)	Q23 (wild-type)	8
			Q79 (mutant)	9
Parkinson's disease (PD)	PARK2	Parkin	wild-type	10
			Q329Stop	11
	SNCA	Alpha-Synuclein	wild-type	12
			A30P	13
			E46K	14
			A53T	15
Spinocerebellar ataxia type 1 (SCA1)	ATXN1	Ataxin-1	Q30 (wild-type)	16
			Q82 (mutant)	17

III.1.2 Validation of protein-protein identifications

Altogether, the assembled NDD protein interaction network contains several PPIs which have been reported in the literature and possess high biological relevance. In line with the already mentioned ATXN1 interaction partners (cf. III.1), many other known interactions were identified, for instance the binding of huntingtin with VCP (Hirabayashi et al., 2001), association of PSEN1 with the oligosaccharyltransferase complex (Lee et al., 2010) or interaction of SNCA with CSNK2A1 (Okochi et al., 2000). To examine whether identified interactors overall exhibit a similar biological function and subcellular localization as their respective bait proteins, interaction partners of each bait protein were subjected to gene ontology analysis (FIG. III.4). Visualization of enriched biological terms was done using hierarchical clustering. In terms of both localization and function, interaction partners showed enrichment in GO terms as expected for the respective bait proteins. For example, interactors of the nuclear proteins ATXN1 and SNCA showed enrichment for the GO term 'nucleus', interactors of the cytoplasmic proteins HTT and PARK2 were enriched in cytosolic-associated compartments and interactors of the transmem-

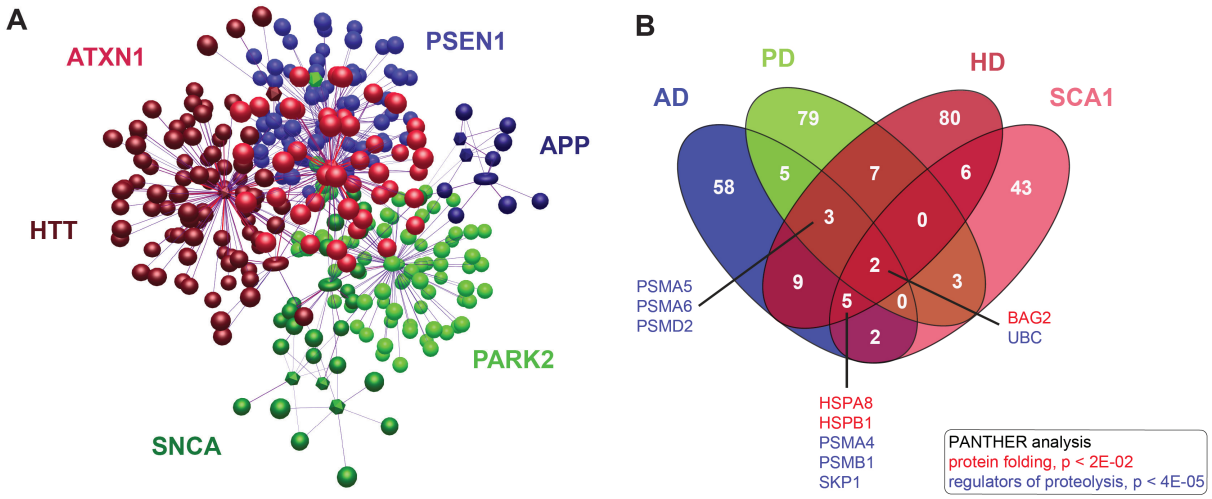

FIG. III.3 | Global properties of the neurodegenerative disease interaction network. (A) A global disease-grouped protein-protein interaction network comprised of 468 interactions in total. Depicted are preys (spheres), wild-type baits (donuts) and mutant baits (dodecahedrons). Red: polyQ diseases; green: Parkinson's disease; blue: Alzheimer's disease. Edges are weighted according to the ratios observed in the SILAC pull-down. (B) A Venn diagram highlights unique and shared interactions between the bait proteins associated with different neurodegenerative diseases. Interactors which are shared between at least three diseases are indicated by name. PANTHER analysis of these ten proteins reveals significant enrichment for either protein folding (red) or regulators of proteolysis (blue).

brane proteins APP and PSEN1 showed enrichment for 'endoplasmatic reticulum'-related GO terms. Similarly, GO analysis of biological processes revealed that interactors share congeneric functional terms with their respected bait proteins. For instance, ATXN1-interactors are enriched in 'mRNA metabolic processes' or 'regulation of gene expression', which is consistent with the supposed function of ATXN1 in splicing and transcriptional regulation (de Chiara et al., 2009; Tsai et al., 2004). Other well-known examples are reflected by the enrichment for HTT interactors in vesicular trafficking (Harjes and Wanker, 2003) or the enrichment of PSEN1 interactors in 'proteolysis' and '*N*-glycosylation' (Lee et al., 2010; Selkoe and Wolfe, 2007). These results indicate that captured PPIs seem to reflect endogenous interactions taking place in the native cellular environments of the distinct bait proteins. To assess the overlap of the identified PPI to already published interactions systematically, the q-AP-MS interactors were mapped to HIPPIE, an integrated human PPI database with experiment-based quality scores

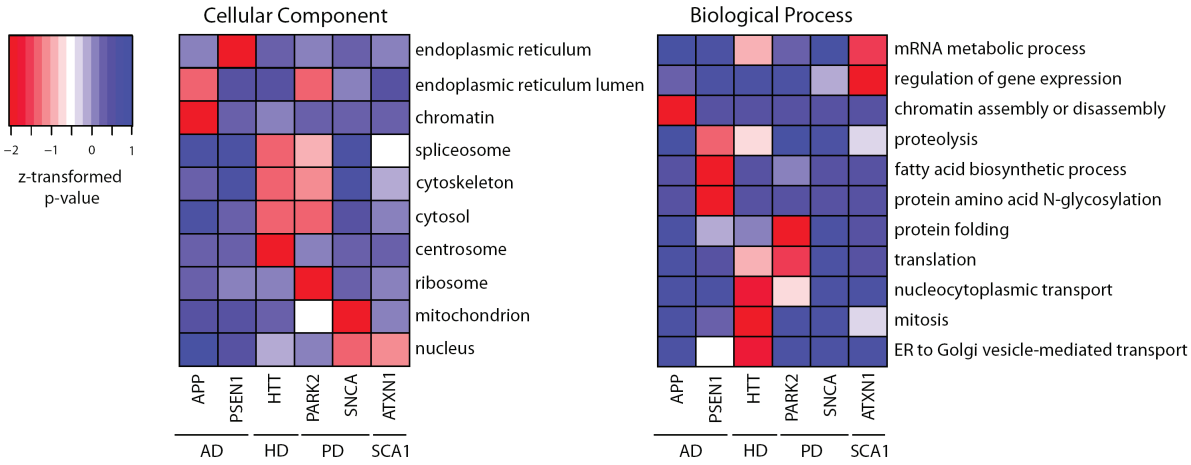

FIG. III.4 | Functional characteristics of selected q-AP-MS targets. Identified interactors were grouped according to the respective bait protein. Visualization of enriched biological terms for the identified interactors was done using hierarchical clustering of z-transformed p-values of significantly ($p < 0.01$) over-represented GO terms (only *Biological Process* and *Cellular Component* apply). Bait proteins are additionally clustered by disease.

(Schaefer et al., 2012). The PPI comparison resulted in a small but highly significant intersection for the ATXN1, HTT, PARK2 and SNCA interactor sets (TAB. III.2). No significant overlap was observed for the two transmembrane proteins APP and PSEN1, although their q-AP-MS interactors are significantly enriched for membrane- and transmembrane-localized proteins, which is consistent with their subcellular localization (FIG. III.4). However, the utilized q-AP-MS screen failed to detect several known interactions, as for instance binding of ATXN1 to RBM17 (Lim et al., 2008) or the association of PSEN1 with APP and other components of the gamma secretase complex (Xia et al., 1997). Missed PPI identification may be due to several reasons, which will be discussed in detail later on (cf. IV).

TAB III.2 | Comparison of identified q-AP-MS targets with HIPPIE. Numbers of interactors of each bait protein are indicated for the HIPPIE repository (Human Integrated Protein-Protein Interaction rEference; Schaefer et al., 2012) and identified q-AP-MS hits from the present thesis. P-values have been assesseed via hypergeometric testing against the estimated number of human protein-coding genes (22,000).

bait protein	HIPPIE	Hosp et al.	overlap	p-value
ATXN1	182	61	8	< 1.0E-08
HTT	328	112	13	< 2.0E-09
PARK2	89	80	3	< 3.0E-03
SNCA	76	24	3	< 5.0E-05
APP	161	9	1	< 0.06
PSEN1	82	75	1	< 0.20

In order to test the reliability of yet unreported interactions identified by q-AP-MS, alternative methods were employed to validate them. At first, co-immunoprecipitation (coIP) of selected novel q-AP-MS hits was performed with myc-tagged bait proteins transiently transfected in HEK293TN cells. Indeed, in 22 out of 22 cases the Western blotting data confirmed the mass spectrometry results (FIG. III.5A). Since tagging and overexpression of the bait protein may alter its interaction behavior, coIP-experiments were additionally performed against the endogenous bait proteins. For these experiments, the neuronal cell line SH-SY5Y was used to more closely resemble the neuronal environment of NDDs. Again, in 8 out of 8 cases the interaction could be validated (FIG. III.5B). Of note, only wild-type interactions could be investigated by coIP in SH-SY5Y cells as detection of disease-associated variant interactions would require stable or transient transfection of the mutant gene product, then again at the cost of expression-mediated adverse effects. Collectively, the conducted validation experiments indicate that the q-AP-MS screening approach can detect PPIs with high specificity.

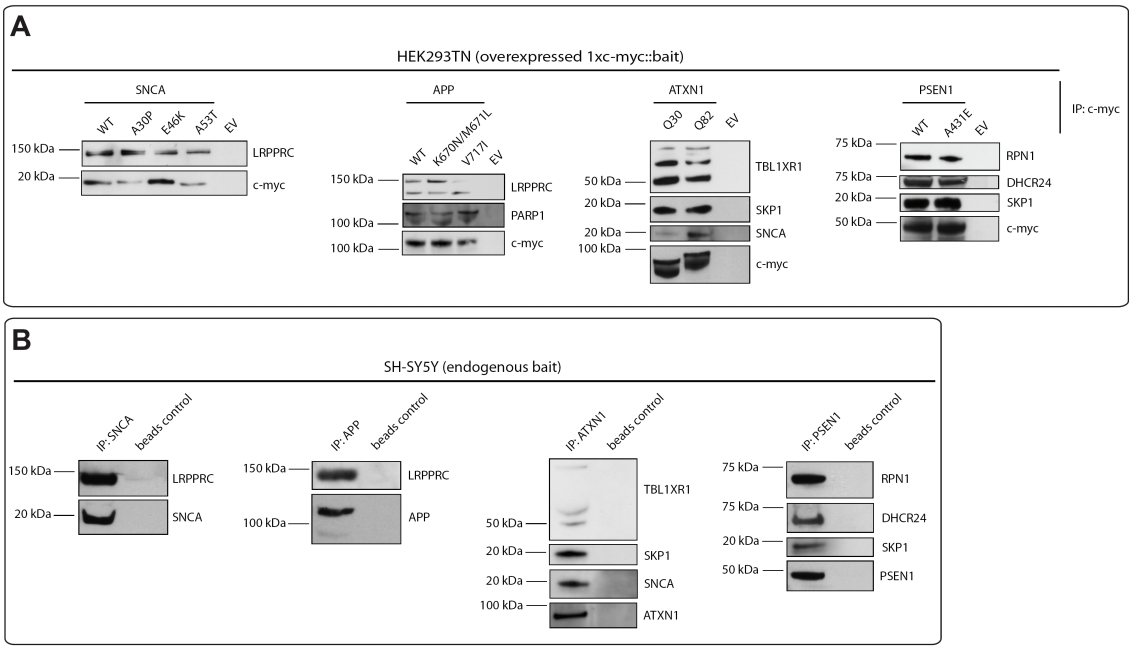

FIG. III.5 | Validation of protein-protein interactions obtained from the q-AP-MS screen. Validation of selected q-AP-MS identifications by co-immunoprecipitation. (A) Co-IPs of overexpressed c-myc-tagged bait proteins from HEK293TN cells. (B) Co-IPs of endogenous bait proteins from SH-SY5Y neuroblastoma cells.

III.1.3 Assessment of bait protein overexpression off-target effects

It is well known that overexpression of a protein in cellular systems can alter the subcellular localization of the protein of interest and can cause changes in the cell's expression profile. In the present thesis, the q-AP-MS screening approach utilizes expression constructs with a human cytomegalovirus (CMV) promoter, which gets cross-activated via the Simian virus 40 large T-antigen stably transformed in HEK293TN cells (Soneoka et al., 1995). This causes a strong overexpression of the gene under control of the cross-activated CMV promoter, which in turn might cause changes in protein levels. Disturbed protein levels might in the end lead to erroneous identification of protein interactors in the present screening approach.

Therefore, it was reasoned to perform additional validation experiments in order to check for potential side effects driven by the overexpression of the bait proteins in HEK293TN cells. For instance, known cellular countermeasures to overexpression of proteins include increased production of heat-shock proteins (HSPs) and chaprones. To get a more thorough overview on HSPs and chaperone binding as a function of bait protein overexpression, all specific interactors of the q-AP-MS screen related to protein folding were clustered against all bait variants (FIG. III.5A). As evident from the heatmap analysis, not a single HSP or chaperone was found to bind to all bait proteins, suggesting no general cellular countermeasure towards the utilized tagged proteins. In fact, the distribution of HSPs and chaperones was quite diverse. While APP and SNCA variants exhibited only very few binders, PARK2-WT and Htt506-Q145 bound many different HSPs and chaperones. This is probably due to the extreme aggregation propensity of Htt506-145 even after 24 hours of expression and the native role of PARK2 as E3-ubiquitin ligase, which binds to many misfolded proteins or targets set to degradation.

Yet, an even more important question to assess is whether the overexpression of the bait proteins might alter the global expression profile of the cell. For instance, upregulation of a transcription factor might change the abundance of certain proteins. Also, the expression of a disease-causing gene product can cause cellular disturbances leading to disturbed PPI formation when compared to cells expressing the wild-type variant of a bait protein. In order to detect

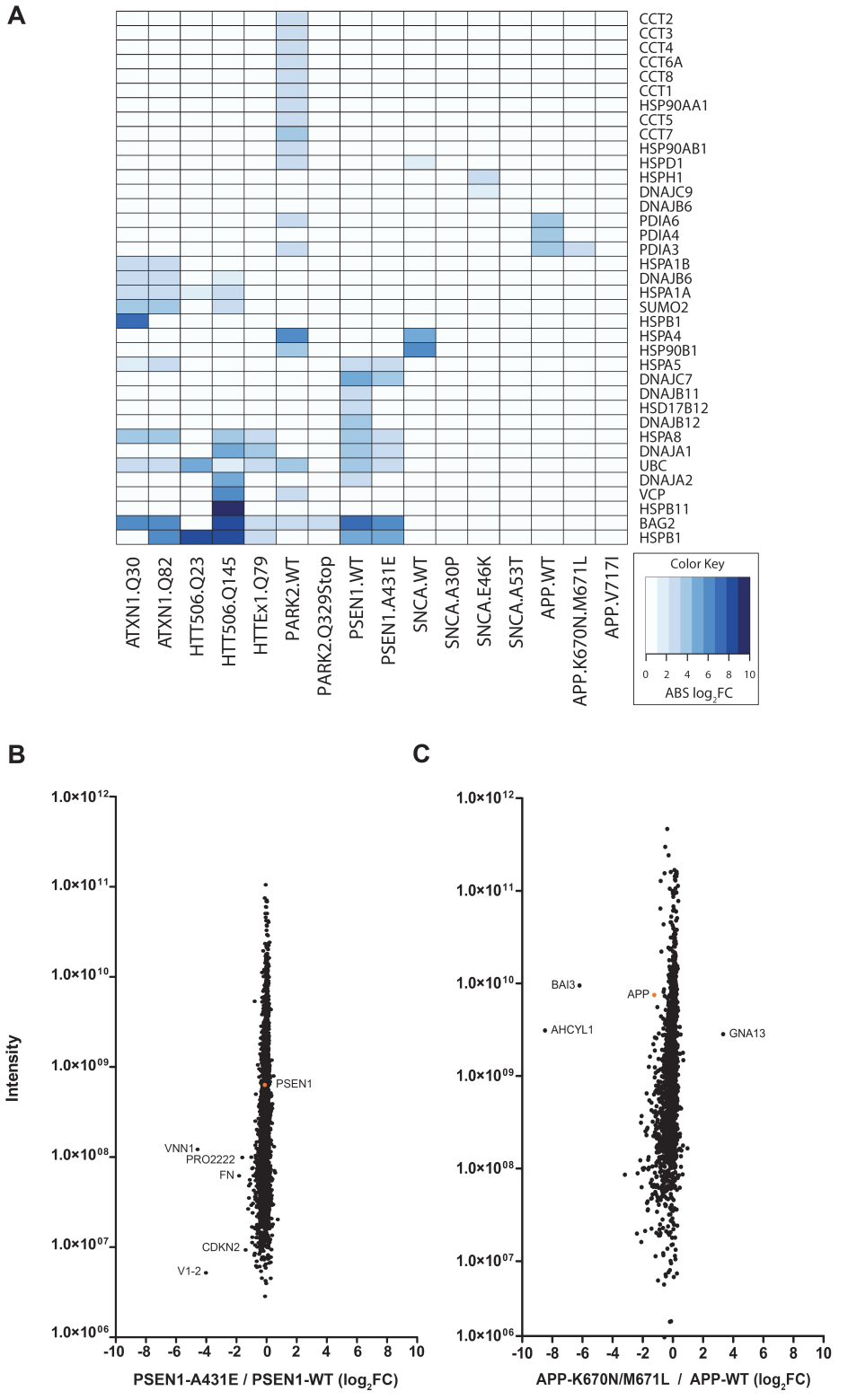

FIG. III.6 | Investigation of potential overexpression off-target effects. (A) Heatmap representation of all identified interactors related to protein folding or regulators of proteolysis across the different bait proteins. (B+C) Global proteome analysis of expression changes between wild-type and disease-associated variants after 24 hrs of bait protein overexpression. No apparent changes can be observed for the two Alzheimer's disease-associated bait proteins PSEN1 and APP.

quantitative changes in the proteome upon expression of the bait candidates, HEK293TN cells were labeled by stable-isotopes and transiently transfected with the respective expression constructs for 24 hours. After harvesting, the two SILAC conditions were combined 1:1 and then subjected to LC-MS/MS analysis. Results from the wild-type versus mutant comparison of the Alzheimer's disease causing proteins APP and PSEN1 are shown (FIG. III.6B and C). After 24 hours of overexpression of the two respective variants, the proteome showed almost no differences between the two conditions, indicating that harvesting cells after 24 hours is a good point of time to minimize off-target effects driven by the overexpression setup. Thus, the overexpression of all bait variants utilized for the q-AP-MS screen was done for 24 hours. In summary, these data indicate that off-target effects driven by the overexpression of the bait proteins do not seem to cause strong cellular responses which would directly interfere with the identification of interactors in the employed screening approach.

III.2 Determination of disease-modifying effects *in vivo*

Validation of identified PPIs is crucial to highlight the specificity of the employed PPI screening method i.e. investigation of false-positive identifications. However, even true PPIs do not necessarily have to be involved in the actual progression of the disease, as they can simply reflect basic cellular functions of the bait protein without any relevance to the disorder. In order to characterize the potential impact of individual PPIs on the pathogenesis of NDDs, selected PPIs were investigated for their possible disease-modifying behavior. Since this requires *in vivo*-derived data, only a subset of the identified q-AP-MS hits could be further examined. In the following, ATXN1-interactors were analyzed via an RNAi approach in *D. melanogaster* and Alzheimer-associated interactions (APP- and PSEN1-interactors) were assessed for their role in Alzheimer's disease by comparing the data with genome-wide association studies (GWAS).

III.2.1 RNAi in a *Drosophila* neurotoxicity model of ATXN1-Q82

The fruit fly *Drosophila melanogaster* has proven to be a valuable model system for neurodegenerative disease research (Bilen and Bonini, 2007; Fernandez-Funez et al., 2000; Kaltenbach et al., 2007; Kazemi-Esfarjani and Benzer, 2000). *Drosophila* compound eyes are made up of about 750 single ommatida, each with eight photoreceptor cells. Perturbations of compound eye developmental pathways or neuronal dysfunction can disturb this highly ordered neuronal structure leading to a so-called rough eye phenotype (REP). REP is accompanied by strong loss of pigmentation and disturbed surface texture. Consequential, expression of neurodegeneration-related proteins under an eye-specific promoter can induce a REP. As the severity of the REP is directly correlated to the loss of underlying photoreceptor neurons and the compound eye is moreover easily accessible by light microscopy, REP determination serves as a good readout to assess the impact of toxic proteins on neurodegeneration *in vivo*. In order to test whether the identified ATXN1 interactors are enriched in modifiers of ATXN1-mediated neurodegeneration *in vivo*, transgenic flies expressing the human ATXN1-Q82 under the eye-

specific *glass* multiple reporter (GMR) within the UAS/GAL4 expression system were utilized (Brand and Perrimon, 1993; Fernandez-Funez et al., 2000). These neurodegeneration model flies exhibit a characteristic REP in comparison to wild-type flies or flies expressing a GMR-driven control protein (FIG. III.7A-C). Subsequently, GMR_ATXN1-Q82 model flies were crossbred with knock-down strains available from the Vienna Drosophila RNAi Center (VDRC). The VDRC RNAi fly strains have been generated by random integration of shRNA-transcribing inverted repeats under the UAS/GAL4 control into the *Drosophila* genome (UAS-shRNA).

Of 61 identified human ATXN1 interaction partners in the q-AP-MS screen, 21 had orthologs in the fly and 20 of those were available as shRNA strains from the VDRC. To exclude off-target effects induced by the shRNA *per se*, all of the VDRC strains were first crossbred with wild-type flies under control of the same eye-specific promoter (GMR-GAL4 driver line). Three of 20 strains exhibited strong changes in the eye morphology in the F1 generation (human/fly gene name: HSPA5/Hsc70-3, PSMA5/Prosalpha5 and PSMB1/Pros26; Supplementary TAB. VII.3), indicating that knock-down of these three genes apparently has detrimental effects on photoreceptor integrity apart from overexpression of the toxic ATXN1-Q82 transgene. Consequently, these three strains were excluded in the subsequent modifier screen. The remaining 17 knock-down strains were then crossbred with the GMR_ATXN1-Q82 flies. As a result, the F1 generation expressed the human ATXN1-Q82 transgene and the respective shRNA. Out of all lines investigated, 6 lines did not show any overt change in ATXN1-Q82-induced REP and were therefore not considered as disease modifying candidates. 11 shRNA-lines did show an apparent change, as either suppression or enhancement of REP was observed. Visible REP changes included occasionally appearing necrotic spots (purple, FIG. III.7E and F), manifesting the degeneration of underlying photoreceptor neurons. Observed disease-modifying effects were classified into three categories (cf. II.4. 'Evaluation of REP modification'), whereas only strong events (++, +++, --, ---) were considered as specific modifiers. In case ATXN1-Q82 expression in combination with gene silencing yielded no viable offspring, this effect was considered as a lethal enhancement (FIG. III.7G). In total, 11 out of 17 shRNA lines (65%) showed a strong REP

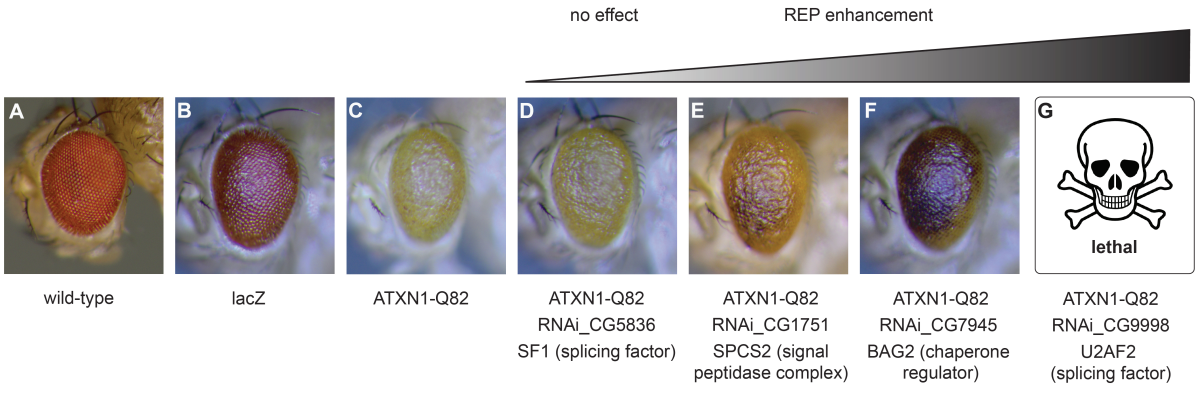

FIG. III.7 | RNAi in a *Drosophila* neurotoxicity model of SCA1. Wild-type (A) and lacZ expressing (B) flies are shown as controls. (C) Expression of ATXN1-Q82 in the fly compound eye induces neurodegeneration (rough eye phenotype, REP). Selected images of ATXN1-Q82 flies crossed with RNAi strains of identified q-AP-MS targets (D-G; purple spots are necrotic lesions). 11/17 (~65 %) tested targets show strong enhancement of the REP (e.g. state F or G; $p < 1.3E-15$), indicating that identified interaction partners are strongly enriched for REP modifiers. Additional control knockdowns of targets in *Drosophila* models of Tau did not induce an apparent change in the Tau REP. RNAi of targets in wild-type fly eyes only also did not show any apparent phenotype.

enhancement (either ++ or +++), suggesting that the identified ATXN1 interactors are significantly enriched (P < 1.3E-15) in modifiers of ATXN1-mediated neurodegeneration *in vivo*. This hit rate of 65% is much higher than in previously conducted forward genetic screens for modifiers of SCA1 in exactly the same fly model strain, ranging from 1-2% (Branco et al., 2008; Fernandez-Funez et al., 2000). Of note, no modifier exhibiting a strong suppression of the REP was observed.

To test whether the observed disease-modifying effects are specific, all shRNA lines were additionally tested in a *Drosophila* model expressing the human Tau protein (GMR_Tau[R406W] line), which is implicated in the progression of other proteopahties such as Alzheimer's and Parkinson's disease. Flies overexpressing the human Tau protein show a very similar REP (Chatterjee et al., 2009). None of the tested shRNA strains did show a strong REP change in the Tau model with the exception of the three strains that already showed an effect in the GMR control screen (Supplementary TAB. VII.3). This indicates that the observed REP-modifiers are specific for ATXN1-Q82-mediated toxic effects but not for effects driven by another neurotoxic protein Tau. Intriguingly, respective knock-down of the two proteins SF1/SF1 and U2AF2/U2af50 (FIG. III.7D and G) results in completely different ATXN1-Q82-induced REP changes, although both proteins bind together in a multi-protein complex involved in pre-mRNA splicing (Abovich and Rosbash, 1997), suggesting that members of the same macromolecular assembly can have a yet strikingly different impact on ATXN1-Q82-mediated pathogenesis in *Drosophila*.

III.2.1 Mapping of PPI data to Alzheimer-specific GWAS

The international HapMap project (The International HapMap Consortium, 2005) resulted in the identification of millions of single nucleotide polymorphisms (SNPs), constituting the most common DNA sequence variation within the human genome linked to disease phenotypes (Gandhi and Wood, 2010). Genome-wide association studies (GWAS) utilize SNP information from selected patients compared to healthy individuals to examine disease association across the entire human genome. Up to now, GWAS have defined several hundreds of genomic regions containing allelic variations predisposing to a multitude of mendelian diseases (McCarthy et al., 2008).

Proteins involved in specific diseases have been reported to frequently interact with each other. Consequently, the combination of protein interaction data with GWAS-derived datasets is a powerful approach to decipher signaling networks related to complex disease phenotypes (Lage et al., 2007, Lim et al., 2006; Rossin et al., 2011). In order to elucidate the role of identified interaction partners of the AD-associated bait proteins APP and PSEN1 in the etiology of Alzheimer's disease, datasets from two independent large genome wide association studies (GWAS) were analyzed. The GWAS data comprised the GenADA set with 753/736 cases controls (Li et al., 2008) and the GERAD set with 3,941/7,848 cases/controls (Harold et al., 2009). First, SNPs of each interaction partner derived from all APP and PSEN1 variants were assembled into SNP sets. Next, it was assessed whether these SNP sets are more likely to be associated in the GWAS than random sets of SNPs (cf. II.13.2 for more details). All SNP sets defined by

the APP disease-associated variants were significantly enriched in both the GenADA and the GERAD studies, while the APP wild-type SNP set was only enriched in the larger GERAD cohort (TAB. III.3). Of the PSEN1 SNP sets, only the A431E-variant SNP set was significantly enriched in the GenADA cohort. However, the combined analysis of both datasets showed a significant enrichment for all APP-defined SNP sets and for interactors of PSEN1-A431E. These findings indicate that SNPs in genes encoding identified interaction partners of APP are significantly more likely to be associated with Alzheimer's disease and suggest that interaction partners of PSEN1-A431E might also be involved in the pathogenesis of AD.

TAB III.3 | GWAS SNP enrichment in two Alzheimer's disease cohorts. Identified q-AP-MS targets of AD were mapped to two independent GWAS datasets for AD (GenADA and GERAD cohorts). SNPs in proximity to interaction partners of APP were more likely to be associated in the GWAS than random sets of SNPs. PSEN1 interactors showed enrichment in only one study, however the combined analysis suggests that interaction partners of PSEN1-A431E are also involved in the pathogenic process.

		GenADA cohort		GERAD cohort		combined
Bait	**Interactors**	**SNPs**	**p-value**	**SNPs**	**p-value**	**p-value**
APP-K670N/M671L	6	121	< 1.3E-03	159	< 5.9E-03	< 1.0E-04
APP-V717I	4	101	< 7.1E-05	120	< 8.1E-05	< 1.2E-07
APP-WT	9	230	< 0.1044	282	< 8.0E-04	< 8.9E-04
PSEN1-A431E	41	1030	< 1.4E-03	1283	< 0.1344	< 1.8E-03
PSEN1-WT	63	1464	< 0.3475	1896	< 0.2073	< 0.2615

III.3 Determination of differential protein-protein interactions

So far, the presented PPI data derived from the q-AP-MS sets was accomplished by performing pull-down experiments of either wild-type or disease-associated variants against an empty vector control. This particular approach is of help to identify PPIs of each individual bait protein alone. However, it is possible that interaction partners, although binding to both wild-type and disease-associated variants, might prefer one over the other. Simply comparing the lists of identified interaction partners derived from individual pull-down experiments cannot identify such differential interaction partners. In addition, potential binders can escape detection in individual q-AP-MS experiments, which is in particular true for low abundant proteins or low-affinity binders. Thus, specific interaction partners identified only for the wild-type bait protein might in fact also bind to mutant bait proteins or vice versa.

To circumvent these limitations and to directly identify interactors with a differential binding behavior, it was sought to directly compare interaction partners of wild-type and disease-associated variant bait proteins in the very same pull-down experiment by q-AP-MS, thus allowing for relative quantification of binding proteins. This approach therefore enables the exploration of interactions that are affected by distinct disease-associated mutations. To this end, the same q-AP-MS approach as in FIG. III.1A was employed, with the exception that HEK293TN cells were transiently transfected with either wild-type or disease-associated variants instead of empty vector controls. Identified proteins were considered as differential interactors when

they were enriched at least by a factor of 1 on average and showed an inverted ratio in the corresponding crossover experiment. As an additional prerequisite, classification of differential interactors was restricted to proteins that were identified in the empty vector control pull-down experiments to exclude false-positive identifications. In total, 107 differential interactors were identified for all 17 bait variants. For example, ten proteins interacted preferentially with wild-type ATXN1-Q30, whereas one protein preferentially bound the disease-associated variant ATXN1-Q82 (FIG. III.8A). In contrast, 37 identified interactors did not show any binding preference towards either wild-type or mutant ATXN1 in the differential q-AP-MS experiment.

Several already known differential interactors were correctly identified in the differential q-AP-MS approach. For instance, when compared to a recent proteomic analysis of differential huntingtin interactors from mouse brain (Culver et al., 2012), 11 out of 68 Htt506-Q145 binders were correctly identified as differential interactors for mutant Huntingtin (FIG. III.8B). Contrariwise, 6 out of 68 Htt506-Q145 binders from the q-AP-MS screen were identified as preferential

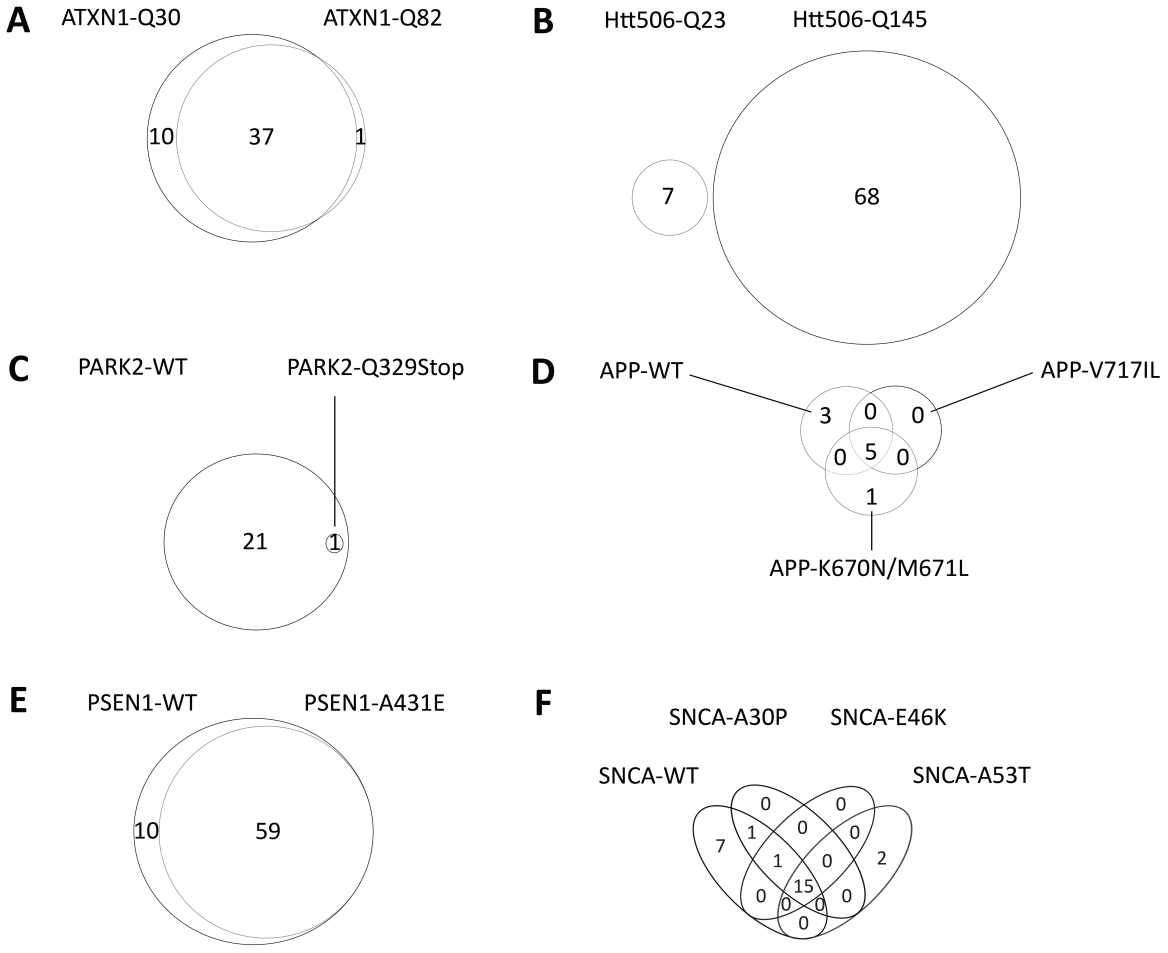

FIG. III.8 | Differential PPIs obtained from q-AP-MS screen. Behavior of of differential protein-protein interactions for (A) Ataxin1-Q30 (wild-type) vs. Ataxin1-Q82 (mutant), (B) Huntingtin506-Q23 (wild-type) vs. Huntingtin506-Q145 (mutant), (C) Parkin (wild-type) vs. Parkin-Q329Stop (mutant), (D) Amyloid Precursor Protein (wild-type) vs. APP-K670N/M671L (Swedish mutation) vs. APP-V717I (London mutation), (E) Presenilin1 (wild-type) vs. Presenilin1-A431E (mutant), (F) Alpha-Synuclein (wild-type) vs. three mutants A30P, E46K and A53T, respectively. Determination of differential PPIs has been restricted to up-front identified PPIs of the respective bait variants compared to empty vector control experiments.

interactors of wild-type huntingtin. It has to be noted that huntingtin constructs of different composition were used in the present thesis and the study from Culver and coworkers, which might have an influence on the PPI formation. Furthermore, the association of CIC towards the wild-type form ATXN1 was correctly identified as preferential binder of wild-type ataxin-1 (FIG. III.8A), reflecting an interaction which is considered to be crucial for neurotoxic effects in the cerebellum of SCA1 mice (Lim et al., 2008).

In order to gain novel insights into mechanistic details of yet unreported differential interactions contributing to disease pathogenesis, functional follow-up experiments were conducted for two selected differential interactors. First, the differential association of the oligosaccharyltransferase (OST) complex towards PSEN1 wild-type was investigated. Second, the preferential binding of LRPPRC towards the APP Swedish mutation was examined in more detail. Both follow-up directions led to distinct findings, suggesting impairments in *N*-glycosylation and mitochondrial function in early-onset Alzheimer's disease and are thus discussed in the following.

III.4 PSEN1 is a mediator of *N*-glycosylation changes in early-onset Alzheimer's disease

Presenilin-1 (PSEN1) is a transmembrane protein and the catalytic subunit of the γ-secretase complex, which is responsible for the proteolytic processing of several important integral membrane proteins such as Notch or APP (Selkoe and Wolfe, 2007). Wild-type PSEN1 has been shown to interact with the translocon subunit Sec61α and the catalytic subunit STT3B of the oligosaccharyltransferase (OST) complex, supporting a mechanism in which newly synthesized polypeptides translocated into the ER are amenable to spatially coordinated posttranslational processing by PSEN1 and *N*-glycosylation by the OST (Lee et al., 2010). Lee and co-workers provided evidence that PSEN1 is involved in *N*-glycan transfer, in particular for the v-ATPase V0a1. Furthermore, they demonstrated that both murine PSEN1 knock-out blastocysts and fibroblast derived from human Alzheimer's disease patients with familial AD mutations in PSEN1 display a similar loss of lysosomal function. The observed autophagosome defect is mediated by inadequate lysosome acidification resulting from the failed *N*-glycosylation of V0a1 in the ER and subsequent PSEN1-dependent faulty trafficking of the v-ATPase (Lee et al., 2010). Consistent with the published interaction of PSEN1 with the OST complex, the q-AP-MS approach identified four out of seven human OST subunits as specific interactors of wild-type PSEN1, including the catalytic subunit STT3A and both regulatory subunits RPN1 and RPN2 (Supplementary TAB. VII.1). Two additional OST subunits (STT3B and OSTC) showed a similar preference for binding to PSEN1-WT but did not reach enough peptide quantification events in both forward and reverse q-AP-MS experiments to pass the applied specificity cutoff. Interestingly, q-AP-MS data derived from the direct comparison of PSEN1-WT versus the AD-associated PSEN1-A431E mutation showed a preferential binding of the OST members towards the wild-type form of PSEN1 (Supplementary TAB. VII.2). These results suggest that the PSEN1-A431E mutation affects the binding to the OST complex and might thus disturb the spatially coordinated process-

ing of nascent polypeptides in the ER by both PSEN1 and the OST complex. Consequently, PSEN1-A431E might have additional detrimental effects on global OST-mediated *N*-glycosylation, besides the already known modulation of γ-secretase activity (Portelius et al., 2010).

III.4.1 PSEN1-A431E changes global *N*-glycosylation pattern in HEK293T cells

In light of the preferential binding of the OST complex towards wild-type PSEN1 and reported observations implying a role of wild-type PSEN1 in both *N*- and *O*-glycosylation of target proteins (Lee et al., 2010; Leem et al., 2002; Nyabi et al., 2003), a more thorough and global analysis of PSEN1-dependent effects on OST-mediated *N*-glycosylation was conducted. Therefore, HEK293TN cells were labeled by a triple SILAC approach and transiently transfected either with an empty vector control, PSEN1-WT or PSEN1-A431E (FIG. III.9A). As an additional control, the selective *N*-glycosylation inhibitor tunicamycin was added in a second experiment to specifically determine OST-mediated *N*-glycosylation effects. After overexpression of the vector constructs for 24 hours, a Concanavalin A (ConA)-pull-down was performed to selectively enrich *N*-glycosylated proteins. ConA is a lectin specifically binding to α-D-glucosyl and α-D-mannosyl residues of glycoproteins. The OST recognizes the tetradecasaccharide $Glc_3Man_9GlcNAc_2$ (three glucose, nine mannose and two *N*-acetylglucosamine residues coupled to an dolichol-pyrophosphate anchor) with high specificity and transfers this complete oligosaccharide to an asparagine residue of an acceptor polypeptide with the appropriate sequon motif N-X-S/T (Mohorko et al., 2011). Consequently, a ConA pull-down should selectively enrich glycoproteins derived by OST-mediated glycosylation. Pull-down experiments were performed for all three SILAC states independently and eluates were combined afterwards in a 1:1:1 fashion and subjected to LC-MS/MS analysis. As PSEN1-WT constructs were transfected in the medium-heavy SILAC state in both experimental setups (FIG. III.9A), the medium-heavy condition served as an internal standard enabling comparison of all tested conditions across both experiments.

FIG. III.9B depicts the relation of fold-changes in protein abundance between tunicamycin-treated versus -untreated cells and PSEN1-WT versus PSEN1-A431E overexpression for approximately 1,500 proteins. Proteins in quadrant III are expected to be hypoglycosylated upon PSEN1-A431E expression and sensitive to the tunicamycin treatment, thus are likely targets of OST-mediated *N*-glycosylation.

To determine whether identified proteins in the ConA pull-down were enriched for Alzheimer-associated proteins, the ConA dataset was additionally mapped to the AlzGene database, which represents the largest collection of putative AD risk factors (Bertram et al., 2007). Although AlzGene entries were found across the whole scatter plot distribution, they were significantly enriched (p-value < 1.0E-07) for hypoglycosylated proteins in quadrant III. Even more, quadrant III contains several high-ranking AlzGene entries such as APP itself, CLPTM1, SORT1 or A2M, suggesting that changes in OST-mediated *N*-glycosylation upon PSEN1-A431E overexpression particularly affect AD-related risk factors.

In an attempt to validate the quantitative ConA pull-down data, selected proteins were examined by additional Western blotting (FIG. III.9C). As apparent from the blotting, the SORLA protein was detected with several bands in mock-treated and PSEN1-WT overexpressing cells, while the highest molecular weight band represents the fully glycosylated SORLA. Tunicamycin treatment results in disappearance of the fully glycosylated SORLA band. Overexpression of PSEN1-A431E leads to a similar expression profile of SORLA where the fully glycosylated form is absent as well. Additional treatment of cell lysates with PNGase F, a glycosidase that specifically cleaves off all asparagine-linked *N*-glycans, causes disappearance of the fully glycosylated SORLA isoforms in mock and PSEN1-overexpressing cells as well, indicating that the highest molecular weight band indeed represents the fully glycosylated isoform of SORLA. A similar behavior can be seen upon detection of the APP protein, however, the visible band shift be-

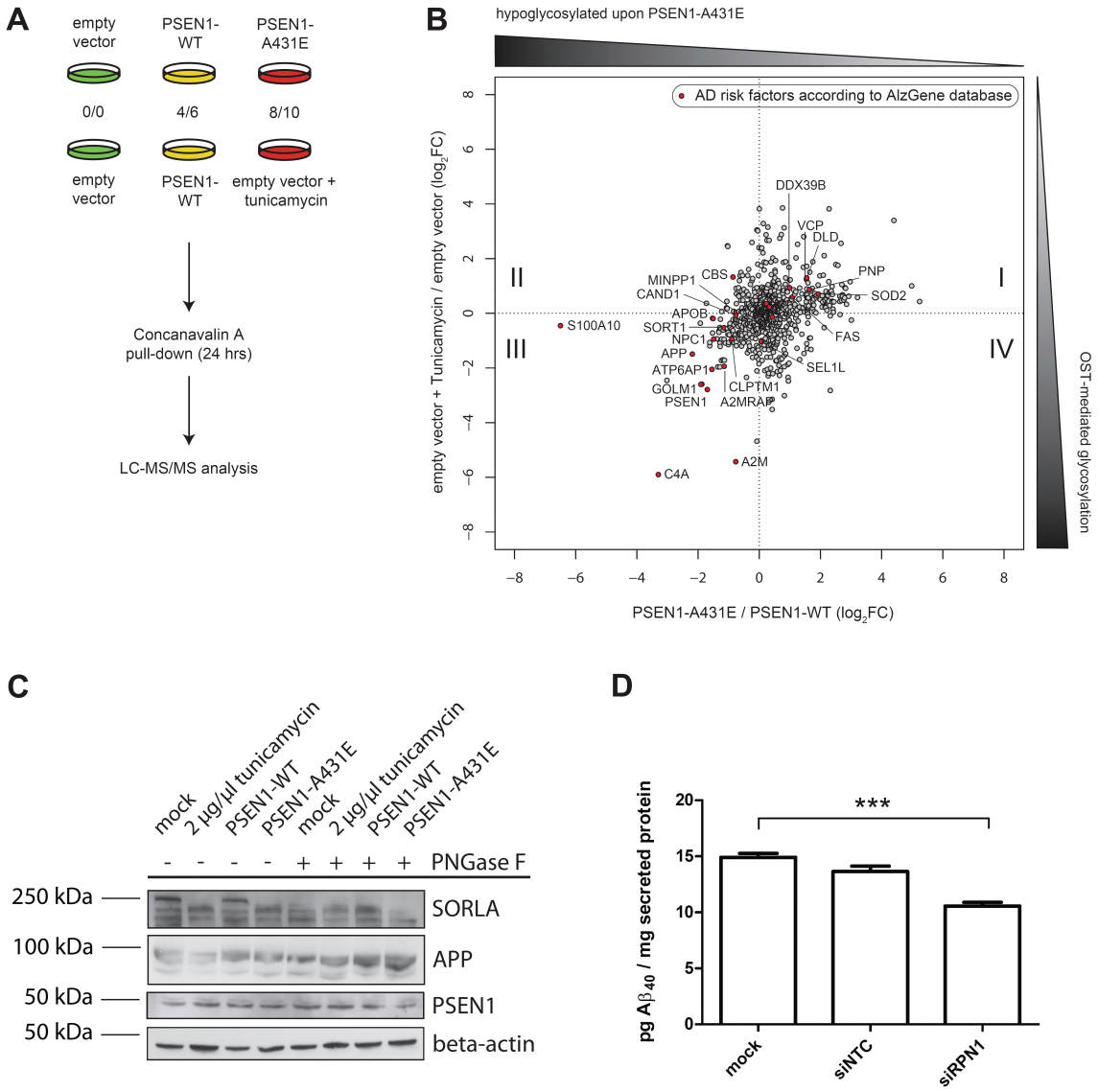

FIG. III.9 | PSEN1-A431E is a mediator of *N*-glycosylation changes in early-onset Alzheimer's disease. (A) Experimental design for the quantitative Concanavalin A pull-down. (B) Changes on global N-glycosylation pattern upon PSEN1-A431E mutation. Proteins that are hypoglycosylated upon A431E expression and *N*-glycosylated via the OST complex show enrichment for Alzheimer's disease candidate genes (marked in red, $p < 1.0E-07$ for quadrant III). (C) Western blot validation of LC-MS/MS results. PNGaseF specifically cleaves *N*-bound glycans. Visible band shift depends on number of N-glycosylations sites (M_W of each $Glc_3Man_9NAc_2$: 2.6 kDa). (D) Secretion of $A\beta_{1-40}$ decreases by ~30% upon siRNA-mediated knockdown of the OST regulatory subunit ribophorin 1 (RPN1) in SH-SY5Y neuroblastoma cells (n=4; ***, $p < 0.001$; NTC: non-targeting control).

tween the fully glycosylated and the non-glycosylated protein is much smaller. This is due to the numbers of *N*-glycosylation sites within the amino acid sequence of a given protein. While SORLA contains 27 predicted *N*-glycosylation sites, APP contains only 1-2 predicted sites, depending on the cell line expressed. Each *N*-glycosylation residue attached to each site additionally adds approximately 2.6 kDa to the molecular weight of the respective glycosylated protein. As the fully glycosylated APP isoform has a molecular weight of around 140 kDa, a 2.6-5.2 kDa shift is more difficult to observe by Western blotting. PSEN1 did not show any apparent band shift behavior in the Western blotting, consistent with previous observations reporting no post-translational modification of PSEN1 by *N*-glycosylation (Walter et al., 1996). Accordingly, the Western blotting data matched the quantitative ConA pull-down observations for the two selected proteins and proved that PSEN1 does not seem to be *N*-glycosylated.

Collectively, these results suggest that the early-onset AD-causing mutation PSEN1-A431E changes the global *N*-glycosylation pattern. In particular, PSEN1-A431E mediates hypoglycosylation of several other AD-related proteins, which might result in disturbed trafficking and/or localization of the affected glycoproteins (Leem et al., 2002) and thereby might potentiate detrimental effects of several AD-related effector proteins to accelerate disease progression.

III.4.2 Processing of APP is regulated by the oligosaccharyltransferase complex

As evident from the quantitative ConA pull-down data, several Alzheimer's-associated gene products are targets of OST-mediated *N*-glycosylation, including the mature APP protein (cf. III.4.1). To determine whether the OST complex modulates the proteolytic processing of APP via the γ-secretase complex, the secretion of Aβ peptides was analyzed as a function of OST activity. For this purpose, SH-SY5Y neuroblastoma cells were mock-treated or transfected with siRNAs directed against RPN1 or a non-targeting control. RPN1 is the substrate-specific regulatory subunit of the OST complex (Wilson and High, 2007) and siRNA-mediated knock-down of RPN1 reduces the overall OST complex activity approximately by 70% (Ruiz-Canada et al., 2009). After 72 hrs of siRNA transfection, fresh medium was added for another 24 hrs and then used in an anti-$A\beta_{1-40}$-directed ELISA. As apparent from the bar chart (FIG. III.9D), the amount of secreted $A\beta_{1-40}$ significantly decreases in RPN1 knock-down cells by almost 30% in contrast to mock-treated cells. Non-targeting controls did not show significant changes when compared to mock-treated SH-SY5Y cells. This observation is consistent with a previous report, in which knock-down of two different OST subunits, namely DC2 and KCP2, also reduced Aβ levels (Wilson et al., 2011). Therefore, the decrease in toxic $A\beta_{1-40}$ levels upon knock-down of different OST subunits indicates that the OST complex specifically alters Aβ production, presumably via its direct interaction with the γ-secretase complex.

III.5 The role of LRPPRC in APPsw-forms of Alzheimer's disease

Leucine-rich pentatricopeptide motif-containing protein (LRPPRC) is a RNA-binding protein that plays a pivotal role in mRNA metabolism in both nuclei and mitochondria. It has been reported to be associated with the nuclear mRNA export machinery (Topisirovic et al., 2009) and to act as a transcriptional regulator for a subset of nuclear-encoded mitochondrial genes through its interaction with peroxisome proliferator-activated receptor coactivator 1-α (PGC-1α) (Cooper et al., 2006). More recently, several publications have focused on the role of LRPPRC within the mitochondria. Here, LRPPRC cooperates with another RNA-binding protein called SLIRP to post-trancriptionally modulate mRNA stability of downstream targets (Sasarman et al., 2010; Sondheimer et al., 2010; Xu et al., 2011), presumably via promoting the polyadenylation of target transcripts and thus suppressing exonucleolytic mRNA decay in mitochondria (Chujo et al., 2012).

LRPPRC is itself a neurodegenerative disease-causing gene product as LRPPRC missense mutations are cause of the rare Leigh syndrome French-Canadian type (LSFC) (Mootha et al., 2003). LSFC patients exhibit dramatic decreases in LRPPRC and cytochrome c oxidase levels, leading to a breakdown of the mitochondrial respiratory chain in cells of the brain stem that is usually fatal.

III.5.1 LRPPRC: novel links to Alzheimer's disease?

LRPPRC was identified as specific interactor in the q-AP-MS screen for the Alzheimer's disease-causing amyloid precursor protein (APP). In more detail, LRPPRC showed a preferential binding towards the double point mutation APP-K670N/M671L (FIG. III.8D and Supplementary TAB. VII.2), which is also called the APP Swedish mutation (APPsw, FIG. I.2). Swedish mutation-based AD varieties are among the most aggressive forms of AD, exhibiting extremely elevated levels of oxidative stress compared to other types of AD based on distinct APP mutations (Bogdanovic et al., 2001; Marques et al., 2003). To validate the differential binding of LRPPRC to APPsw, co-immunoprecipitation experiments were performed in HEK293TN cells overexpressing three different APP variants (FIG. III.10A). Immunoprecipitation of APP revealed a similar protein expression level for all APP variants yet a stronger signal in the APPsw lane when co-stained for LRPPRC. The reciprocal coIP in the same overexpression background showed similar results: pull-down of LRPPRC exhibited equal LRPPRC expression levels but a stronger signal in the APPsw lane when co-stained with an anti-APP antibody. Together, both the q-AP-MS results for APP and the coIP/Western blotting data indicate that LRPPRC seems to preferentially bind the APPsw variant over APP wild-type or APP London mutation (APP-V717I). Furthermore, the interaction between LRPPRC and wild-type APP was validated by co-immunoprecipitation with wild-type mouse brain lysate (FIG. III.10B), indicating that the interaction seems to be functionally relevant *in vivo*.

III.5.2 Oxidative stress phenotypes of APPsw cells can be rescued by LRPPRC

Almost all NDDs exhibit severe deficiencies in mitochondrial integrity, however, the precise causes for underlying mitochondrial dysfunction are yet unclear in most diseases (Lin and Beal, 2006). As LRPPRC is one of the most potent regulators of mitochondrial gene expression and now has been identified as differential binder of APPsw, it was reasoned that LRPPRC could represent a novel link to mitochondrial impairment in early-onset AD. Therefore, the impact of LRPPRC and APPsw on mitochondrial metabolism was studied more closely. HEK293TN cells were transiently transfected with different expression constructs alone, co-transfected with LRPPRC overexpression constructs or siRNAs directed against LRPPRC (FIG. III.10C). After 48 hours of expression, the cells were gently lysed to preserve subcellular compartments and the mitochondria were subsequently isolated from these cells. Next, mitochondrial function was spectrometrically assessed by measuring the enzymatic activity of the mitochondrial enzyme aconitase. Aconitase contains an iron-sulfur cluster in its enzymatic center and is therefore extremely sensitive to oxidative stress agents as they reduce the [4Fe-4S] to an [3Fe-4s] cluster, hence inactivating the enzymatic activity of aconitase. Measuring the mitochondrial aconitase activity thus represents a good readout system for monitoring oxidative stress levels in mitochondria (Yan et al., 1997).

Expression of LRPPRC increased the aconitase activity in each condition, while knock-down of LRPPRC drastically reduced aconitase activity, suggesting that LRPPRC is essential for proper mitochondrial function, which is consistent with the literature (Xu et al., 2011). Expression of APPsw causes a significant ($p < 0.005$) reduction of aconitase activity when compared to APP-WT expressing cells. Co-expression of LRPPRC together with APPsw was able to partially rescue the stress phenotype, suggesting that APPsw-induced stress may be related to LRPPRC. Interestingly, no significant difference in aconitase activity could be found between APP-WT and APP-V717I expressing cells, indicating that the stress phenotype is specific for APPsw but not for another early-onset variant of AD.

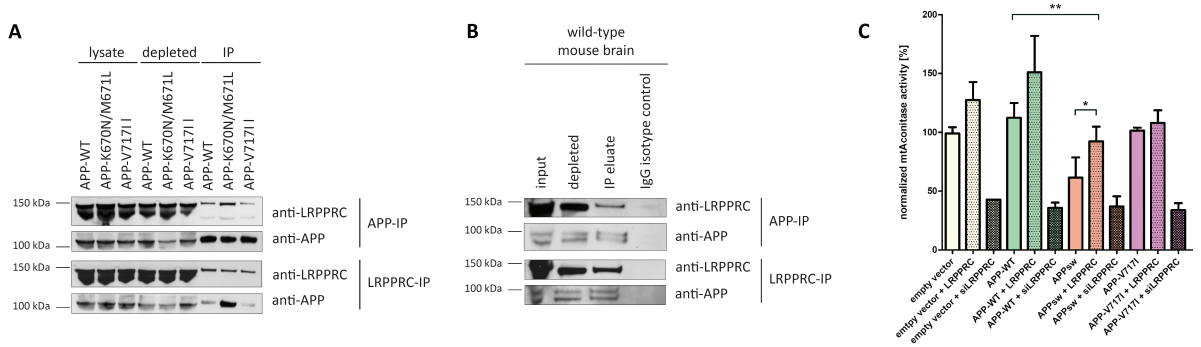

FIG. III.10 | LRPPRC preferentially binds APPsw and partially rescues APPsw-phenotypes. (A) Western blot of APP-IP or reciprocal LRPPRC-IP after overexpression of APP variants in HEK293TN cells. LRPPRC binds stronger to APPsw (K670N/M671L) compared to APP wild-type or APP-V717I. (B) LRPPRC can be co-immunoprecipitated with endogenous APP from wild-type mouse brain lysate and vice versa in reciprocal coIP experiments. (C) Overexpression of APPsw causes significantly reduced aconitase activity in isolated mitochondria compared to wild-type APP, indicating higher levels of oxidative stress. Co-expression of LRPPRC in APPsw-expressing cells partly rescues the stress phenotype (mean ± SD; n=4; **, $p < 0.005$; *, $p < 0.05$).

III.5.3 The APPsw-mediated phenotype is accompanied by decreased levels of LPPPRC and its downstream targets

While the determination of aconitase activity revealed deficits in the mitochondrial activity of APPsw compared to wild-type APP expressing cells, tracking only one mitochondrial enzyme might be too simplistic for assessing the overall mitochondrial fidelity, thus a more global study was reasoned.

At first, triple stable-isotope labeled HEK293TN cells were transfected for 48 hrs with either APP-WT, APPsw or APPsw co-transfected with LRPPRC in order to characterize global proteome changes. Expression of APPsw induced downregulation of both LRPPRC and SLIRP compared to cells expressing wild-type APP (FIG. III.11A, proteins marked in red). In addition, well-known targets of LRPPRC and SLIRP, e.g. different subunits of the cytochrome c oxidase (Complex IV) or NADH dehydrogenase (Complex I), exhibited reduced protein levels upon APPsw expression (FIG. III.11A, proteins marked in yellow), which is consistent with previous reports on mitochondrial responses to loss of LRPPRC (Gohil et al., 2010). Co-expression of LRPPRC together with APPsw was able to partially rescue the expression phenotype, shifting the protein levels of LRPPRC, SLIRP and their downstream targets back to almost wild-type APP expression levels (FIG. III.11B).

As both LRPPRC and SLIRP are RNA-binding proteins that regulate the mRNA stability of their downstream targets, it was straightforward to investigate mRNA levels of the respective gene products as well. Quantitative RT-PCR analysis revealed a decrease of the corresponding mRNA levels of LRPPRC and COX1 in cells expressing APPsw compared to wild-type APP (FIG. III.11C).

All the aforementioned findings suggest a yet unreported interplay between LRPPRC and the amyloid precursor protein APP and, in particular, with the APP Swedish mutation. Paradoxically, overall LRPPRC levels seem to be downregulated upon APPsw expression, while at the same time the interaction between APPsw and LRPPRC is enhanced compared to cells expressing wild-type APP. Therefore, in an attempt to characterize the molecular details of the APP/LRPPRC mechanisms more closely, several follow-up experiments were conducted. However, neither impaired trafficking of the nuclear-encoded LRPPRC into mitochondria was observed (Supplementary FIG. VII.3), nor enhanced degradation of LRPPRC as investigated by pulsed SILAC analysis (Supplementary FIG. VII.4). However, ongoing quantitative RT-PCR experiments additionally link LRPPRC to APP: cells expressing APPsw in contrast to APP-WT displayed both a reduction of LRPPRC- and COX1-mRNA (FIG. III.11C) and dimished binding of these mRNAs in anti-LRPPRC RNA-immunoprecipiations experiments (FIG. III.11D).

Besides the already known binding of LRPPRC to COX1 mRNA (Gohil et al., 2009; Ruzzenente et al., 2011), these results suggest that LRPPRC protein could bind its own mRNA as well. On the other hand, the data indicate that the APPsw mutation impairs binding of LRPPRC protein towards COX1 and LRPPRC mRNA.

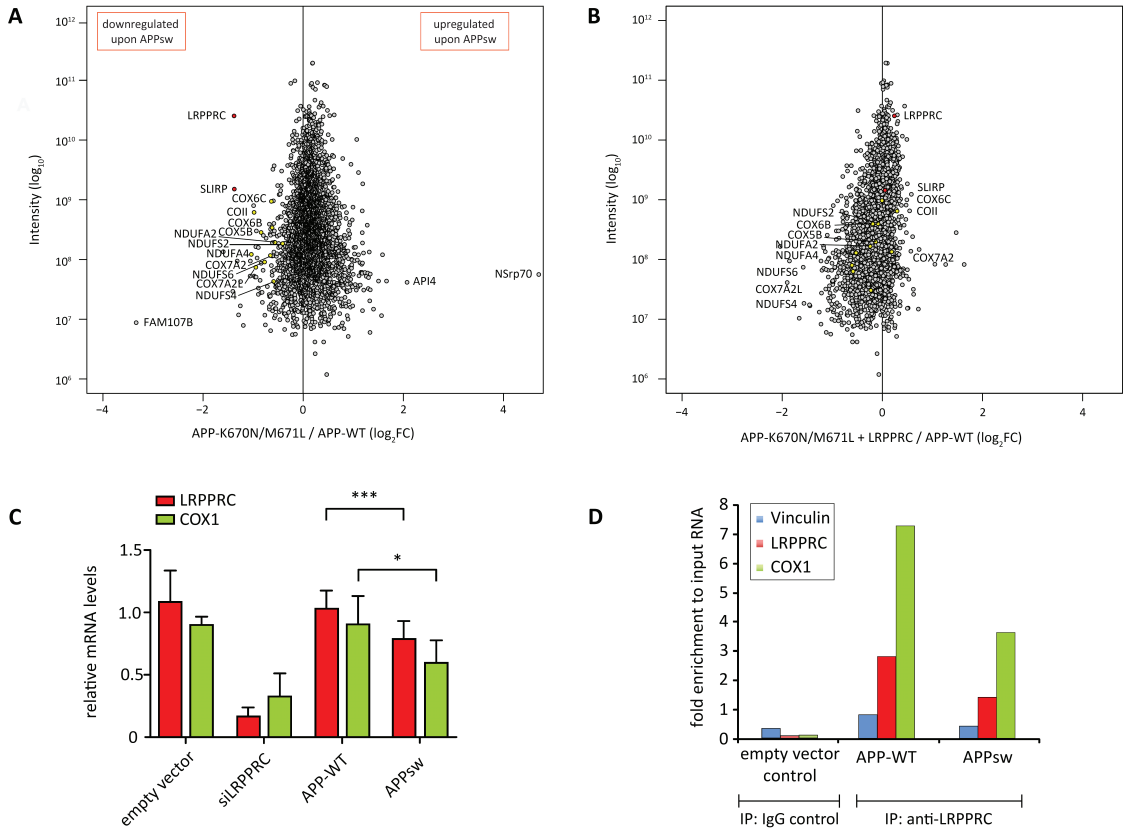

FIG. III.11 | LRPPRC is a novel effector in APPsw-mediated Alzheimer's disease. (A) Global proteome changes in HEK293T cells as measured by SILAC-based mass spectrometry analysis. APPsw overexpression reduces LRPPRC and SLIRP levels (marked in red) and proteins of the mitochdonrial electron transport chain (marked in yellow). (B) LRPPRC overexpression partially rescues the effect of APPsw. (C) mRNA levels of LRPPRC and its downstream target COX1 are reduced in APPsw compared to APP wild-type expressing cells; mean ±SD, n=5, ***, *P*<0.005; *, *P*<0.05, two-tailed Student's *t*-test. (D) LRPPRC- and COX1-mRNA can be enriched by immunoprecipitation of LRPPRC protein, suggesting that LRPPRC binds its own mRNA in APP-WT-expressing cells. LRPPRC- and COX1-mRNA enrichment is markedly reduced after pull-down of LRPPRC in APPsw-expressing cells; n=2.

IV Discussion

IV.1 Q-AP-MS strategy and protein-protein interactions

In the present thesis, a quantitative affinity purification followed by mass spectrometry (q-AP-MS) approach has been utilized to screen for interactors of proteins involved in neurodegenerative diseases. In particular, q-AP-MS was applied to identify differential interactions that might be affected by distinct disease-associated mutations. The q-AP-MS approach is widely used in the proteomic community to address various biological questions and is now considered to represent to most unbiased method to study PPIs with high throughput and high reproducibility (Vermeulen et al., 2008). However, given their inherent design, all AP-MS approaches suffer from the tradeoff between specificity and sensitivity. In the present thesis, the implementation of stable isotope labeling and crossover experiments enabled to differentiate unspecific binders from specific interactors (FIG. III.1B and C, FIG. III.2). Moreover shown by the functional characteristics of the identified interactors (FIG. III.4) and further validation experiments (FIG. III.5). At the same time, however, it was observed that the overlap to many known interactions reported in the HIPPIE database was small, though highly significant for most cases (TAB. III.2). As the HIPPIE collection is comprised of data derived from different detection methods and various biological sources, a strong overlap to the HIPPIE database was initially not anticipated. Comparative assessment of PPI data derived from distinct high-throughput methods has been shown to poorly correlate, giving rise to complementary datasets with particular biases towards protein abundance and localization (von Mering et al., 2002). Although the HIPPIE database does represent the largest collection of NDD-associated PPIs, it is still imperfect: manual inspection of the identified q-AP-MS targets has highlighted several known PPIs reported in the literature (e.g. binding of PSEN1 to different subunits of the OST), which are conversely not listed in HIPPIE. Thus, the defined overlap in TAB. III.2 underestimates the true intersection of identified q-AP-MS targets with known PPIs from the literature.

Surprisingly, while comparing the q-AP-MS raw data and HIPPIE-listed entries, it became apparent that many literature-reported interactors were actually identified in the pull-down experiments performed in the present thesis but did not exhibit the “anticipated“ ratios, thus they were not classified as interactors by the q-AP-MS screen. This discrepancy may be due to missing adaptor proteins in HEK293TN cells, which are necessary for the formation of certain complexes. Consequently, a putative prey protein might still be expressed in HEK293TN cells, but is not part of the complex interacting with the prey in a different cellular system. A second possibility are insufficient peptide quantification events for distinct candidate peptides. Therefore, true interactors might be rejected by the applied specificity cutoffs. Softening of the applied rules could account for such cases, however, adversely affecting false-positive identifications at the same time. On the contrary, the HIPPIE database could also be contaminated by false-positive identifications reported in previous publications. For instance, as apparent from FIG. III.1B and 1C most of the identified proteins show roughly 1:1 ratios, thus indicating un-

specific binding. Such proteins cannot be discriminated from specific interactors in traditional, non-quantitative AP-MS experiments that are included in HIPPIE. Hence, many reported "true" interactors might in fact be unspecific binders. This issue can only be solved by additional validation experiments.

Still, the small overlap and the failure of the applied q-AP-MS screening approach to detect several known interactors from the literature indicates limitations of the method. Possible explanations for false-negative identifications in the present thesis might be (i) interference of the tag, (ii) missing expression of prey proteins or particular scaffold proteins mediating binding of the bait to certain prey proteins in the utilized HEK293TN cell system or (iii) too stringent washing conditions. All the aforementioned issues are related to the tradeoff between experimental simplicity and biological relevance. While HEK293TN are easy to work with regarding cultivation, SILAC and transient transfection, they are not neuronal cells. Performing the q-AP-MS approach with neuroblastoma cells for instance would most certainly lead to the finding of partially distinct interactions that have not been found in the HEK cells, as they do not express neuron-specific proteins.

A further subject of debate is the utilization of N-terminal c-myc-tagged bait proteins within the q-AP-MS screen. Tagging facilitated the pull-down procedure, as the same anti-c-myc antibody was used for all pull-down experiments. In order to minimize tag-related side-effects regarding unspecific interactions or solubilization issues, the N-terminal c-myc tag (EQKLISEEDL, ten amino acids) was used as a rather small and frequently used tag (Jarvik and Telmer, 1998). Nevertheless, it cannot be ruled out that the tag might influence certain PPIs.

Beyond that, potential off-targets effects introduced by the overexpression constructs were investigated (FIG. III.6). While these experiments did not provide evidence for a strong change in the protein expression profile, it cannot be excluded that changes in cellular protein abundance caused by the overexpression had an impact on the results. Stress-responsive proteins might therefore have been detected as specific interactors. However, given the co-immunoprecipitation experiments for the endogenous bait proteins (FIG. III.5B), where all selected interactions have been validated, it is expected that the provided PPI dataset is highly specific.

Finally, it is worth mentioning that a generic q-AP-MS protocol was applied to all bait proteins to conduct a straightforward PPI screening. Considering the distinct cellular functions of all bait proteins under investigation, it is conceivable that the binding affinities towards their respective interactors can differ quite substantially. Hence, the generic pull-down and washing procedure might need optimization for each and every bait protein in order to maximize the PPI identification output, which would be extremely costly in terms of time and was therefore not carried out.

As follows from the discussion above, a proper assessment of both false-positive and false-negative rates is almost impossible, since no available set of 'true' PPIs can be used for accurate error rate estimation. Given all technical and biological replicates, crossover-experiments and subsequent validation experiments, it can be reasoned that the present data derived from the q-AP-MS screen is of high specificity and satisfying sensitivity.

With the exception of two publications (Lim et al., 2006; Limviphuvadh et al., 2007) no comparative analysis combining two or more NDDs has been performed so far. Thus, the present thesis represents the first experimental attempt to generate a PPI network across several non-related NDDs. While Lim and coworkers developed an interaction network for 23 different inherited ataxias, only SCA1 was under investigation in the present thesis. Consequently, no cross-comparative results can be drawn on from this particular dataset. Limviphuvadh and coworkers generated an *in silico* PPI network of six NDDs, three of them shared with the present thesis. While investigating 201 bait proteins, only five proteins were commonly found in at least three diseases. This minor overlap between the different diseases is consistent with the present findings that only few proteins are actually shared between different NDDs and most interactions are unique to the distinct disorders (FIG. III.3B).

Potentially the most interesting results have been obtained through screening for differential PPIs (FIG. III.8 and Supplementary TAB. VII.2). These differential PPIs might directly reveal proteins functionally involved in NDD progression. It has to be stressed again that only interactors identified in the original screen were considered for differential binding behavior, in order to reduce increased false-positive identifications. The observed distribution of differential interactions (FIG. III.8) in part reflects the unique characteristics of the respective bait variants. For example, the huge difference between interactions of PARK2 wild-type and Q329Stop can be explained by the early stop codon mutation that renders the mutated PARK2 protein completely dysfunctional. Similarly, the utilized huntingtin construct Htt506-Q145 has an extremely high aggregation propensity thus sequestering a plethora of proteins. It is therefore not surprising that both HTT and PARK2 had many differential interactors. Surprisingly, in the ataxin-1 experiment only one protein showed a preferential binding towards the mutant ataxin-1 construct ATXN1-Q82. As already mentioned earlier, it is more likely that the ATXN1-polyQ expansion is shifting PPI complex formation between wild-type and mutant forms in a quantitative rather than a qualitative way (cf. III.1).

Interestingly, all the bait proteins with point mutations (APP, PSEN1 and SNCA) showed a large overlap of interactions and only very few differential interactions. The majority of them exhibited a preference for the wild-type variant of each respective bait protein. Single point mutations might not dramatically change the interactome, unless the point mutation directly affects a binding domain or a very important feature of the protein structure. This observation suggests that the effect of the employed disease-associated point mutations on PPI formation is subtle. It is expected that the differential interactions provided in the present thesis represent a rich source for fellow scientists, allowing to identify novel disease mechanisms with direct implications in selected NDDs.

IV.2 Determination of disease-modifying effects *in vivo*

Recently, Kaltenbach and coworkers showed that genetic modifiers of NDDs are enriched for interactors of the disease-causing proteins *in vivo* (Kaltenbach et al., 2007). Moreover, two ATXN1-interactors have been shown to be genetic modifiers of SCA1, critically for progression of the disease in the cerebellum of SCA1-mouse models (Lam et al., 2006; Lim et al., 2008). These data show that interaction partners of disease proteins can be informative for disease phenotypes. The assessment of disease-modifying effects for ataxin-1 interactors in the *Drosophila* neurotoxicity model of SCA1 in the present thesis has now led to an extremely significant and exalted hit rate (FIG. III.7) which is roughly 30-fold higher than in previous large-scale screens performed in the very same model (Branco et al., 2008; Fernandez-Funez et al., 2000). Combined, these results demonstrate that large-scale PPI screening combined with genetic interaction studies in *Drosophila* represent a powerful tool to identify novel candidate modifiers of ATXN1-mediated neurotoxicity.

In the end, however, only 30% of all ataxin-1 interactors identified in the q-AP-MS screen could be assessed in the fly neurotoxicity model. As the remaining 70% did not have any ortholog gene in the fly or no shRNA strain was available, the vast majority of potentially interesting modifiers of ATXN1-mediated neurodegeneration could not be investigated. All of the 11 identified disease modifiers enhanced the rough eye phenotype. Hence, no REP suppressors were identified in the present thesis. However, previous screens with the very same but also with different disease models exhibited both REP enhancers and suppressors at the same time (Branco et al., 2008; Fernandez-Funez et al., 2000; Muqit and Feany, 2002). In earlier publications, the ratio between identified suppressors:enhancers is roughly 1:3. Given the small sample size, the failed suppressor detection might simply be a random event. Alternatively, it is also possible that physical interaction partners of ATXN1 have a protective role preventing neurodegeneration.

Surprisingly, approximately 40% of all tested *Drosophila* shRNA strains exhibited lethal phenotypes in the F1 generation (Supplementary FIG. VII.2) when crossbred with the GMR_ATXN1-Q82 flies. This high number of genes leading to lethal interactions was unexpected, as the expression of the toxic ATXN1-Q82 protein is restricted to differentiated cells of the compound eye, which should not interfere with the vitality of the flies under investigation. Yet, the employed GMR promoter has been reported to drive protein expression not only posterior to the morphogenetic furrow of the eye disc, but also in a small population of cells in the fly brain (Ellis et al, 1993; Moses and Rubin, 1991). Consequently, demise of these non-retinal GMR-positive cells might potentiate deleterious effects of progressing degeneration in the compound eye. Also, necrosis of affected GMR-positive cells might spread to neighboring tissue without any ATXN1-Q82 expression or might release further toxic molecules, thus preventing normal fly morphogenesis and hatching of the fly larvae. It is important to point out that the SCA1 neurotoxicity model in *Drosophila* represents a rather artificial system to screen for genetic modifiers. Besides the overexpression of a human transgene in an invertebrate animal model,

the additional knock-down of selected genes might constitute a factitious system which exhibits more off-target, i.e. lethal effects than expected (Ma et al, 2006; Moffat et al., 2007). However, neither the RNAi knock-downs in wild-type flies nor control screens in Tau model flies showed any obvious phenotype (Supplementary TAB. VII.3), suggesting that the observed lethal interactions are specific for ATXN1-Q82.

Arguably, the most significant assessment of NDD-modifying effects would be an experimental investigation of human patient material. This is very difficult to achieve due to several reasons. As an alternative, the PPI data was compared to genome-wide association studies (GWAS). Overall, a significant SNP set enrichment was replicated in two independent GWAS cohorts for all but the PSEN1-WT SNP set. While SNP sets of interactors for all disease-associated but not wild-type bait variants showed a significant enrichment in the smaller GenADA cohort, this finding could not be replicated in the much bigger GERAD dataset (TAB. III.3). This inconsistency might be explained by the fact that GWAS cohorts are assorted with patients showing apparent phenotypical symptoms of Alzheimer's disease, however the exact disease-causing mutations of each participating individual is not determined. Consequently, the GenADA but not the GERAD cohort might be biased by patients exhibiting similar mutations as the ones selected for the q-AP-MS screening.

Noteworthy, no individual SNP reached the threshold of genome-wide significance (p-value < 1.0E-07) currently applied in most GWAS publications (Gandhi and Wood, 2010). Still, even larger p-values might become significant, when considering combinatorial effects of individual SNPs in distinct genes that could contribute to disease onset or progression (Unoki et al., 2008). In this way, PPI data might considerably increase the usefulness of GWAS data: combination of both datasets could identify potential disease-associated genes, which are currently falling below commonly used genome-wide significance cutoffs.

IV.3 Implications of PSEN1-A431E on *N*-glycosylation changes in Alzheimer's disease

Recent findings have assigned a direct role of PSEN1 in the initial steps of protein *N*-glycosylation in the ER (Lee et al., 2010). In the present thesis, this hypothesis was corroborated by validation of the interaction between PSEN1 and a large fraction of the oligosaccharyltransferase complex (OST) subunits, which are responsible for initial *N*-glycosylation. Moreover, the early-onset AD variant PSEN1-A431E was shown to disturb the global *N*-glycosylation pattern in HEK-293TN cells (FIG. III.9B), most likely due to impaired coordination of PSEN1- and OST-regulated post-translational processing events in the ER.

A potential pitfall of the quantitative ConA experiment performed in this study (cf. III.4.1) is the risk of false-positive identifications. Specifically, some proteins might show a significant ratio in the experiment although their glycosylation is not affected. These false-positive identifications might be technical in nature, e.g. contaminations derived from the ConA specificity or

the washing conditions, or linked to other biological effects. As an example, PSEN1 was identified in the quantitative ConA pull-down experiments in quadrant III (FIG. III.9B) - indicating reduced expression and hypoglycosylation in the PSEN1-A431E condition. However, PSEN1 is reported not to be *N*-glycosylated (Walter et al., 1996) and did not exhibit an apparent band shift in the Western blot validation experiments (FIG. III.9C), thus raising the question how it showed up as specific target of OST-mediated glycosylation. One possible explanation might be a "co-purification" of PSEN1 through binding to another quadrant III-target, as for instance to its reported binding partner APP which is a known glycoprotein.

Surprisingly, many proteins pulled-down by ConA were not sensitive for the tunicamycin treatment (FIG. III.9B, quadrant I and II). This could connote that these proteins are either not glycosylated at all or glycosylated in an OST-independent manner. As ConA normally displays high specificity and also the applied washing conditions during the ConA pull-down were quite stringent, it seemed implausible that so many of the identified proteins were not glycosylated at all. It is tempting to speculate that an alternative glycosylation mechanism is responsible for their identification in the ConA pull-down. As there is no comprehensive *N*-glycosylation resource or database available, a number of proteins displayed in quadrants I and II were manually inspected for different post-translational glycan modifications reported in the literature. It was found that several of the inspected proteins (e.g. ENO1, GAPDH, IDH3A, LDHA, MDH1, SOD1) are experimentally validated targets of so-called glycation, a non-enzymatic form of carbohydrate transfer (Heath et al., 1996; Kato et al., 2000; Kil and Lee., 2004; Morgan et al., 2002; Pietkiewicz et al., 2009), turning them into so-called advanced glycation end-products (AGEs) (Singh et al., 2001). Glycation is thought to take place under normal physiological conditions but is extremely elevated upon increased age or certain pathologic conditions such as oxidative or carbonyl stress, both hallmarks of NDDs (Munch et al, 1997; Vicente Miranda and Outeiro, 2010). As many more tunicamycin-insensitive proteins were identified in quadrant I (specific for PSEN1-A431E) than in quadrant II (specific for PSEN1-WT), it seems that overexpression of the mutant PSEN1-A431E could induce glycation events. In fact, several different PSEN1 mutations increase both cellular levels of oxidative stress and reactive carbonyl compounds (Guo et al., 1997; LaFontaine et al., 2002), leading to accumulation of AGEs in more than 75% of pyramidal neurons in human AD patients with PSEN1 mutations (Munch et al., 2002). The present findings could indicate a similar role for PSEN1-A431 in provoking increased glycation events in Alzheimer's disease.

In a very recent publication, Coen and coworkers were unable to reproduce the findings proposed by Lee et al. (Coen et al., 2012), showing that *N*-glycosylation is not a necessary prerequisite for proper targeting of the v-ATPase V0a1 in PSEN$^{-/-}$ cells. In contrast, the data from the present thesis did identify the related v-ATPase subunit V1a (ATP6AP1, FIG. III.9B, quadrant III) as strongly regulated upon PSEN1-A431E expression, going along with the original data by Lee and coworkers. Still, the proposed role of PSEN1 in early *N*-glycosylation steps must be critically scrutinized in further validation experiments to provide additional support for this hypothesis.

IV.4 Identification of LRPPRC as novel effector for oxidative stress in APPsw-mediated forms of Alzheimer's disease

Early-onset Alzheimer's disease is caused by mutations in either APP or PSEN1/2. Simultaneously, increased oxidative stress levels might play an additional role in the progression of AD (cf. I.1.2). APP Swedish mutation (APPsw)-mediated forms are among the most aggressive types of AD, as they exhibit extremely elevated levels of oxidative stress (III.5.1), accompanied by a very rapid disease progression. However, the distinct underlying mechanisms for this are yet unknown.

The present work revealed preferential binding of LRPPRC to APPsw compared to APP wild-type or the APP-V717I mutation. So far, the conducted experiments show reduced levels of both LRPPRC protein and mRNA in APPsw-expressing cells (FIG. III.11A and C). In addition, co-expression of LRPPRC with APPsw partially rescued APPsw-mediated oxidative stress in mitochondria (FIG. III.10C), suggesting a direct role of LRPPRC in APPsw-mediated forms of AD. Since neither trafficking impairments nor enhanced degradation of LRPPRC protein could account for the observed mitochondrial deficits (Supplementary FIG. VII.3 and VII.4), the reduced LRPPRC levels thus cannot be explained by translational or post-translational effects on LRPPRC driven by APPsw. However, given the reported role of LRPPRC in post-transcriptional regulation and the data obtained from the RNA-immnuoprecipitations (FIG. III.11D), a novel feedback mechanism of LRPPRC is proposed on the basis of the data available (FIG. IV.1), which includes post-transcriptional regulatory effects as well. According to this model, LRPPRC stabilizes its own transcript in wild-type APP-expressing cells, hence maintaining mitochondrial function through positive regulation of respiratory chain-encoded gene products. In contrast, sequestration of LRPPRC by APPsw causes reduced stabilization of its own and target mRNAs leading to diminished levels of these targets and LRPPRC itself. Since RNA-binding proteins such as LRPPRC play crucial roles in gene expression, their spatio-temporal abundance is itself tightly regulated, often times by autoregulatory mechanisms (Kishore et al., 2010). It is likely that the observed decline of the LRPPRC protein levels might in the end be a combinatory effect of both impaired transcript stability and reduced translation efficiency, due to the proposed LRPPRC-mediated mRNA regulation in human mitochondria (Chujo et al., 2012).

This hypothesis is based on the assumption that LRPPRC could bind its own mRNA, as suggested by the performed RIP experiments. Yet, pull-down of LRPPRC could be complicated by LRPPRC protein that is actually just being translated and thus associated with its own mRNA. In a way to provide final evidence for binding of LRPPRC to its own transcript, PAR-CLIP (Photoactivatable-Ribonucleoside-Enhanced Crosslinking and Immunoprecipitation) analysis would be desirable (Hafner, Landthaler et al., 2010) and is envisaged within the near future. Hence, not only the mRNA-protein interaction but also the direct binding sites could be mapped accordingly.

The aforementioned follow-up experiments suggest a novel role of LRPPRC in APPsw-mediated early onset forms of Alzheimer's disease. Still, the normal cellular function of LRPPRC binding to wild-type APP remains unaddressed so far. The actual subcellular location of the interaction is of particular interest. Both proteins exhibit a large intersection of subcellular locations: while APP is mainly located at the cell surface and the secretory compartment (De Strooper and Annaert, 2000), proteolytic fragments have been detected in the cytoplasm (Gao and Pimplikar; 2001) and the nuclei of neurons as well (Baek et al., 2002; von Rotz et al., 2004). Moreover, APP can also be targeted to mitochondria (Anandatheerthavarada et al., 2003). On the other side, LRPPRC is mainly mitochondrial (Mili and Pinol-Roma, 2003), but has a significant role in the nucleus (Cooper et al., 2006; Topisirovic et al., 2009) and is present in the cytoplasm during translation. Successive immunofluorescence co-localization studies on APP and LRPPRC have not generated satisfying results (data not shown), thus no conclusive statement can be made so far and further studies have to investigate the exact site of the interaction in more detail.

Nevertheless, based on several published findings with regard to the transcriptional activity of APP, which is exerted through its proteolytic fragment AICD (cf. III.1.2.), it is tempting to speculate that the interaction between APP and LRPPRC takes place in the nucleus. As described earlier, both proteins can act as transcriptional regulators. Interestingly, expression of the APPsw not only correlates with the preferential binding of LRPPRC to APP but also with enhanced processing of APP to both Aβ and AICD (Kim et al., 2003; Belyaev et al., 2010). APPsw-driven and enhanced generation of AICD would sequester LRPPRC in the nucleus, which subsequently leads to the observed effects on mitochondrial gene expression (cf. IV.1). This assumption would be consistent with published findings, which link AICD to mitochondrial function (Hamid et al., 2007; Ward et al., 2010). Although very tempting, this hypothesis is not entirely consistent with the current q-AP-MS and follow-up data: as the initial PPI screen was performed with N-terminal c-myc-tagged APP variants, the observed interaction must happen with either the full-length protein or the ß-secretase-cleaved sAPPß fragment, which still carries the N-terminal myc-tag. The AICD fragment is cleaved off from the C-terminus of the full-length APP protein, thus it does not carry the N-terminal tag anymore when translocated into the nucleus in the present experimental setup.

Given the present data, three possible explanations await further investigation: (i) the interaction independently takes place in the nucleus and an additional compartment; (ii) the interaction takes place in only one specific compartment not yet determined; (iii) the interaction is an artifact that occurs post-lysis. While (i) requires a much more complex mode of action, (ii) is at present considered more unlikely as full-length APP has not been detected so far in the mitochondrial matrix (main LRPPRC environment) and LRPPRC has not been detected at the plasma membrane or the secretory compartment (main full-length APP environment). Hence, high-resolution confocal microscopy experiments should enable a more thorough co-localization study of LRPPRC and full-length APP protein. The results of these experiments would allow drawing conclusions about the main site of the interaction in more detail.

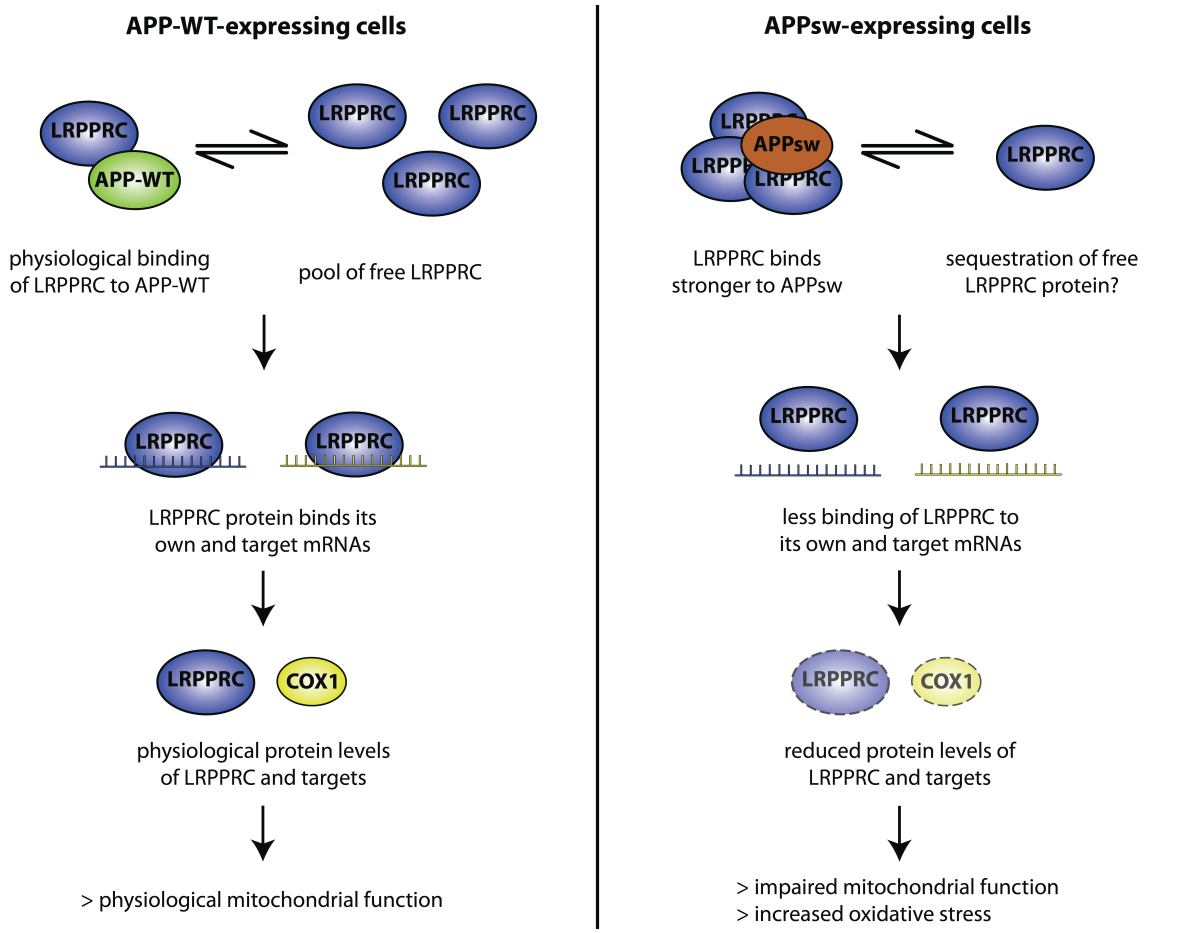

FIG. IV.1 | Hypothetical feedback mechanism of LRPPRC in cells expressing either wild-type or Swedish mutation APP. (Left panel) LRPPRC binds wild-type APP to act in a yet unknown fashion. LRPPRC protein levels remain physiological, thus allowing proper binding of LRPPRC towards its own (blue) and target mRNAs (yellow; COX1 as exemplified target). LRPPRC-bound mRNAs are post-transcriptionally stabilized (Chujo et al., 2012), mitochondria function normally. (Right panel) LRPPRC binds stronger towards APPsw, thus less free LRPPRC protein molecules are amenable for mRNA regulation. Downstream mRNA targets are destabilized and mitochondrial function is hence affected.

V Conclusions and Outlook

Protein-protein interaction networks offer a way to generate predictions of pathogenic pathways in human diseases involving complex molecular processes (Jordan et al., 2012). This systems perspective was harnessed in the present thesis to generate the first comparative analysis of four neurodegenerative disorders at the molecular level and to establish the first systematic quantitative PPI screen for normal and disease-associated variants of neurodegenerative disease proteins. The obtained PPI data corroborated the hypothesis that the four diseases under investigation indeed share some functional characteristics. In fact, all of them being responses to well-known protein misfolding events in these disorders. However, most interactions were unique for each disease, possibly explaining their very different phenotypical manifestations and clinical symptoms. Moreover, a significant link to disease phenotypes *in vivo* was established for AD and SCA1 interactors, thus the present PPI dataset provides a promising entity of protein binders which seem to play a critical role in the pathogenesis of NDDs.

The present findings on LRPPRC and its role in APP-expressing cells may of help to better understand the underlying mechanisms responsible for the extensive mitochondrial deficits observed in AD patients carrying the APP Swedish mutation. LRPPRC potentially represents a novel effector protein for these specific early-onset AD cases. In this context, it will be of particular interest to further investigate the role of LRPPRC in AD. Based on the present findings, ongoing work is centered on the validation of the LPPPRC interaction with APP in human brain samples derived from AD patients with the Swedish mutation. Also, investigation of metabolic changes in APPsw-conditions and flux analysis of selected metabolites is currently performed.

Consequently, all work in that direction has important practical implications. Given the similarity of contact surfaces of temporary protein complexes with the active sites of enzymes, PPIs represent challenging but attractive targets for small molecules or drugs (Archakov et al., 2003; Sugya et al., 2007). Since there is currently no prospect of total cure for any of the aforementioned neurodegenerative diseases, much effort is now spend towards developing small molecule inhibitors of several proteins involved in NDDs (Blazer and Neubig, 2009). The respective knowledge on the most relevant PPIs is an imperative prerequisite in order to develop feasible treatment options to eventually cure these devastating disorders. The assembled PPI network for NDDs gained in the present work and, more importantly, the differential PPIs may thus be explored for further conceivable drug targets.

VI REFERENCES

1. Abovich, N., and Rosbash, M. (1997). Cross-intron bridging interactions in the yeast commitment complex are conserved in mammals. Cell 89, 403-412.

2. Aebersold, R., and Mann, M. (2003). Mass spectrometry-based proteomics. Nature 422, 198-207.

3. Alzheimer, A. (1907). Ueber eine eigenartige Erkrankung der Hirnrinde. Allg Z Psychiat Psych-Gerichtl Med 64, 146-148.

4. Anandatheerthavarada, H.K., Biswas, G., Robin, M.A., and Avadhani, N.G. (2003). Mitochondrial targeting and a novel transmembrane arrest of Alzheimer's amyloid precursor protein impairs mitochondrial function in neuronal cells. J Cell Biol 161, 41-54.

5. Anderson, N.L., and Anderson, N.G. (2002). The human plasma proteome: history, character, and diagnostic prospects. Mol Cell Proteomics 1, 845-867.

6. Anfinsen, C.B. (1973). Principles that govern the folding of protein chains. Science 181, 223-230.

7. Archakov, A.I., Govorun, V.M., Dubanov, A.V., Ivanov, Y.D., Veselovsky, A.V., Lewi, P., and Janssen, P. (2003). Protein-protein interactions as a target for drugs in proteomics. Proteomics 3, 380-391.

8. Baek, S.H., Ohgi, K.A., Rose, D.W., Koo, E.H., Glass, C.K., and Rosenfeld, M.G. (2002). Exchange of N-CoR corepressor and Tip60 coactivator complexes links gene expression by NF-kappaB and beta-amyloid precursor protein. Cell 110, 55-67.

9. Bai, Y., Markham, K., Chen, F., Weerasekera, R., Watts, J., Horne, P., Wakutani, Y., Bagshaw, R., Mathews, P.M., Fraser, P.E., et al. (2008). The in vivo brain interactome of the amyloid precursor protein. Mol Cell Proteomics 7, 15-34.

10. Ballatore, C., Lee, V.M., and Trojanowski, J.Q. (2007). Tau-mediated neurodegeneration in Alzheimer's disease and related disorders. Nat Rev Neurosci 8, 663-672.

11. Belyaev, N.D., Kellett, K.A., Beckett, C., Makova, N.Z., Revett, T.J., Nalivaeva, N.N., Hooper, N.M., and Turner, A.J. (2010). The transcriptionally active amyloid precursor protein (APP) intracellular domain is preferentially produced from the 695 isoform of APP in a {beta}-secretase-dependent pathway. J Biol Chem 285, 41443-41454.

12. Bence, N.F., Sampat, R.M., and Kopito, R.R. (2001). Impairment of the ubiquitin-proteasome system by protein aggregation. Science 292, 1552-1555.

13. Benilova, I., Karran, E., and De Strooper, B. (2012). The toxic Abeta oligomer and Alzheimer's disease: an emperor in need of clothes. Nat Neurosci 15, 349-357.

14. Berke, S.J., and Paulson, H.L. (2003). Protein aggregation and the ubiquitin proteasome pathway: gaining the UPPer hand on neurodegeneration. Curr Opin Genet Dev 13, 253-261.

15. Berrios, G.E. (1990). Alzheimer's disease: A conceptual history. Int J Geriat Psychiatry 5, 355-365.

16. Bertram, L., Lill, C.M., and Tanzi, R.E. (2010). The genetics of Alzheimer disease: back to the future. Neuron 68, 270-281.

17. Bertram, L., McQueen, M.B., Mullin, K., Blacker, D., and Tanzi, R.E. (2007). Systematic meta-analyses of Alzheimer disease genetic association studies: the AlzGene database. Nat Genet 39, 17-23.

18. Bertram, L., and Tanzi, R.E. (2008). Thirty years of Alzheimer's disease genetics: the implications of systematic meta-analyses. Nat Rev Neurosci 9, 768-778.

19. Bilen, J., and Bonini, N.M. (2007). Genome-wide screen for modifiers of ataxin-3 neurodegeneration in Drosophila. PLoS Genet 3, 1950-1964.

20. Blagoev, B., Kratchmarova, I., Ong, S.E., Nielsen, M., Foster, L.J., and Mann, M. (2003). A proteomics strategy to elucidate functional protein-protein interactions applied to EGF signaling. Nat Biotechnol 21, 315-318.

21. Blazer, L.L., and Neubig, R.R. (2009). Small molecule protein-protein interaction inhibitors as CNS therapeutic agents: current progress and future hurdles. Neuropsychopharmacology 34, 126-141.

22. Bogdanovic, N., Zilmer, M., Zilmer, K., Rehema, A., and Karelson, E. (2001). The Swedish APP670/671 Alzheimer's disease mutation: the first evidence for strikingly increased oxidative injury in the temporal inferior cortex. Dement Geriatr Cogn Disord 12, 364-370.

23. Bosetti, F., Brizzi, F., Barogi, S., Mancuso, M., Siciliano, G., Tendi, E.A., Murri, L., Rapoport, S.I., and Solaini, G. (2002). Cytochrome c oxidase and mitochondrial F1F0-ATPase (ATP synthase) activities in platelets and brain from patients with Alzheimer's disease. Neurobiol Aging 23, 371-376.

24. Branco, J., Al-Ramahi, I., Ukani, L., Perez, A.M., Fernandez-Funez, P., Rincon-Limas, D., and Botas, J. (2008). Comparative analysis of genetic modifiers in Drosophila points to common and distinct mechanisms of pathogenesis among polyglutamine diseases. Hum Mol Genet 17, 376-390.

25. Brand, A.H., and Perrimon, N. (1993). Targeted gene expression as a means of altering cell fates and generating dominant phenotypes. Development 118, 401-415.

26. Brand, M., Ranish, J.A., Kummer, N.T., Hamilton, J., Igarashi, K., Francastel, C., Chi, T.H., Crabtree, G.R., Aebersold, R., and Groudine, M. (2004). Dynamic changes in transcription factor complexes during erythroid differentiation revealed by quantitative proteomics. Nat Struct Mol Biol 11, 73-80.

27. Bu, G. (2009). Apolipoprotein E and its receptors in Alzheimer's disease: pathways, pathogenesis and therapy. Nat Rev Neurosci 10, 333-344.

28. Buchberger, A., Bukau, B., and Sommer, T. (2010). Protein quality control in the cytosol and the endoplasmic reticulum: brothers in arms. Mol Cell 40, 238-252.

29. Burns, J.M., Cronk, B.B., Anderson, H.S., Donnelly, J.E., Thomas, G.P., Harsha, A., Brooks, W.M., and Swerdlow, R.H. (2008). Cardiorespiratory fitness and brain atrophy in early Alzheimer disease. Neurology 71, 210-216.

30. Castellani, R., Hirai, K., Aliev, G., Drew, K.L., Nunomura, A., Takeda, A., Cash, A.D., Obrenovich, M.E., Perry, G., and Smith, M.A. (2002). Role of mitochondrial dysfunction in Alzheimer's disease. J Neurosci Res 70, 357-360.

31. Cha, J.H. (2000). Transcriptional dysregulation in Huntington's disease. Trends Neurosci 23, 387-392.

32. Chatterjee, S., Sang, T.K., Lawless, G.M., and Jackson, G.R. (2009). Dissociation of tau toxicity and phosphorylation: role of GSK-3beta, MARK and Cdk5 in a Drosophila model. Hum Mol Genet 18, 164-177.

33. Chen, H.K., Fernandez-Funez, P., Acevedo, S.F., Lam, Y.C., Kaytor, M.D., Fernandez, M.H., Aitken, A., Skoulakis, E.M., Orr, H.T., Botas, J., et al. (2003). Interaction of Akt-phosphorylated ataxin-1 with 14-3-3 mediates neurodegeneration in spinocerebellar ataxia type 1. Cell 113, 457-468.

34. Chiti, F., and Dobson, C.M. (2006). Protein misfolding, functional amyloid, and human disease. Annu Rev Biochem 75, 333-366.

35. Choi, H., Larsen, B., Lin, Z.Y., Breitkreutz, A., Mellacheruvu, D., Fermin, D., Qin, Z.S., Tyers, M., Gingras, A.C., and Nesvizhskii, A.I. (2010). SAINT: probabilistic scoring of affinity purification-mass spectrometry data. Nat Methods 8, 70-73.

36. Chujo, T., Ohira, T., Sakaguchi, Y., Goshima, N., Nomura, N., Nagao, A., and Suzuki, T. (2012). LRPPRC/SLIRP suppresses PNPase-mediated mRNA decay and promotes polyadenylation in human mitochondria. Nucleic Acids Res.

37. Chung, M.Y., Ranum, L.P., Duvick, L.A., Servadio, A., Zoghbi, H.Y., and Orr, H.T. (1993). Evidence for a mechanism predisposing to intergenerational CAG repeat instability in spinocerebellar ataxia type I. Nat Genet 5, 254-258.

38. Clarke, G., Collins, R.A., Leavitt, B.R., Andrews, D.F., Hayden, M.R., Lumsden, C.J., and McInnes, R.R. (2000). A one-hit model of cell death in inherited neuronal degenerations. Nature 406, 195-199.

39. Cleary, J.P., Walsh, D.M., Hofmeister, J.J., Shankar, G.M., Kuskowski, M.A., Selkoe, D.J., and Ashe, K.H. (2005). Natural oligomers of the amyloid-beta protein specifically disrupt cognitive function. Nat Neurosci 8, 79-84.

40. Coen, K., Flannagan, R.S., Baron, S., Carraro-Lacroix, L.R., Wang, D., Vermeire, W., Michiels, C., Munck, S., Baert, V., Sugita, S., et al. (2012). Lysosomal calcium homeostasis defects, not proton pump defects, cause endo-lysosomal dysfunction in PSEN-deficient cells. J Cell Biol 198, 23-35.

41. Cohen, T.J., Guo, J.L., Hurtado, D.E., Kwong, L.K., Mills, I.P., Trojanowski, J.Q., and Lee, V.M. (2011). The acetylation of tau inhibits its function and promotes pathological tau aggregation. Nat Commun 2, 252.

42. Cooper, M.P., Qu, L., Rohas, L.M., Lin, J., Yang, W., Erdjument-Bromage, H., Tempst, P., and Spiegelman, B.M. (2006). Defects in energy homeostasis in Leigh syndrome French Canadian variant through PGC-1alpha/LRP130 complex. Genes Dev 20, 2996-3009.

43. Corder, E.H., Saunders, A.M., Strittmatter, W.J., Schmechel, D.E., Gaskell, P.C., Small, G.W., Roses, A.D., Haines, J.L., and Pericak-Vance, M.A. (1993). Gene dose of apolipoprotein E type 4 allele and the risk of Alzheimer's disease in late onset families. Science 261, 921-923.

44. Corral-Debrinski, M., Horton, T., Lott, M.T., Shoffner, J.M., McKee, A.C., Beal, M.F., Graham, B.H., and Wallace, D.C. (1994). Marked changes in mitochondrial DNA deletion levels in Alzheimer brains. Genomics 23, 471-476.

45. Coskun, P.E., Beal, M.F., and Wallace, D.C. (2004). Alzheimer's brains harbor somatic mtDNA control-region mutations that suppress mitochondrial transcription and replication. Proc Natl Acad Sci U S A 101, 10726-10731.

46. Coux, O., Tanaka, K., and Goldberg, A.L. (1996). Structure and functions of the 20S and 26S proteasomes. Annu Rev Biochem 65, 801-847.

47. Cox, J., and Mann, M. (2008). MaxQuant enables high peptide identification rates, individualized p.p.b.-range mass accuracies and proteome-wide protein quantification. Nat Biotechnol 26, 1367-1372.

48. Cox, J., Neuhauser, N., Michalski, A., Scheltema, R.A., Olsen, J.V., and Mann, M. (2011a). Andromeda: a peptide search engine integrated into the MaxQuant environment. J Proteome Res 10, 1794-1805.

49. Cox, J., and Mann, M. (2011b). Quantitative, high-resolution proteomics for data-driven systems biology. Annu Rev Biochem 80, 273-299.

50. Cox, J., Matic, I., Hilger, M., Nagaraj, N., Selbach, M., Olsen, J.V., and Mann, M. (2009). A practical guide to the MaxQuant computational platform for SILAC-based quantitative proteomics. Nat Protoc 4, 698-705.

51. Craft, S., Peskind, E., Schwartz, M.W., Schellenberg, G.D., Raskind, M., and Porte, D., Jr. (1998). Cerebrospinal fluid and plasma insulin levels in Alzheimer's disease: relationship to severity of dementia and apolipoprotein E genotype. Neurology 50, 164-168.

52. Cravatt, B.F., Simon, G.M., and Yates, J.R., 3rd (2007). The biological impact of mass-spectrometry-based proteomics. Nature 450, 991-1000.

53. Cuervo, A.M., Stefanis, L., Fredenburg, R., Lansbury, P.T., and Sulzer, D. (2004). Impaired degradation of mutant alpha-synuclein by chaperone-mediated autophagy. Science 305, 1292-1295.

54. Davranche, A., Aviolat, H., Zeder-Lutz, G., Busso, D., Altschuh, D., Trottier, Y., and Klein, F.A. (2011). Huntingtin affinity for partners is not changed by polyglutamine length: aggregation itself triggers aberrant interactions. Hum Mol Genet 20, 2795-2806.

55. de Chiara, C., Menon, R.P., Strom, M., Gibson, T.J., and Pastore, A. (2009). Phosphorylation of S776 and 14-3-3 binding modulate ataxin-1 interaction with splicing factors. PLoS One 4, e8372.

56. De Strooper, B., and Annaert, W. (2000). Proteolytic processing and cell biological functions of the amyloid precursor protein. J Cell Sci 113 (Pt 11), 1857-1870.

57. Dill, K.A., Ozkan, S.B., Shell, M.S., and Weikl, T.R. (2008). The protein folding problem. Annu Rev Biophys 37, 289-316.

58. Dobson, C.M. (2003). Protein folding and misfolding. Nature 426, 884-890.

59. Dobson, C.M., Sali, A., and Karplus, M. (1998). Protein Folding: A Perspective from Theory and Experiment. Angewandte Chemie Int Ed 37, 868-893.

60. Domon, B., and Aebersold, R. (2006). Mass spectrometry and protein analysis. Science 312, 212-217.

61. Eisele, Y.S., Obermuller, U., Heilbronner, G., Baumann, F., Kaeser, S.A., Wolburg, H., Walker, L.C., Staufenbiel, M., Heikenwalder, M., and Jucker, M. (2010). Peripherally applied Abeta-containing inoculates induce cerebral beta-amyloidosis. Science 330, 980-982.

62. Ellis, M.C., O'Neill, E.M., and Rubin, G.M. (1993). Expression of Drosophila glass protein and evidence for negative regulation of its activity in non-neuronal cells by another DNA-binding protein. Development 119, 855-865.

63. Emamian, E.S., Kaytor, M.D., Duvick, L.A., Zu, T., Tousey, S.K., Zoghbi, H.Y., Clark, H.B., and Orr, H.T. (2003). Serine 776 of ataxin-1 is critical for polyglutamine-induced disease in SCA1 transgenic mice. Neuron 38, 375-387.

64. Ewing, R.M., Chu, P., Elisma, F., Li, H., Taylor, P., Climie, S., McBroom-Cerajewski, L., Robinson, M.D., O'Connor, L., Li, M., et al. (2007). Large-scale mapping of human protein-protein interactions by mass spectrometry. Mol Syst Biol 3, 89.

65. Fernandez-Funez, P., Nino-Rosales, M.L., de Gouyon, B., She, W.C., Luchak, J.M., Martinez, P., Turiegano, E., Benito, J., Capovilla, M., Skinner, P.J., et al. (2000). Identification of genes that modify ataxin-1-induced neurodegeneration. Nature 408, 101-106.

66. Fields, S., and Song, O. (1989). A novel genetic system to detect protein-protein interactions. Nature 340, 245-246.

67. Fink, A.L. (1999). Chaperone-mediated protein folding. Physiol Rev 79, 425-449.

68. Friedlander, R., Jarosch, E., Urban, J., Volkwein, C., and Sommer, T. (2000). A regulatory link between ER-associated protein degradation and the unfolded-protein response. Nat Cell Biol 2, 379-384.

69. Gandhi, S., and Wood, N.W. (2010). Genome-wide association studies: the key to unlocking neurodegeneration? Nat Neurosci 13, 789-794.

70. Gandy, S., Simon, A.J., Steele, J.W., Lublin, A.L., Lah, J.J., Walker, L.C., Levey, A.I., Krafft, G.A., Levy, E., Checler, F., et al. (2010). Days to criterion as an indicator of toxicity associated with human Alzheimer amyloid-beta oligomers. Ann Neurol 68, 220-230.

71. Gao, Y., and Pimplikar, S.W. (2001). The gamma -secretase-cleaved C-terminal fragment of amyloid precursor protein mediates signaling to the nucleus. Proc Natl Acad Sci U S A 98, 14979-14984.

72. Gatchel, J.R., and Zoghbi, H.Y. (2005). Diseases of unstable repeat expansion: mechanisms and common principles. Nat Rev Genet 6, 743-755.

73. Gavin, A.C., Aloy, P., Grandi, P., Krause, R., Boesche, M., Marzioch, M., Rau, C., Jensen, L.J., Bastuck, S., Dumpelfeld, B., et al. (2006). Proteome survey reveals modularity of the yeast cell machinery. Nature 440, 631-636.

74. Gavin, A.C., Maeda, K., and Kuhner, S. (2011). Recent advances in charting protein-protein interaction: mass spectrometry-based approaches. Curr Opin Biotechnol 22, 42-49.

75. Geiger, T., Cox, J., Ostasiewicz, P., Wisniewski, J.R., and Mann, M. (2010). Super-SILAC mix for quantitative proteomics of human tumor tissue. Nat Methods 7, 383-385.

76. Geiger, T., Wehner, A., Schaab, C., Cox, J., and Mann, M. (2012). Comparative proteomic analysis of eleven common cell lines reveals ubiquitous but varying expression of most proteins. Mol Cell Proteomics 11, M111 014050.

77. Gingras, A.C., Gstaiger, M., Raught, B., and Aebersold, R. (2007). Analysis of protein complexes using mass spectrometry. Nat Rev Mol Cell Biol 8, 645-654.

78. Giuffrida, M.L., Caraci, F., De Bona, P., Pappalardo, G., Nicoletti, F., Rizzarelli, E., and Copani, A. (2010). The monomer state of beta-amyloid: where the Alzheimer's disease protein meets physiology. Rev Neurosci 21, 83-93.

79. Glickman, M.H., and Ciechanover, A. (2002). The ubiquitin-proteasome proteolytic pathway: destruction for the sake of construction. Physiol Rev 82, 373-428.

80. Goehler, H., Lalowski, M., Stelzl, U., Waelter, S., Stroedicke, M., Worm, U., Droege, A., Lindenberg, K.S., Knoblich, M., Haenig, C., et al. (2004). A protein interaction network links GIT1, an enhancer of huntingtin aggregation, to Huntington's disease. Mol Cell 15, 853-865.

81. Gohil, V.M., Nilsson, R., Belcher-Timme, C.A., Luo, B., Root, D.E., and Mootha, V.K. (2010). Mitochondrial and nuclear genomic responses to loss of LRPPRC expression. J Biol Chem 285, 13742-13747.

82. Gouw, J.W., Tops, B.B., and Krijgsveld, J. (2011). Metabolic labeling of model organisms using heavy nitrogen (15N). Methods Mol Biol 753, 29-42.

83. Gruhler, A., Olsen, J.V., Mohammed, S., Mortensen, P., Faergeman, N.J., Mann, M., and Jensen, O.N. (2005). Quantitative phosphoproteomics applied to the yeast pheromone signaling pathway. Mol Cell Proteomics 4, 310-327.

84. Grundke-Iqbal, I., Iqbal, K., Tung, Y.C., Quinlan, M., Wisniewski, H.M., and Binder, L.I. (1986). Abnormal phosphorylation of the microtubule-associated protein tau (tau) in Alzheimer cytoskeletal pathology. Proc Natl Acad Sci U S A 83, 4913-4917.

85. Guo, Q., Sopher, B.L., Furukawa, K., Pham, D.G., Robinson, N., Martin, G.M., and Mattson, M.P. (1997). Alzheimer's presenilin mutation sensitizes neural cells to apoptosis induced by trophic factor withdrawal and amyloid beta-peptide: involvement of calcium and oxyradicals. J Neurosci 17, 4212-4222.

86. Gygi, S.P., Rist, B., Gerber, S.A., Turecek, F., Gelb, M.H., and Aebersold, R. (1999). Quantitative analysis of complex protein mixtures using isotope-coded affinity tags. Nat Biotechnol 17, 994-999.

87. Hafner, M., Landthaler, M., Burger, L., Khorshid, M., Hausser, J., Berninger, P., Rothballer, A., Ascano, M., Jr., Jungkamp, A.C., Munschauer, M., et al. (2010). Transcriptome-wide identification of RNA-binding protein and microRNA target sites by PAR-CLIP. Cell 141, 129-141.

88. Hamid, R., Kilger, E., Willem, M., Vassallo, N., Kostka, M., Bornhovd, C., Reichert, A.S., Kretzschmar, H.A., Haass, C., and Herms, J. (2007). Amyloid precursor protein intracellular domain modulates cellular calcium homeostasis and ATP content. J Neurochem 102, 1264-1275.

89. Hardy, J., and Selkoe, D.J. (2002). The amyloid hypothesis of Alzheimer's disease: progress and problems on the road to therapeutics. Science 297, 353-356.

90. Hardy, J.A., and Higgins, G.A. (1992). Alzheimer's disease: the amyloid cascade hypothesis. Science 256, 184-185.

91. Harjes, P., and Wanker, E.E. (2003). The hunt for huntingtin function: interaction partners tell many different stories. Trends Biochem Sci 28, 425-433.

92. Harold, D., Abraham, R., Hollingworth, P., Sims, R., Gerrish, A., Hamshere, M.L., Pahwa, J.S., Moskvina, V., Dowzell, K., Williams, A., et al. (2009). Genome-wide association study identifies variants at CLU and PICALM associated with Alzheimer's disease. Nat Genet 41, 1088-1093.

93. Heath, M.M., Rixon, K.C., and Harding, J.J. (1996). Glycation-induced inactivation of malate dehydrogenase protection by aspirin and a lens molecular chaperone, alpha-crystallin. Biochim Biophys Acta 1315, 176-184.

94. Heinig, M., Petretto, E., Wallace, C., Bottolo, L., Rotival, M., Lu, H., Li, Y., Sarwar, R., Langley, S.R., Bauerfeind, A., et al. (2010). A trans-acting locus regulates an anti-viral expression network and type 1 diabetes risk. Nature 467, 460-464.

95. Hershko, A., and Ciechanover, A. (1998). The ubiquitin system. Annu Rev Biochem 67, 425-479.

96. Higgins, L.S., Murphy, G.M., Jr., Forno, L.S., Catalano, R., and Cordell, B. (1996). P3 beta-amyloid peptide has a unique and potentially pathogenic immunohistochemical profile in Alzheimer's disease brain. Am J Pathol 149, 585-596.

97. Hirabayashi, M., Inoue, K., Tanaka, K., Nakadate, K., Ohsawa, Y., Kamei, Y., Popiel, A.H., Sinohara, A., Iwamatsu, A., Kimura, Y., et al. (2001). VCP/p97 in abnormal protein aggregates, cytoplasmic vacuoles, and cell death, phenotypes relevant to neurodegeneration. Cell Death Differ 8, 977-984.

98. Hsiao, K., Chapman, P., Nilsen, S., Eckman, C., Harigaya, Y., Younkin, S., Yang, F., and Cole, G. (1996). Correlative memory deficits, Abeta elevation, and amyloid plaques in transgenic mice. Science 274, 99-102.

99. Huang, Y., and Mucke, L. (2012). Alzheimer mechanisms and therapeutic strategies. Cell 148, 1204-1222.

100. Ideker, T., and Sharan, R. (2008). Protein networks in disease. Genome Res 18, 644-652.

101. Iqbal, K., Liu, F., Gong, C.X., and Grundke-Iqbal, I. (2010). Tau in Alzheimer disease and related tauopathies. Curr Alzheimer Res 7, 656-664.

102. Jarvik, J.W., and Telmer, C.A. (1998). Epitope tagging. Annu Rev Genet 32, 601-618.

103. Jin, J., Li, G.J., Davis, J., Zhu, D., Wang, Y., Pan, C., and Zhang, J. (2007). Identification of novel proteins associated with both alpha-synuclein and DJ-1. Mol Cell Proteomics 6, 845-859.

104. Johnson, D.K., Wilkins, C.H., and Morris, J.C. (2006). Accelerated weight loss may precede diagnosis in Alzheimer disease. Arch Neurol 63, 1312-1317.

105. Johnston, J.A., Ward, C.L., and Kopito, R.R. (1998). Aggresomes: a cellular response to misfolded proteins. J Cell Biol 143, 1883-1898.

106. Jordan, F., Nguyen, T.P., and Liu, W.C. (2012). Studying protein-protein interaction networks: a systems view on diseases. Brief Funct Genomics.

107. Kaltenbach, L.S., Romero, E., Becklin, R.R., Chettier, R., Bell, R., Phansalkar, A., Strand, A., Torcassi, C., Savage, J., Hurlburt, A., et al. (2007). Huntingtin interacting proteins are genetic modifiers of neurodegeneration. PLoS Genet 3, e82.

108. Kane, M.D., Lipinski, W.J., Callahan, M.J., Bian, F., Durham, R.A., Schwarz, R.D., Roher, A.E., and Walker, L.C. (2000). Evidence for seeding of beta -amyloid by intracerebral infusion of Alzheimer brain extracts in beta -amyloid precursor protein-transgenic mice. J Neurosci 20, 3606-3611.

109. Kang, S., and Hong, S. (2009). Molecular pathogenesis of spinocerebellar ataxia type 1 disease. Mol Cells 27, 621-627.

110. Kato, S., Horiuchi, S., Liu, J., Cleveland, D.W., Shibata, N., Nakashima, K., Nagai, R., Hirano, A., Takikawa, M., Kato, M., et al. (2000). Advanced glycation endproduct-modified superoxide dismutase-1 (SOD1)-positive inclusions are common to familial amyotrophic lateral sclerosis patients with SOD1 gene mutations and transgenic mice expressing human SOD1 with a G85R mutation. Acta Neuropathol 100, 490-505.

111. Kazemi-Esfarjani, P., and Benzer, S. (2000). Genetic suppression of polyglutamine toxicity in Drosophila. Science 287, 1837-1840.

112. Kenworthy, A.K. (2001). Imaging protein-protein interactions using fluorescence resonance energy transfer microscopy. Methods 24, 289-296.

113. Khan, S.M., Cassarino, D.S., Abramova, N.N., Keeney, P.M., Borland, M.K., Trimmer, P.A., Krebs, C.T., Bennett, J.C., Parks, J.K., Swerdlow, R.H., et al. (2000). Alzheimer's disease cybrids replicate beta-amyloid abnormalities through cell death pathways. Ann Neurol 48, 148-155.

114. Kil, I.S., Lee, J.H., Shin, A.H., and Park, J.W. (2004). Glycation-induced inactivation of NADP(+)-dependent isocitrate dehydrogenase: implications for diabetes and aging. Free Radic Biol Med 37, 1765-1778.

115. Kim, H.S., Kim, E.M., Lee, J.P., Park, C.H., Kim, S., Seo, J.H., Chang, K.A., Yu, E., Jeong, S.J., Chong, Y.H., et al. (2003). C-terminal fragments of amyloid precursor protein exert neurotoxicity by inducing glycogen synthase kinase-3beta expression. FASEB J 17, 1951-1953.

116. King, M.E., Kan, H.M., Baas, P.W., Erisir, A., Glabe, C.G., and Bloom, G.S. (2006). Tau-dependent microtubule disassembly initiated by prefibrillar beta-amyloid. J Cell Biol 175, 541-546.

117. Kishore, S., Luber, S., and Zavolan, M. (2010). Deciphering the role of RNA-binding proteins in the post-transcriptional control of gene expression. Brief Funct Genomics 9, 391-404.

118. Klement, I.A., Skinner, P.J., Kaytor, M.D., Yi, H., Hersch, S.M., Clark, H.B., Zoghbi, H.Y., and Orr, H.T. (1998). Ataxin-1 nuclear localization and aggregation: role in polyglutamine-induced disease in SCA1 transgenic mice. Cell 95, 41-53.

119. Kocher, T., and Superti-Furga, G. (2007). Mass spectrometry-based functional proteomics: from molecular machines to protein networks. Nat Methods 4, 807-815.

120. Kruger, M., Moser, M., Ussar, S., Thievessen, I., Luber, C.A., Forner, F., Schmidt, S., Zanivan, S., Fassler, R., and Mann, M. (2008). SILAC mouse for quantitative proteomics uncovers kindlin-3 as an essential factor for red blood cell function. Cell 134, 353-364.

121. LaFontaine, M.A., Mattson, M.P., and Butterfield, D.A. (2002). Oxidative stress in synaptosomal proteins from mutant presenilin-1 knock-in mice: implications for familial Alzheimer's disease. Neurochem Res 27, 417-421.

122. Lage, K., Karlberg, E.O., Storling, Z.M., Olason, P.I., Pedersen, A.G., Rigina, O., Hinsby, A.M., Tumer, Z., Pociot, F., Tommerup, N., et al. (2007). A human phenome-interactome network of protein complexes implicated in genetic disorders. Nat Biotechnol 25, 309-316.

123. Lalowski, M., Golabek, A., Lemere, C.A., Selkoe, D.J., Wisniewski, H.M., Beavis, R.C., Frangione, B., and Wisniewski, T. (1996). The "nonamyloidogenic" p3 fragment (amyloid beta17-42) is a major constituent of Down's syndrome cerebellar preamyloid. J Biol Chem 271, 33623-33631.

124. Lam, Y.C., Bowman, A.B., Jafar-Nejad, P., Lim, J., Richman, R., Fryer, J.D., Hyun, E.D., Duvick, L.A., Orr, H.T., Botas, J., et al. (2006). ATAXIN-1 interacts with the repressor Capicua in its native complex to cause SCA1 neuropathology. Cell 127, 1335-1347.

125. Lansbury, P.T., Jr. (1997). Structural neurology: are seeds at the root of neuronal degeneration? Neuron 19, 1151-1154.

126. Larance, M., Bailly, A.P., Pourkarimi, E., Hay, R.T., Buchanan, G., Coulthurst, S., Xirodimas, D.P., Gartner, A., and Lamond, A.I. (2011). Stable-isotope labeling with amino acids in nematodes. Nat Methods 8, 849-851.

127. Lee, J.H., Yu, W.H., Kumar, A., Lee, S., Mohan, P.S., Peterhoff, C.M., Wolfe, D.M., Martinez-Vicente, M., Massey, A.C., Sovak, G., et al. (2010). Lysosomal proteolysis and autophagy require presenilin 1 and are disrupted by Alzheimer-related PS1 mutations. Cell 141, 1146-1158.

128. Leem, J.Y., Saura, C.A., Pietrzik, C., Christianson, J., Wanamaker, C., King, L.T., Veselits, M.L., Tomita, T., Gasparini, L., Iwatsubo, T., et al. (2002). A role for presenilin 1 in regulating the delivery of amyloid precursor protein to the cell surface. Neurobiol Dis 11, 64-82.

129. Levinthal, C. (1968). Are there pathways for protein folding? J Chim Phys 65, 44-45.

130. Li, H., Wetten, S., Li, L., St Jean, P.L., Upmanyu, R., Surh, L., Hosford, D., Barnes, M.R., Briley, J.D., Borrie, M., et al. (2008). Candidate single-nucleotide polymorphisms from a genomewide association study of Alzheimer disease. Arch Neurol 65, 45-53.

131. Lim, J., Crespo-Barreto, J., Jafar-Nejad, P., Bowman, A.B., Richman, R., Hill, D.E., Orr, H.T., and Zoghbi, H.Y. (2008). Opposing effects of polyglutamine expansion on native protein complexes contribute to SCA1. Nature 452, 713-718.

132. Lim, J., Hao, T., Shaw, C., Patel, A.J., Szabo, G., Rual, J.F., Fisk, C.J., Li, N., Smolyar, A., Hill, D.E., et al. (2006). A protein-protein interaction network for human inherited ataxias and disorders of Purkinje cell degeneration. Cell 125, 801-814.

133. Limviphuvadh, V., Tanaka, S., Goto, S., Ueda, K., and Kanehisa, M. (2007). The commonality of protein interaction networks determined in neurodegenerative disorders (NDDs). Bioinformatics 23, 2129-2138.

134. Lin, M.T., and Beal, M.F. (2006). Mitochondrial dysfunction and oxidative stress in neurodegenerative diseases. Nature 443, 787-795.

135. Looso, M., Borchardt, T., Kruger, M., and Braun, T. (2010). Advanced identification of proteins in uncharacterized proteomes by pulsed in vivo stable isotope labeling-based mass spectrometry. Mol Cell Proteomics 9, 1157-1166.

136. Lu, T., Pan, Y., Kao, S.Y., Li, C., Kohane, I., Chan, J., and Yankner, B.A. (2004). Gene regulation and DNA damage in the ageing human brain. Nature 429, 883-891.

137. Ma, Y., Creanga, A., Lum, L., and Beachy, P.A. (2006). Prevalence of off-target effects in Drosophila RNA interference screens. Nature 443, 359-363.

138. Makarov, A. (2000). Electrostatic axially harmonic orbital trapping: a high-performance technique of mass analysis. Anal Chem 72, 1156-1162.

139. Makarov, A., Denisov, E., Kholomeev, A., Balschun, W., Lange, O., Strupat, K., and Horning, S. (2006a). Performance evaluation of a hybrid linear ion trap/orbitrap mass spectrometer. Anal Chem 78, 2113-2120.

140. Makarov, A., Denisov, E., Lange, O., and Horning, S. (2006b). Dynamic range of mass accuracy in LTQ Orbitrap hybrid mass spectrometer. J Am Soc Mass Spectrom 17, 977-982.

141. Mallick, P., and Kuster, B. (2010). Proteomics: a pragmatic perspective. Nat Biotechnol 28, 695-709.

142. Malovannaya, A., Lanz, R.B., Jung, S.Y., Bulynko, Y., Le, N.T., Chan, D.W., Ding, C., Shi, Y., Yucer, N., Krenciute, G., et al. (2011). Analysis of the human endogenous coregulator complexome. Cell 145, 787-799.

143. Manczak, M., Anekonda, T.S., Henson, E., Park, B.S., Quinn, J., and Reddy, P.H. (2006). Mitochondria are a direct site of A beta accumulation in Alzheimer's disease neurons: implications for free radical generation and oxidative damage in disease progression. Hum Mol Genet 15, 1437-1449.

144. Markesbery, W.R. (1997). Oxidative stress hypothesis in Alzheimer's disease. Free Radic Biol Med 23, 134-147.

145. Marques, C.A., Keil, U., Bonert, A., Steiner, B., Haass, C., Muller, W.E., and Eckert, A. (2003). Neurotoxic mechanisms caused by the Alzheimer's disease-linked Swedish amyloid precursor protein mutation: oxidative stress, caspases, and the JNK pathway. J Biol Chem 278, 28294-28302.

146. Martin, J.B. (1999). Molecular basis of the neurodegenerative disorders. N Engl J Med 340, 1970-1980.

147. Martinez-Vicente, M., and Cuervo, A.M. (2007). Autophagy and neurodegeneration: when the cleaning crew goes on strike. Lancet Neurol 6, 352-361.

148. McCarthy, M.I., Abecasis, G.R., Cardon, L.R., Goldstein, D.B., Little, J., Ioannidis, J.P., and Hirschhorn, J.N. (2008). Genome-wide association studies for complex traits: consensus, uncertainty and challenges. Nat Rev Genet 9, 356-369.

149. McLean, C.A., Cherny, R.A., Fraser, F.W., Fuller, S.J., Smith, M.J., Beyreuther, K., Bush, A.I., and Masters, C.L. (1999). Soluble pool of Abeta amyloid as a determinant of severity of neurodegeneration in Alzheimer's disease. Ann Neurol 46, 860-866.

150. Meyer-Luehmann, M., Coomaraswamy, J., Bolmont, T., Kaeser, S., Schaefer, C., Kilger, E., Neuenschwander, A., Abramowski, D., Frey, P., Jaton, A.L., et al. (2006). Exogenous induction of cerebral beta-amyloidogenesis is governed by agent and host. Science 313, 1781-1784.

151. Michalski, A., Damoc, E., Hauschild, J.P., Lange, O., Wieghaus, A., Makarov, A., Nagaraj, N., Cox, J., Mann, M., and Horning, S. (2011). Mass spectrometry-based proteomics using Q Exactive, a high-performance benchtop quadrupole Orbitrap mass spectrometer. Mol Cell Proteomics 10, M111 011015.

152. Mili, S., and Pinol-Roma, S. (2003). LRP130, a pentatricopeptide motif protein with a noncanonical RNA-binding domain, is bound in vivo to mitochondrial and nuclear RNAs. Mol Cell Biol 23, 4972-4982.

153. Moffat, J., Reiling, J.H., and Sabatini, D.M. (2007). Off-target effects associated with long dsRNAs in Drosophila RNAi screens. Trends Pharmacol Sci 28, 149-151.

154. Mohorko, E., Glockshuber, R., and Aebi, M. (2011). Oligosaccharyltransferase: the central enzyme of N-linked protein glycosylation. J Inherit Metab Dis 34, 869-878.

155. Molina, H., Yang, Y., Ruch, T., Kim, J.W., Mortensen, P., Otto, T., Nalli, A., Tang, Q.Q., Lane, M.D., Chaerkady, R., et al. (2009). Temporal profiling of the adipocyte proteome during differentiation using a five-plex SILAC based strategy. J Proteome Res 8, 48-58.

156. Mootha, V.K., Lepage, P., Miller, K., Bunkenborg, J., Reich, M., Hjerrild, M., Delmonte, T., Villeneuve, A., Sladek, R., Xu, F., et al. (2003). Identification of a gene causing human cytochrome c oxidase deficiency by integrative genomics. Proc Natl Acad Sci U S A 100, 605-610.

157. Morgan, P.E., Dean, R.T., and Davies, M.J. (2002). Inactivation of cellular enzymes by carbonyls and protein-bound glycation/glycoxidation products. Arch Biochem Biophys 403, 259-269.

158. Morimoto, R.I. (2008). Proteotoxic stress and inducible chaperone networks in neurodegenerative disease and aging. Genes Dev 22, 1427-1438.

159. Moses, K., and Rubin, G.M. (1991). Glass encodes a site-specific DNA-binding protein that is regulated in response to positional signals in the developing Drosophila eye. Genes Dev 5, 583-593.

160. Mousson, F., Kolkman, A., Pijnappel, W.W., Timmers, H.T., and Heck, A.J. (2008). Quantitative proteomics reveals regulation of dynamic components within TATA-binding protein (TBP) transcription complexes. Mol Cell Proteomics 7, 845-852.

161. Muchowski, P.J., and Wacker, J.L. (2005). Modulation of neurodegeneration by molecular chaperones. Nat Rev Neurosci 6, 11-22.

162. Mucke, L. (2009). Neuroscience: Alzheimer's disease. Nature 461, 895-897.

163. Munch, G., Shepherd, C.E., McCann, H., Brooks, W.S., Kwok, J.B., Arendt, T., Hallupp, M., Schofield, P.R., Martins, R.N., and Halliday, G.M. (2002). Intraneuronal advanced glycation endproducts in presenilin-1 Alzheimer's disease. Neuroreport 13, 601-604.

164. Munch, G., Thome, J., Foley, P., Schinzel, R., and Riederer, P. (1997). Advanced glycation endproducts in ageing and Alzheimer's disease. Brain Res Brain Res Rev 23, 134-143.

165. Muqit, M.M., and Feany, M.B. (2002). Modelling neurodegenerative diseases in Drosophila: a fruitful approach? Nat Rev Neurosci 3, 237-243.

166. Naslund, J., Haroutunian, V., Mohs, R., Davis, K.L., Davies, P., Greengard, P., and Buxbaum, J.D. (2000). Correlation between elevated levels of amyloid beta-peptide in the brain and cognitive decline. JAMA 283, 1571-1577.

167. Nesvizhskii, A.I., and Aebersold, R. (2005). Interpretation of shotgun proteomic data: the protein inference problem. Mol Cell Proteomics 4, 1419-1440.

168. Nunomura, A., Perry, G., Aliev, G., Hirai, K., Takeda, A., Balraj, E.K., Jones, P.K., Ghanbari, H., Wataya, T., Shimohama, S., et al. (2001). Oxidative damage is the earliest event in Alzheimer disease. J Neuropathol Exp Neurol 60, 759-767.

169. Nyabi, O., Bentahir, M., Horre, K., Herreman, A., Gottardi-Littell, N., Van Broeckhoven, C., Merchiers, P., Spittaels, K., Annaert, W., and De Strooper, B. (2003). Presenilins mutated at Asp-257 or Asp-385 restore Pen-2 expression and Nicastrin glycosylation but remain catalytically inactive in the absence of wild type Presenilin. J Biol Chem 278, 43430-43436.

170. Okochi, M., Walter, J., Koyama, A., Nakajo, S., Baba, M., Iwatsubo, T., Meijer, L., Kahle, P.J., and Haass, C. (2000). Constitutive phosphorylation of the Parkinson's disease associated alpha-synuclein. J Biol Chem 275, 390-397.

171. Olsen, J.V., Blagoev, B., Gnad, F., Macek, B., Kumar, C., Mortensen, P., and Mann, M. (2006). Global, in vivo, and site-specific phosphorylation dynamics in signaling networks. Cell 127, 635-648.

172. Olsen, J.V., Macek, B., Lange, O., Makarov, A., Horning, S., and Mann, M. (2007). Higher-energy C-trap dissociation for peptide modification analysis. Nat Methods 4, 709-712.

173. Ong, S.E., Blagoev, B., Kratchmarova, I., Kristensen, D.B., Steen, H., Pandey, A., and Mann, M. (2002). Stable isotope labeling by amino acids in cell culture, SILAC, as a simple and accurate approach to expression proteomics. Mol Cell Proteomics 1, 376-386.

174. Ong, S.E., and Mann, M. (2006). A practical recipe for stable isotope labeling by amino acids in cell culture (SILAC). Nat Protoc 1, 2650-2660.

175. Orr, H.T., Chung, M.Y., Banfi, S., Kwiatkowski, T.J., Jr., Servadio, A., Beaudet, A.L., McCall, A.E., Duvick, L.A., Ranum, L.P., and Zoghbi, H.Y. (1993). Expansion of an unstable trinucleotide CAG repeat in spinocerebellar ataxia type 1. Nat Genet 4, 221-226.

176. Pandey, A., and Mann, M. (2000). Proteomics to study genes and genomes. Nature 405, 837-846.

177. Park, S.K., Liao, L., Kim, J.Y., and Yates, J.R., 3rd (2009). A computational approach to correct arginine-to-proline conversion in quantitative proteomics. Nat Methods 6, 184-185.

178. Parker, W.D., Jr. (1991). Cytochrome oxidase deficiency in Alzheimer's disease. Ann N Y Acad Sci 640, 59-64.

179. Paul, F.E., Hosp, F., and Selbach, M. (2011). Analyzing protein-protein interactions by quantitative mass spectrometry. Methods 54, 387-395.

180. Pflieger, D., Junger, M.A., Muller, M., Rinner, O., Lee, H., Gehrig, P.M., Gstaiger, M., and Aebersold, R. (2008). Quantitative proteomic analysis of protein complexes: concurrent identification of interactors and their state of phosphorylation. Mol Cell Proteomics 7, 326-346.

181. Pierce, M.M., Raman, C.S., and Nall, B.T. (1999). Isothermal titration calorimetry of protein-protein interactions. Methods 19, 213-221.

182. Pietkiewicz, J., Gamian, A., Staniszewska, M., and Danielewicz, R. (2009). Inhibition of human muscle-specific enolase by methylglyoxal and irreversible formation of advanced glycation end products. J Enzyme Inhib Med Chem 24, 356-364.

183. Portelius, E., Andreasson, U., Ringman, J.M., Buerger, K., Daborg, J., Buchhave, P., Hansson, O., Harmsen, A., Gustavsson, M.K., Hanse, E., et al. (2010). Distinct cerebrospinal fluid amyloid beta peptide signatures in sporadic and PSEN1 A431E-associated familial Alzheimer's disease. Mol Neurodegener 5, 2.

184. Pratico, D., Uryu, K., Leight, S., Trojanoswki, J.Q., and Lee, V.M. (2001). Increased lipid peroxidation precedes amyloid plaque formation in an animal model of Alzheimer amyloidosis. J Neurosci 21, 4183-4187.

185. Querfurth, H.W., and LaFerla, F.M. (2010). Alzheimer's disease. N Engl J Med 362, 329-344.

186. Rappsilber, J., Ishihama, Y., and Mann, M. (2003). Stop and go extraction tips for matrix-assisted laser desorption/ionization, nanoelectrospray, and LC/MS sample pretreatment in proteomics. Anal Chem 75, 663-670.

187. Rechavi, O., Kalman, M., Fang, Y., Vernitsky, H., Jacob-Hirsch, J., Foster, L.J., Kloog, Y., and Goldstein, I. (2010). Trans-SILAC: sorting out the non-cell-autonomous proteome. Nat Methods 7, 923-927.

188. Rigaut, G., Shevchenko, A., Rutz, B., Wilm, M., Mann, M., and Seraphin, B. (1999). A generic protein purification method for protein complex characterization and proteome exploration. Nat Biotechnol 17, 1030-1032.

189. Ross, C.A., and Poirier, M.A. (2004). Protein aggregation and neurodegenerative disease. Nat Med 10 Suppl, S10-17.

190. Ross, C.A., and Poirier, M.A. (2005). Opinion: What is the role of protein aggregation in neurodegeneration? Nat Rev Mol Cell Biol 6, 891-898.

191. Ross, P.L., Huang, Y.N., Marchese, J.N., Williamson, B., Parker, K., Hattan, S., Khainovski, N., Pillai, S., Dey, S., Daniels, S., et al. (2004). Multiplexed protein quantitation in Saccharomyces cerevisiae using amine-reactive isobaric tagging reagents. Mol Cell Proteomics 3, 1154-1169.

192. Rossin, E.J., Lage, K., Raychaudhuri, S., Xavier, R.J., Tatar, D., Benita, Y., Cotsapas, C., and Daly, M.J. (2011). Proteins encoded in genomic regions associated with immune-mediated disease physically interact and suggest underlying biology. PLoS Genet 7, e1001273.

193. Rubinsztein, D.C. (2006). The roles of intracellular protein-degradation pathways in neurodegeneration. Nature 443, 780-786.

194. Rubinsztein, D.C., Leggo, J., Coles, R., Almqvist, E., Biancalana, V., Cassiman, J.J., Chotai, K., Connarty, M., Crauford, D., Curtis, A., et al. (1996). Phenotypic characterization of individuals with 30-40 CAG repeats in the Huntington disease (HD) gene reveals HD cases with 36 repeats and apparently normal elderly individuals with 36-39 repeats. Am J Hum Genet 59, 16-22.

195. Ruiz-Canada, C., Kelleher, D.J., and Gilmore, R. (2009). Cotranslational and posttranslational N-glycosylation of polypeptides by distinct mammalian OST isoforms. Cell 136, 272-283.

196. Ruzzenente, B., Metodiev, M.D., Wredenberg, A., Bratic, A., Park, C.B., Camara, Y., Milenkovic, D., Zickermann, V., Wibom, R., Hultenby, K., et al. (2011). LRPPRC is necessary for polyadenylation and coordination of translation of mitochondrial mRNAs. EMBO J 31, 443-456.

197. Sardiu, M.E., Cai, Y., Jin, J., Swanson, S.K., Conaway, R.C., Conaway, J.W., Florens, L., and Washburn, M.P. (2008). Probabilistic assembly of human protein interaction networks from label-free quantitative proteomics. Proc Natl Acad Sci U S A 105, 1454-1459.

198. Sasarman, F., Brunel-Guitton, C., Antonicka, H., Wai, T., and Shoubridge, E.A. (2010). LRPPRC and SLIRP interact in a ribonucleoprotein complex that regulates posttranscriptional gene expression in mitochondria. Mol Biol Cell 21, 1315-1323.

199. Savva, G.M., Wharton, S.B., Ince, P.G., Forster, G., Matthews, F.E., and Brayne, C. (2009). Age, neuropathology, and dementia. N Engl J Med 360, 2302-2309.

200. Schaefer, M.H., Fontaine, J.F., Vinayagam, A., Porras, P., Wanker, E.E., and Andrade-Navarro, M.A. (2012). HIPPIE: Integrating protein interaction networks with experiment based quality scores. PLoS One 7, e31826.

201. Scherzinger, E., Lurz, R., Turmaine, M., Mangiarini, L., Hollenbach, B., Hasenbank, R., Bates, G.P., Davies, S.W., Lehrach, H., and Wanker, E.E. (1997). Huntingtin-encoded polyglutamine expansions form amyloid-like protein aggregates in vitro and in vivo. Cell 90, 549-558.

202. Schoenheimer, R., and Rittenberg, D. (1938). The Application of Isotopes to the Study of Intermediary Metabolism. Science 87, 221-226.

203. Schubert, U., Anton, L.C., Gibbs, J., Norbury, C.C., Yewdell, J.W., and Bennink, J.R. (2000). Rapid degradation of a large fraction of newly synthesized proteins by proteasomes. Nature 404, 770-774.

204. Schupf, N., and Sergievsky, G.H. (2002). Genetic and host factors for dementia in Down's syndrome. Br J Psychiatry 180, 405-410.

205. Schuster-Bockler, B., and Bateman, A. (2008). Protein interactions in human genetic diseases. Genome Biol 9, R9.

206. Scott, J.D., and Pawson, T. (2009). Cell signaling in space and time: where proteins come together and when they're apart. Science 326, 1220-1224.

207. Seet, B.T., Dikic, I., Zhou, M.M., and Pawson, T. (2006). Reading protein modifications with interaction domains. Nat Rev Mol Cell Biol 7, 473-483.

208. Selkoe, D.J. (1991). The molecular pathology of Alzheimer's disease. Neuron 6, 487-498.

209. Selkoe, D.J. (2001). Alzheimer's disease: genes, proteins, and therapy. Physiol Rev 81, 741-766.

210. Selkoe, D.J. (2004). Cell biology of protein misfolding: the examples of Alzheimer's and Parkinson's diseases. Nat Cell Biol 6, 1054-1061.

211. Selkoe, D.J., and Wolfe, M.S. (2007). Presenilin: running with scissors in the membrane. Cell 131, 215-221.

212. Shevchenko, A., Tomas, H., Havlis, J., Olsen, J.V., and Mann, M. (2006). In-gel digestion for mass spectrometric characterization of proteins and proteomes. Nat Protoc 1, 2856-2860.

213. Singh, R., Barden, A., Mori, T., and Beilin, L. (2001). Advanced glycation end-products: a review. Diabetologia 44, 129-146.

214. Singleton, A.B., Farrer, M., Johnson, J., Singleton, A., Hague, S., Kachergus, J., Hulihan, M., Peuralinna, T., Dutra, A., Nussbaum, R., et al. (2003). alpha-Synuclein locus triplication causes Parkinson's disease. Science 302, 841.

215. Smith, M.A., Rottkamp, C.A., Nunomura, A., Raina, A.K., and Perry, G. (2000). Oxidative stress in Alzheimer's disease. Biochim Biophys Acta 1502, 139-144.

216. Soler-Lopez, M., Zanzoni, A., Lluis, R., Stelzl, U., and Aloy, P. (2011). Interactome mapping suggests new mechanistic details underlying Alzheimer's disease. Genome Res 21, 364-376.

217. Sondheimer, N., Fang, J.K., Polyak, E., Falk, M.J., and Avadhani, N.G. (2010). Leucine-rich pentatricopeptide-repeat containing protein regulates mitochondrial transcription. Biochemistry 49, 7467-7473.

218. Soneoka, Y., Cannon, P.M., Ramsdale, E.E., Griffiths, J.C., Romano, G., Kingsman, S.M., and Kingsman, A.J. (1995). A transient three-plasmid expression system for the production of high titer retroviral vectors. Nucleic Acids Res 23, 628-633.

219. Song, W., Chen, J., Petrilli, A., Liot, G., Klinglmayr, E., Zhou, Y., Poquiz, P., Tjong, J., Pouladi, M.A., Hayden, M.R., et al. (2011). Mutant huntingtin binds the mitochondrial fission GTPase dynamin-related protein-1 and increases its enzymatic activity. Nat Med 17, 377-382.

220. Soto, C. (2003). Unfolding the role of protein misfolding in neurodegenerative diseases. Nat Rev Neurosci 4, 49-60.

221. Sowa, M.E., Bennett, E.J., Gygi, S.P., and Harper, J.W. (2009). Defining the human deubiquitinating enzyme interaction landscape. Cell 138, 389-403.

222. Steen, H., and Mann, M. (2004). The ABC's (and XYZ's) of peptide sequencing. Nat Rev Mol Cell Biol 5, 699-711.

223. Strittmatter, W.J., Saunders, A.M., Schmechel, D., Pericak-Vance, M., Enghild, J., Salvesen, G.S., and Roses, A.D. (1993). Apolipoprotein E: high-avidity binding to beta-amyloid and increased frequency of type 4 allele in late-onset familial Alzheimer disease. Proc Natl Acad Sci U S A 90, 1977-1981.

224. Sugars, K.L., and Rubinsztein, D.C. (2003). Transcriptional abnormalities in Huntington disease. Trends Genet 19, 233-238.

225. Sugaya, N., Ikeda, K., Tashiro, T., Takeda, S., Otomo, J., Ishida, Y., Shiratori, A., Toyoda, A., Noguchi, H., Takeda, T., et al. (2007). An integrative in silico approach for discovering candidates for drug-targetable protein-protein interactions in interactome data. BMC Pharmacol 7, 10.

226. Sury, M.D., Chen, J.X., and Selbach, M. (2010). The SILAC fly allows for accurate protein quantification in vivo. Mol Cell Proteomics 9, 2173-2183.

227. Swerdlow, R.H., Burns, J.M., and Khan, S.M. (2010). The Alzheimer's disease mitochondrial cascade hypothesis. J Alzheimers Dis 20 Suppl 2, S265-279.

228. Swerdlow, R.H., and Khan, S.M. (2004). A “mitochondrial cascade hypothesis” for sporadic Alzheimer’s disease. Med Hypotheses 63, 8-20.

229. Tanaka, Y., Engelender, S., Igarashi, S., Rao, R.K., Wanner, T., Tanzi, R.E., Sawa, A., V, L.D., Dawson, T.M., and Ross, C.A. (2001). Inducible expression of mutant alpha-synuclein decreases proteasome activity and increases sensitivity to mitochondria-dependent apoptosis. Hum Mol Genet 10, 919-926.

230. Tanzi, R.E., Haines, J.L., Watkins, P.C., Stewart, G.D., Wallace, M.R., Hallewell, R., Wong, C., Wexler, N.S., Conneally, P.M., and Gusella, J.F. (1988). Genetic linkage map of human chromosome 21. Genomics 3, 129-136.

231. Tarassov, K., Messier, V., Landry, C.R., Radinovic, S., Serna Molina, M.M., Shames, I., Malitskaya, Y., Vogel, J., Bussey, H., and Michnick, S.W. (2008). An in vivo map of the yeast protein interactome. Science 320, 1465-1470.

232. Taylor, J.P., Hardy, J., and Fischbeck, K.H. (2002). Toxic proteins in neurodegenerative disease. Science 296, 1991-1995.

233. Terry, R.D., Masliah, E., Salmon, D.P., Butters, N., DeTeresa, R., Hill, R., Hansen, L.A., and Katzman, R. (1991). Physical basis of cognitive alterations in Alzheimer’s disease: synapse loss is the major correlate of cognitive impairment. Ann Neurol 30, 572-580.

234. Thathiah, A., and De Strooper, B. (2009). G protein-coupled receptors, cholinergic dysfunction, and Abeta toxicity in Alzheimer’s disease. Sci Signal 2, re8.

235. The Huntington’s Disease Collaborative Research Group (1993). A novel gene containing a trinucleotide repeat that is expanded and unstable on Huntington’s disease chromosomes. The Huntington’s Disease Collaborative Research Group. Cell 72, 971-983.

236. The International HapMap Consortium (2005). A haplotype map of the human genome. Nature 437, 1299-1320.

237. Topisirovic, I., Siddiqui, N., Lapointe, V.L., Trost, M., Thibault, P., Bangeranye, C., Pinol-Roma, S., and Borden, K.L. (2009). Molecular dissection of the eukaryotic initiation factor 4E (eIF4E) export-competent RNP. EMBO J 28, 1087-1098.

238. Travers, K.J., Patil, C.K., Wodicka, L., Lockhart, D.J., Weissman, J.S., and Walter, P. (2000). Functional and genomic analyses reveal an essential coordination between the unfolded protein response and ER-associated degradation. Cell 101, 249-258.

239. Trifunovic, A., Wredenberg, A., Falkenberg, M., Spelbrink, J.N., Rovio, A.T., Bruder, C.E., Bohlooly, Y.M., Gidlof, S., Oldfors, A., Wibom, R., et al. (2004). Premature ageing in mice expressing defective mitochondrial DNA polymerase. Nature 429, 417-423.

240. Trinkle-Mulcahy, L., Boulon, S., Lam, Y.W., Urcia, R., Boisvert, F.M., Vandermoere, F., Morrice, N.A., Swift, S., Rothbauer, U., Leonhardt, H., et al. (2008). Identifying specific protein interaction partners using quantitative mass spectrometry and bead proteomes. J Cell Biol 183, 223-239.

241. Tsai, C.C., Kao, H.Y., Mitzutani, A., Banayo, E., Rajan, H., McKeown, M., and Evans, R.M. (2004). Ataxin 1, a SCA1 neurodegenerative disorder protein, is functionally linked to the silencing mediator of retinoid and thyroid hormone receptors. Proc Natl Acad Sci U S A 101, 4047-4052.

242. Unoki, H., Takahashi, A., Kawaguchi, T., Hara, K., Horikoshi, M., Andersen, G., Ng, D.P., Holmkvist, J., Borch-Johnsen, K., Jorgensen, T., et al. (2008). SNPs in KCNQ1 are associated with susceptibility to type 2 diabetes in East Asian and European populations. Nat Genet 40, 1098-1102.

243. Valla, J., Berndt, J.D., and Gonzalez-Lima, F. (2001). Energy hypometabolism in posterior cingulate cortex of Alzheimer's patients: superficial laminar cytochrome oxidase associated with disease duration. J Neurosci 21, 4923-4930.

244. Vermeulen, M., Hubner, N.C., and Mann, M. (2008). High confidence determination of specific protein-protein interactions using quantitative mass spectrometry. Curr Opin Biotechnol 19, 331-337.

245. Vicente Miranda, H., and Outeiro, T.F. (2010). The sour side of neurodegenerative disorders: the effects of protein glycation. J Pathol 221, 13-25.

246. Vidal, M., Cusick, M.E., and Barabasi, A.L. (2011). Interactome networks and human disease. Cell 144, 986-998.

247. von Mering, C., Krause, R., Snel, B., Cornell, M., Oliver, S.G., Fields, S., and Bork, P. (2002). Comparative assessment of large-scale data sets of protein-protein interactions. Nature 417, 399-403.

248. von Rotz, R.C., Kohli, B.M., Bosset, J., Meier, M., Suzuki, T., Nitsch, R.M., and Konietzko, U. (2004). The APP intracellular domain forms nuclear multiprotein complexes and regulates the transcription of its own precursor. J Cell Sci 117, 4435-4448.

249. Walhout, A.J., and Vidal, M. (2001). Protein interaction maps for model organisms. Nat Rev Mol Cell Biol 2, 55-62.

250. Walsh, D.M., Klyubin, I., Fadeeva, J.V., Cullen, W.K., Anwyl, R., Wolfe, M.S., Rowan, M.J., and Selkoe, D.J. (2002). Naturally secreted oligomers of amyloid beta protein potently inhibit hippocampal long-term potentiation in vivo. Nature 416, 535-539.

251. Walter, J., Capell, A., Grunberg, J., Pesold, B., Schindzielorz, A., Prior, R., Podlisny, M.B., Fraser, P., Hyslop, P.S., Selkoe, D.J., et al. (1996). The Alzheimer's disease-associated presenilins are differentially phosphorylated proteins located predominantly within the endoplasmic reticulum. Mol Med 2, 673-691.

252. Ward, M.W., Concannon, C.G., Whyte, J., Walsh, C.M., Corley, B., and Prehn, J.H. (2010). The amyloid precursor protein intracellular domain(AICD) disrupts actin dynamics and mitochondrial bioenergetics. J Neurochem 113, 275-284.

253. Wilkins, M.R., Pasquali, C., Appel, R.D., Ou, K., Golaz, O., Sanchez, J.C., Yan, J.X., Gooley, A.A., Hughes, G., Humphery-Smith, I., et al. (1996). From proteins to proteomes: large scale protein identification by two-dimensional electrophoresis and amino acid analysis. Biotechnology (N Y) 14, 61-65.

254. Williams, A., Jahreiss, L., Sarkar, S., Saiki, S., Menzies, F.M., Ravikumar, B., and Rubinsztein, D.C. (2006). Aggregate-prone proteins are cleared from the cytosol by autophagy: therapeutic implications. Curr Top Dev Biol 76, 89-101.

255. Wilson, C.M., and High, S. (2007). Ribophorin I acts as a substrate-specific facilitator of N-glycosylation. J Cell Sci 120, 648-657.

256. Wilson, C.M., Magnaudeix, A., Yardin, C., and Terro, F. (2011). DC2 and keratinocyte-associated protein 2 (KCP2), subunits of the oligosaccharyltransferase complex, are regulators of the gamma-secretase-directed processing of amyloid precursor protein (APP). J Biol Chem 286, 31080-31091.

257. Xia, W., Zhang, J., Perez, R., Koo, E.H., and Selkoe, D.J. (1997). Interaction between amyloid precursor protein and presenilins in mammalian cells: implications for the pathogenesis of Alzheimer disease. Proc Natl Acad Sci U S A 94, 8208-8213.

258. Xu, F., Addis, J.B., Cameron, J.M., and Robinson, B.H. (2011). LRPPRC mutation suppresses cytochrome oxidase activity by altering mitochondrial RNA transcript stability in a mouse model. Biochem J 441, 275-283.

259. Yamin, G. (2009). NMDA receptor-dependent signaling pathways that underlie amyloid beta-protein disruption of LTP in the hippocampus. J Neurosci Res 87, 1729-1736.

260. Yan, L.J., Levine, R.L., and Sohal, R.S. (1997). Oxidative damage during aging targets mitochondrial aconitase. Proc Natl Acad Sci U S A 94, 11168-11172.

261. Yao, J., Irwin, R.W., Zhao, L., Nilsen, J., Hamilton, R.T., and Brinton, R.D. (2009). Mitochondrial bioenergetic deficit precedes Alzheimer's pathology in female mouse model of Alzheimer's disease. Proc Natl Acad Sci U S A 106, 14670-14675.

262. Yao, X., Freas, A., Ramirez, J., Demirev, P.A., and Fenselau, C. (2001). Proteolytic 18O labeling for comparative proteomics: model studies with two serotypes of adenovirus. Anal Chem 73, 2836-2842.

263. Zhu, M., Li, J., and Fink, A.L. (2003). The association of alpha-synuclein with membranes affects bilayer structure, stability, and fibril formation. J Biol Chem 278, 40186-40197.

264. Zoghbi, H.Y., and Orr, H.T. (2000). Glutamine repeats and neurodegeneration. Annu Rev Neurosci 23, 217-247.

265. Zoghbi, H.Y., and Orr, H.T. (2009). Pathogenic mechanisms of a polyglutamine-mediated neurodegenerative disease, spinocerebellar ataxia type 1. J Biol Chem 284, 7425-7429.

VII SUPPLEMENTARY INFORMATION

VII.1 PUBLICATION LIST

Publications derived from the main PhD thesis project

- **Hosp F**, Vossfeldt H, Heinig M, Wyler E, Schmidt V, Willnow T, Landthaler M, Huebner N, Wanker EE, Lalowski M, Voigt A, Kempa S, Selbach M (2012) „A quantitative interaction screen for neurodegenerative disease proteins“ *manuscript in preparation*
- Paul FE, **Hosp F**, Selbach M (2011) „Analyzing protein-protein interactions by quantitative mass spectrometry” *Methods* 54 (4):387-95

Publications derived from cooperation projects (not described in the PhD thesis)

- Moeller A, Xie SQ, **Hosp F**, Lang B, Phatnani HP, James S, Ramirez F, Collin GB, Naggert JK, Babu MM, Greenleaf AL, Selbach M, Pombo A (2012) „Proteomic analysis of mitotic RNA polymerase II reveals novel interactors and association with proteins dysfunctional in disease” *Molecular and Cellular Proteomics* 11 (6):M111.011767, 1–16

Publications prior to the PhD thesis

- Wirtz M, Birke H, Mueller C, **Hosp F**, Throm C, Koenig S, Feldman-Salit A, Rippe K, Petersen G, Wade RC, Rybin V, Scheffzek K, Hell R (2010) „Structure and function of the hetero-oligomeric cysteine synthase complex in plants”, *Journal of Biological Chemistry* 285:32810-17

Berlin, den 04.02.2013

Fabian Hosp

VII.2 Posters and Talks

- **Keystone Symposium 'Proteomics & Interactomes' 2012, Stockholm, Sweden.** "Quantitative interaction proteomics identifies LRPPRC as novel target for APPsw-mediated forms of Alzheimer's disease (Poster presentation)
- **4th EU Summer School in Proteomics 2010, Bressanone/Brixen, Italy.** "Quantitative interactome profiling of proteins contributing to neurodegenerative diseases" (Poster presentation)
- **12th MDC/FMP PhD Retreat 2010, Rheinsberg, Germany.** "Quantitative interactome profiling of proteins contributing to neurodegenerative diseases" (Oral presentation)
- **2nd Annual Meeting NGFN-Plus and NGFN-Transfer in the Programme of Medical Genome Research 2009, Berlin, Germany.** "Constructing a functional network for a polyQ-disease model using quantitative proteomics and probabilistic modeling" (Poster presentation)
- **Proteomic Forum 2009, Berlin, Germany.** "Quantiative proteomics combined with gene interaction analysis reveals Huntington's disease mechanisms " (Poster presentation)
- **11th MDC/FMP PhD Retreat 2009, Kremmen, Germany.** "Quantiative proteomics combined with gene interaction analysis reveals Huntington's disease mechanisms " (Poster presentation)
- **1st Annual Meeting NGFN-Plus and NGFN-Transfer in the Programme of Medical Genome Research 2008, Munich, Germany.** "Identification and quantification of protein-protein interactions in neurodegenerative diseases" (Poster presentation)
- **10th MDC/FMP PhD Retreat 2008, Templin, Germany.** "A protein-protein interaction screening approach by quantitative proteomics" (Poster presentation)

VII.3 SUPPLEMENTARY DATA

VII.3.1 Supplementary figures

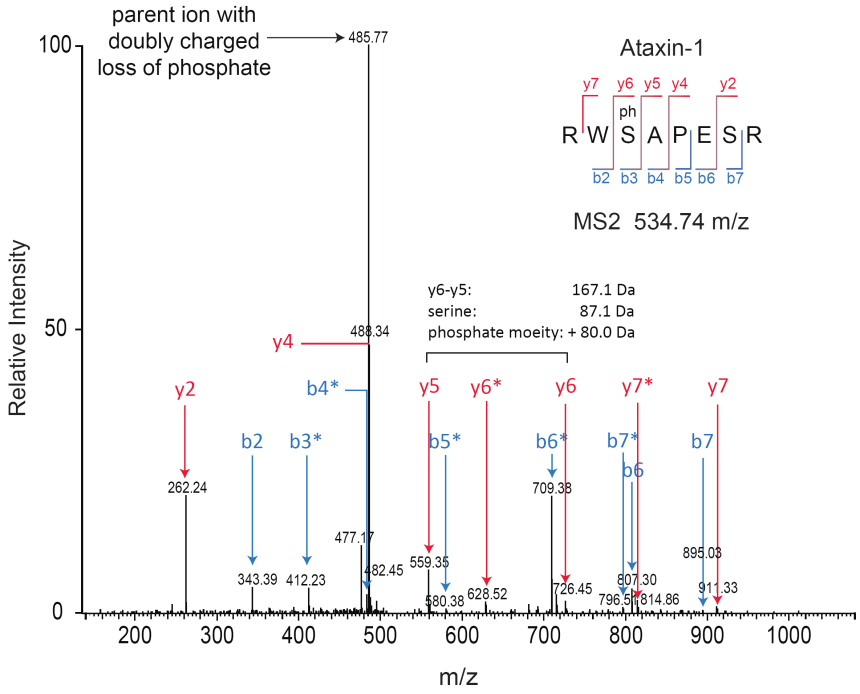

Supplementary Figure VII.1 | Detection of phosphorylation-dependent interactions. Phosphorylation of Ataxin-1 at Serine776 facilitates binding of Ataxin-1 to the 14-3-3 protein. Shown is the MS/MS spectrum of the corresponding peptide RWS(p)APESR of Ataxin1 with annotated b- and y-ions. The mass shift of respective b- and y-ions comprising a phosphate moeity is indicated by asteriks.

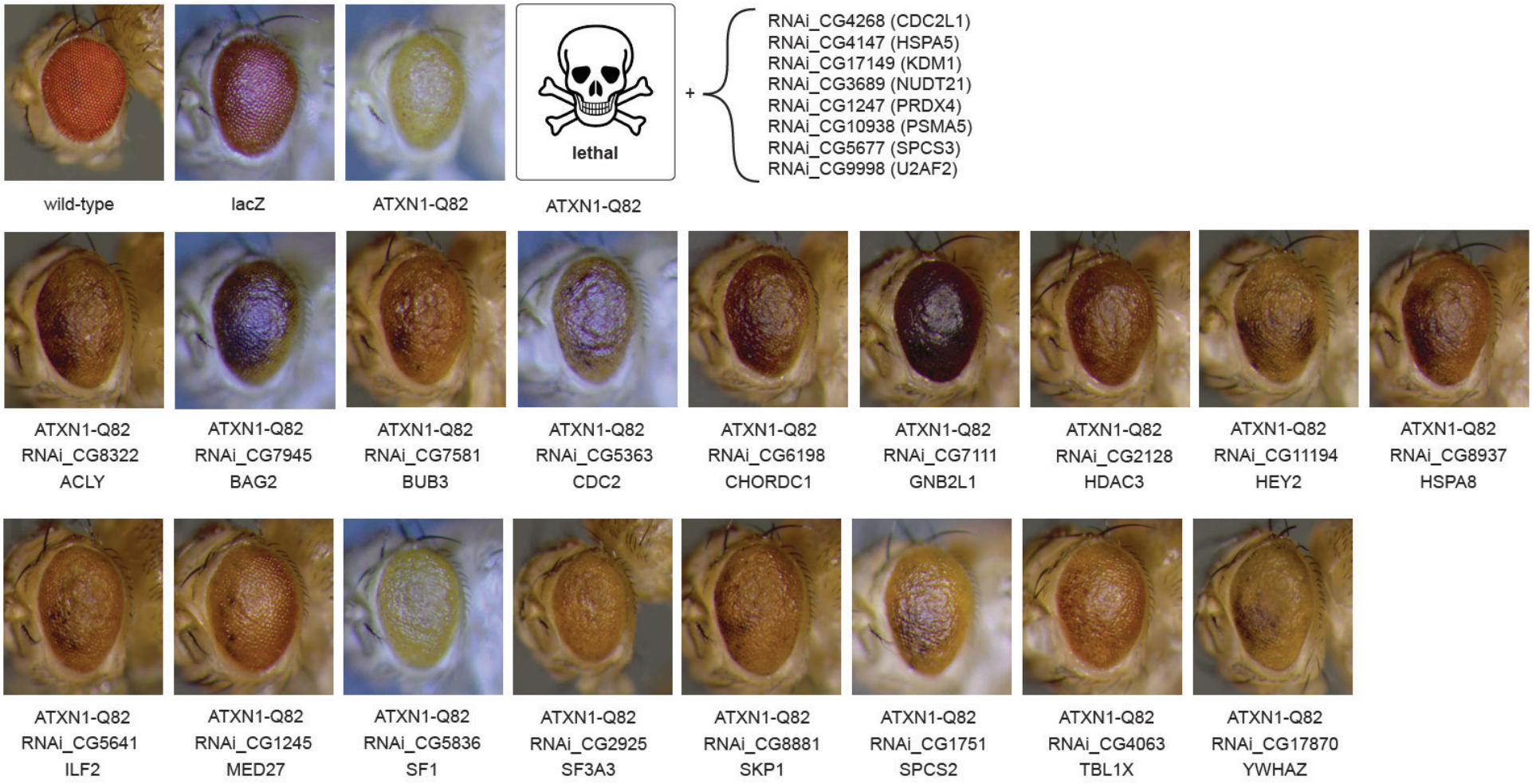

Supplementary Figure VII.2 | Documentation of rough eye phenotype assessment. Refer to Supplementary TAB. VII.3 for detailed information on strain IDs and REP classification.

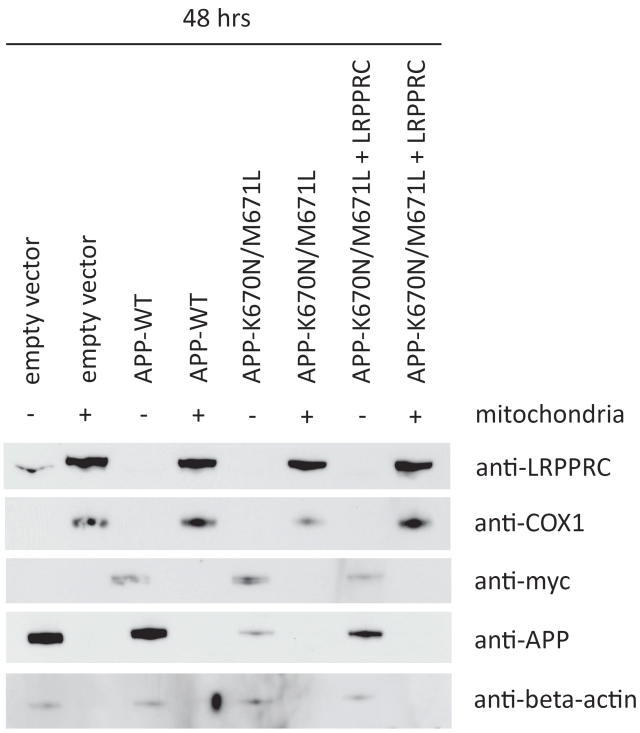

Supplementary FIG. VII.3 | APPsw does not impair LRPPRC trafficking. HEK293TN cells were transiently transfected with indicated expression constructs for 48 hrs. Subsequent Western blot analysis of isolated mitochondrial fractions and mitochondria-depleted cellular lysates is depicted. Consistent with reported publications, mitochondrial localization can be observed for LRPPRC and COX1, whereas APP is not located to the mitochondria. Protein levels of LRPPRC do not show an apparent change in mitochondrial localization or retention in the cytosol upon expression of the APP Swedish mutation K670N/M671L, thus indicating that LRPPRC trafficking is not disturbed in APPsw-expressing cells compared to wild-type APP cells.

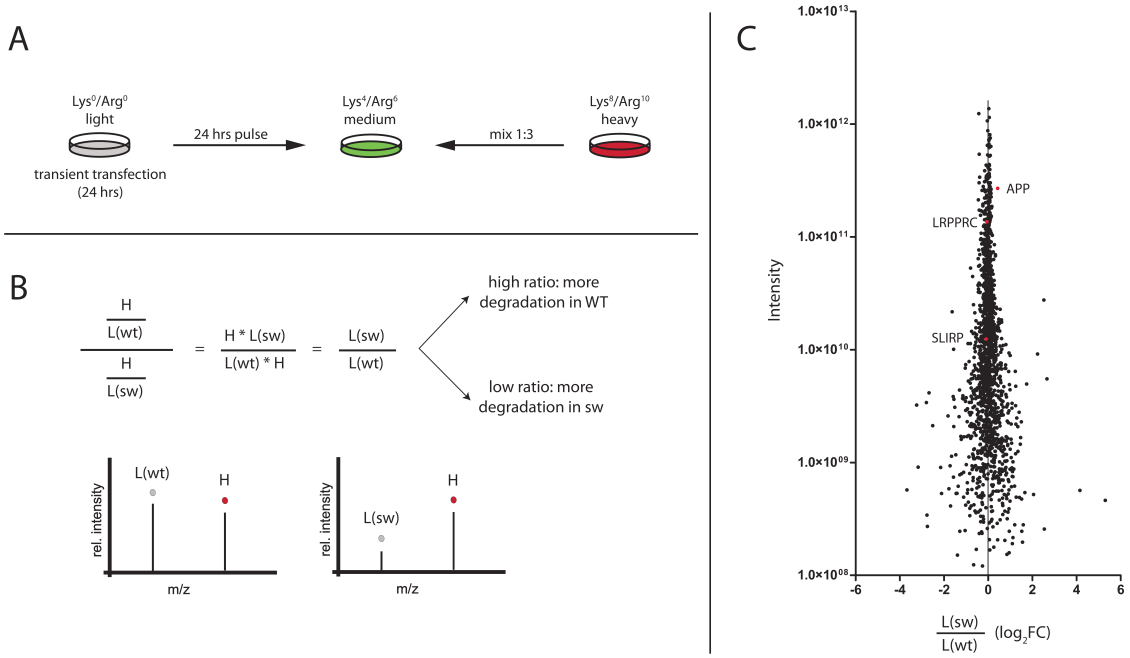

Supplementary Figure VII.4 | pSILAC analysis reveals no degradation of LRPPRC upon APPsw expression. (A) Light labeled HEK293TN cells were transfected with either empty vector control, APP-WT or APPsw. After 24 hrs of expression, light cells were pulsed for 24 hrs with medium-heavy medium. 48 hrs post-transfection, medium-heavy cells were harvested and heavy cells were spiked in 1:3 to each condition as internal reference control. (B) Heavy peptide peaks were used as reference to compare the degradation of light-derived peaks from APP-WT- versus APPsw-transfected cells over time by LC-MS/MS analysis, thus allowing ratio-of-ratio generation. (C) Global protein expression changes for roughly 1,600 proteins do not show any apparent degradation effect for LRPPRC or SLIRP. Individual protein ratios are normalized to median changes of all proteins quantified.

VII.3.2. Supplementary tables

Supplementary Table VII.1 | Identified prey proteins from q-AP-MS screen
Listed are gene names of identified interactors from the q-AP-MS screen for each bait variant, respectively (for specificity assessment cf. III.1). *Log_2FC* reflects the absolute logarithmized H/L ratio fold changes from the combined forward and reverse experiment, compared to the empty vector control pull-down. If an H/L ratio could not be assigned by the MaxQuant analysis software due to extreme H/L ratios, however, ion intensities have been detected for both the corresponding light and heavy peptide peaks, an infinite ratio was assigned (= INF).

Disease	Bait variant	Prey	Log_2FC	Disease	Bait variant	Prey	Log_2FC
PD	PARK2-WT	PCBP1	2.021	SCA1	ATXN1-Q30	CDC2	2.001
PD	PARK2-WT	RPL11	2.032	SCA1	ATXN1-Q30	HSPA5	2.111
PD	PARK2-WT	RPLP2	2.033	SCA1	ATXN1-Q30	PPP2R1A	2.456
PD	PARK2-WT	TUBB2C	2.037	SCA1	ATXN1-Q30	MYOM2	2.470
PD	PARK2-WT	AIFM1	2.083	SCA1	ATXN1-Q30	HSPA1A	2.478
PD	PARK2-WT	RUVBL2	2.102	SCA1	ATXN1-Q30	MED27	2.586
PD	PARK2-WT	PGK1	2.138	SCA1	ATXN1-Q30	OBSCN	2.622
PD	PARK2-WT	CFL1	2.162	SCA1	ATXN1-Q30	HSPA1B	2.624
PD	PARK2-WT	TUBB	2.164	SCA1	ATXN1-Q30	UBC	2.648
PD	PARK2-WT	YWHAZ	2.178	SCA1	ATXN1-Q30	ELAVL1	2.762
PD	PARK2-WT	RPS25	2.190	SCA1	ATXN1-Q30	NID1	3.076
PD	PARK2-WT	TUBA1C	2.196	SCA1	ATXN1-Q30	DNAJB6	3.169
PD	PARK2-WT	TUFM	2.200	SCA1	ATXN1-Q30	KDM1	3.212
PD	PARK2-WT	RPLP0	2.250	SCA1	ATXN1-Q30	U2AF1	3.252
PD	PARK2-WT	HNRNPH1	2.333	SCA1	ATXN1-Q30	PCMT1	3.283
PD	PARK2-WT	P4HB	2.341	SCA1	ATXN1-Q30	PSMB1	3.318
PD	PARK2-WT	CCT6A	2.423	SCA1	ATXN1-Q30	GSPT1	3.423
PD	PARK2-WT	CCT2	2.444	SCA1	ATXN1-Q30	HSPA8	3.423
PD	PARK2-WT	XRCC5	2.465	SCA1	ATXN1-Q30	HDAC3	3.502
PD	PARK2-WT	TXN	2.509	SCA1	ATXN1-Q30	PSMA4	3.599
PD	PARK2-WT	BAG2	2.511	SCA1	ATXN1-Q30	SF1	3.720
PD	PARK2-WT	MATR3	2.524	SCA1	ATXN1-Q30	SKP1	3.739
PD	PARK2-WT	PGAM1	2.571	SCA1	ATXN1-Q30	CDK2	3.815
PD	PARK2-WT	EEF1A1	2.575	SCA1	ATXN1-Q30	BUB3	4.198
PD	PARK2-WT	VCP	2.595	SCA1	ATXN1-Q30	SUMO2	4.279
PD	PARK2-WT	HNRNPF	2.609	SCA1	ATXN1-Q30	TLE4	4.311
PD	PARK2-WT	PKM2	2.611	SCA1	ATXN1-Q30	EIF4E2	4.499
PD	PARK2-WT	MYL12B	2.631	SCA1	ATXN1-Q30	RNH1	4.500
PD	PARK2-WT	ACTBL2	2.637	SCA1	ATXN1-Q30	WDR68	4.603
PD	PARK2-WT	CCT3	2.646	SCA1	ATXN1-Q30	MLF1	4.936
PD	PARK2-WT	PDIA6	2.662	SCA1	ATXN1-Q30	SQSTM1	5.364
PD	PARK2-WT	CCT1	2.671	SCA1	ATXN1-Q30	PRDX4	5.683
PD	PARK2-WT	ACTG1	2.696	SCA1	ATXN1-Q30	MLF2	6.123
PD	PARK2-WT	CCT4	2.699	SCA1	ATXN1-Q30	CDC2L1	6.163

PD	PARK2-WT	ACTC1	2.750	SCA1	ATXN1-Q30	BAG2	6.283
PD	PARK2-WT	MDH2	2.771	SCA1	ATXN1-Q30	MBNL1	6.383
PD	PARK2-WT	HSPD1	2.778	SCA1	ATXN1-Q30	YWHAB	6.613
PD	PARK2-WT	RPS13	2.839	SCA1	ATXN1-Q30	YWHAZ	6.893
PD	PARK2-WT	EIF5A	2.859	SCA1	ATXN1-Q30	YWHAE	6.934
PD	PARK2-WT	NCL	2.898	SCA1	ATXN1-Q30	YWHAG	6.975
PD	PARK2-WT	PDIA3	2.901	SCA1	ATXN1-Q30	HSPB1	7.382
PD	PARK2-WT	HNRNPA2B1	2.926	SCA1	ATXN1-Q30	U2AF2	7.442
PD	PARK2-WT	CCT5	2.936	SCA1	ATXN1-Q30	YWHAH	7.752
PD	PARK2-WT	PPIA	2.969	SCA1	ATXN1-Q30	TBL1XR1	7.845
PD	PARK2-WT	HNRNPA1	3.084	SCA1	ATXN1-Q30	YWHAQ	8.069
PD	PARK2-WT	ENO1	3.088	SCA1	ATXN1-Q30	CIC	INF
PD	PARK2-WT	ANXA11	3.114	SCA1	ATXN1-Q30	CDC16	INF
PD	PARK2-WT	FKBP4	3.118	SCA1	ATXN1-Q30	TBC1D9B	INF
PD	PARK2-WT	NME1-NME2	3.128	SCA1	ATXN1-Q30	UBQLN1	INF
PD	PARK2-WT	GAPDH	3.129	SCA1	ATXN1-Q30	UBQLN2	INF
PD	PARK2-WT	CCT8	3.141	SCA1	ATXN1-Q82	C15ORF24	2.001
PD	PARK2-WT	EZR	3.155	SCA1	ATXN1-Q82	PYCRL	2.069
PD	PARK2-WT	PRDX2	3.157	SCA1	ATXN1-Q82	MED27	2.194
PD	PARK2-WT	NACA	3.185	SCA1	ATXN1-Q82	PTPN1	2.266
PD	PARK2-WT	PRDX1	3.186	SCA1	ATXN1-Q82	HSPA5	2.310
PD	PARK2-WT	CSE1L	3.203	SCA1	ATXN1-Q82	SPCS3	2.374
PD	PARK2-WT	GSTP1	3.206	SCA1	ATXN1-Q82	OBSCN	2.466
PD	PARK2-WT	HSP90AB1	3.240	SCA1	ATXN1-Q82	CHORDC1	2.487
PD	PARK2-WT	TPI1	3.286	SCA1	ATXN1-Q82	DNAJB6	2.505
PD	PARK2-WT	HSP90AA1	3.333	SCA1	ATXN1-Q82	NID1	2.507
PD	PARK2-WT	CCT7	3.398	SCA1	ATXN1-Q82	MYOM2	2.520
PD	PARK2-WT	NPM1	3.434	SCA1	ATXN1-Q82	UBC	2.611
PD	PARK2-WT	TKT	3.494	SCA1	ATXN1-Q82	HSPA1A	2.660
PD	PARK2-WT	UBC	3.496	SCA1	ATXN1-Q82	PSMB1	2.677
PD	PARK2-WT	HSP90B1	3.552	SCA1	ATXN1-Q82	SNCA	2.717
PD	PARK2-WT	EEF2	3.555	SCA1	ATXN1-Q82	WDR68	2.793
PD	PARK2-WT	PSMD2	3.597	SCA1	ATXN1-Q82	HSPA1B	2.797
PD	PARK2-WT	FASN	3.762	SCA1	ATXN1-Q82	SF1	3.168
PD	PARK2-WT	LDHB	3.795	SCA1	ATXN1-Q82	GSPT1	3.224
PD	PARK2-WT	AHCY	3.894	SCA1	ATXN1-Q82	U2AF1	3.408
PD	PARK2-WT	PFN1	3.918	SCA1	ATXN1-Q82	SKP1	3.423
PD	PARK2-WT	PSMA5	4.002	SCA1	ATXN1-Q82	HSPA8	3.477
PD	PARK2-WT	PSMA6	4.223	SCA1	ATXN1-Q82	ZNF207	3.540
PD	PARK2-WT	HNRNPAB	4.271	SCA1	ATXN1-Q82	PCMT1	3.555
PD	PARK2-WT	LDHA	4.384	SCA1	ATXN1-Q82	SUMO2	4.054
PD	PARK2-WT	ALDOA	4.873	SCA1	ATXN1-Q82	TLE4	4.880
PD	PARK2-WT	PA2G4	4.900	SCA1	ATXN1-Q82	BUB3	4.895
PD	PARK2-WT	MTHFD1	5.393	SCA1	ATXN1-Q82	ARG1	5.131

PD	PARK2-WT	MAT2A	5.516	SCA1	ATXN1-Q82	RNH1	5.668
PD	PARK2-WT	HSPA4	6.600	SCA1	ATXN1-Q82	BAG2	5.709
PD	PARK2-Q329STOP	BAG2	2.767	SCA1	ATXN1-Q82	TPM3	5.934
PD	SNCA-WT	CSNK2A1	1.282	SCA1	ATXN1-Q82	SYNE2	5.979
PD	SNCA-WT	NCL	4.511	SCA1	ATXN1-Q82	HDAC3	6.211
PD	SNCA-WT	NOL7	3.161	SCA1	ATXN1-Q82	YWHAB	6.251
PD	SNCA-WT	ILF2	3.380	SCA1	ATXN1-Q82	MLF2	6.303
PD	SNCA-WT	ILF3	3.464	SCA1	ATXN1-Q82	HSPB1	6.373
PD	SNCA-WT	NOL11	2.818	SCA1	ATXN1-Q82	CDC2L1	6.424
PD	SNCA-WT	PARK7	6.945	SCA1	ATXN1-Q82	YWHAG	6.664
PD	SNCA-WT	HSP90B1	5.596	SCA1	ATXN1-Q82	U2AF2	6.765
PD	SNCA-WT	HSPA4	5.048	SCA1	ATXN1-Q82	YWHAE	6.846
PD	SNCA-WT	TTLL12	3.960	SCA1	ATXN1-Q82	TBL1XR1	7.110
PD	SNCA-WT	PSMA2	3.790	SCA1	ATXN1-Q82	YWHAZ	7.220
PD	SNCA-WT	HSPD1	1.686	SCA1	ATXN1-Q82	YWHAH	7.634
PD	SNCA-WT	UBA1	3.348	SCA1	ATXN1-Q82	YWHAQ	7.986
PD	SNCA-WT	LRPPRC	3.683	SCA1	ATXN1-Q82	CIC	INF
PD	SNCA-WT	YWHAZ	2.757	SCA1	ATXN1-Q82	CDC16	INF
PD	SNCA-WT	PSMC3	2.575	SCA1	ATXN1-Q82	TBC1D9B	INF
PD	SNCA-WT	YWHAB	2.121	SCA1	ATXN1-Q82	UBQLN1	INF
PD	SNCA-WT	YWHAE	4.147	SCA1	ATXN1-Q82	UBXN1	INF
PD	SNCA-A30P	NCL	4.152	HD	HTT506-Q23	CSNK2A1	2.080
PD	SNCA-A30P	NOL11	1.859	HD	HTT506-Q23	HSPA1A	2.213
PD	SNCA-A30P	ILF2	2.154	HD	HTT506-Q23	RUVBL1	2.423
PD	SNCA-A30P	ILF3	2.182	HD	HTT506-Q23	IPO9	2.444
PD	SNCA-E46K	NOL8	2.050	HD	HTT506-Q23	DHX30	2.762
PD	SNCA-E46K	CSNK2A1	2.148	HD	HTT506-Q23	IPO7	3.316
PD	SNCA-E46K	DNAJC9	2.096	HD	HTT506-Q23	VIM	3.657
PD	SNCA-E46K	NOL11	1.661	HD	HTT506-Q23	ACTG1	4.072
PD	SNCA-E46K	GTPBP4	2.056	HD	HTT506-Q23	IPO4	4.099
PD	SNCA-E46K	NOLC1	2.927	HD	HTT506-Q23	ACTA1	4.194
PD	SNCA-E46K	HSPH1	2.669	HD	HTT506-Q23	UBC	4.519
PD	SNCA-A53T	THRAP3	4.326	HD	HTT506-Q23	KPNB1	5.938
PD	SNCA-A53T	NOL11	1.088	HD	HTT506-Q23	HSPB1	7.899
PD	SNCA-A53T	NCL	1.484	HD	HTT506-Q145	RANGAP1	2.006
PD	SNCA-A53T	ILF3	1.206	HD	HTT506-Q145	DNAJB6	2.012
PD	SNCA-A53T	NOL7	1.269	HD	HTT506-Q145	FASN	2.084
PD	SNCA-A53T	ILF2	1.292	HD	HTT506-Q145	UBC	2.089
PD	SNCA-A53T	NOL8	1.319	HD	HTT506-Q145	CAD	2.090
PD	SNCA-A53T	CSNK2A1	1.444	HD	HTT506-Q145	BAT3	2.116
AD	PSEN1-WT	PCBP2	2.062	HD	HTT506-Q145	RUVBL1	2.147
AD	PSEN1-WT	SCD	2.068	HD	HTT506-Q145	FLOT1	2.243
AD	PSEN1-WT	ARF4	2.070	HD	HTT506-Q145	DDB1	2.337
AD	PSEN1-WT	SSR3	2.076	HD	HTT506-Q145	MATR3	2.513

AD	PSEN1-WT	ARL1	2.123	HD	HTT506-Q145	HBXIP	2.595
AD	PSEN1-WT	SAR1A	2.134	HD	HTT506-Q145	HSPA1A	2.706
AD	PSEN1-WT	CNOT7	2.136	HD	HTT506-Q145	WDR61	2.719
AD	PSEN1-WT	SLC1A5	2.145	HD	HTT506-Q145	AP2B1	2.758
AD	PSEN1-WT	RDH11	2.193	HD	HTT506-Q145	SUMO2	2.904
AD	PSEN1-WT	PSMD14	2.201	HD	HTT506-Q145	ACLY	2.906
AD	PSEN1-WT	PGRMC1	2.250	HD	HTT506-Q145	PPP1R10	3.026
AD	PSEN1-WT	PTPLAD1	2.310	HD	HTT506-Q145	POLR2H	3.027
AD	PSEN1-WT	RANGAP1	2.332	HD	HTT506-Q145	PPIH	3.031
AD	PSEN1-WT	TMCO1	2.342	HD	HTT506-Q145	POLR1C	3.072
AD	PSEN1-WT	PSMA6	2.364	HD	HTT506-Q145	PSMD6	3.096
AD	PSEN1-WT	ZW10	2.381	HD	HTT506-Q145	KPNB1	3.161
AD	PSEN1-WT	TMED10	2.403	HD	HTT506-Q145	PSMA4	3.207
AD	PSEN1-WT	DNAJA2	2.405	HD	HTT506-Q145	PSMB1	3.227
AD	PSEN1-WT	EIF4G1	2.472	HD	HTT506-Q145	PSMB2	3.261
AD	PSEN1-WT	FADS1	2.571	HD	HTT506-Q145	EPPK1	3.290
AD	PSEN1-WT	PSMA2	2.613	HD	HTT506-Q145	ALDOA	3.328
AD	PSEN1-WT	SSR4	2.686	HD	HTT506-Q145	VPS28	3.353
AD	PSEN1-WT	SSR1	2.757	HD	HTT506-Q145	KDM1	3.406
AD	PSEN1-WT	ATP2A2	2.773	HD	HTT506-Q145	EIF3B	3.432
AD	PSEN1-WT	HSD17B12	2.804	HD	HTT506-Q145	GEMIN7	3.562
AD	PSEN1-WT	PSMD2	2.825	HD	HTT506-Q145	HNRNPM	3.566
AD	PSEN1-WT	TBL3	2.827	HD	HTT506-Q145	COMMD1	3.574
AD	PSEN1-WT	ERLIN2	2.890	HD	HTT506-Q145	LSM5	3.577
AD	PSEN1-WT	RPL38	2.961	HD	HTT506-Q145	HGS	3.653
AD	PSEN1-WT	STT3A	2.967	HD	HTT506-Q145	IMMT	3.694
AD	PSEN1-WT	PSMC2	2.985	HD	HTT506-Q145	PSMA6	3.761
AD	PSEN1-WT	TMEM33	3.002	HD	HTT506-Q145	PSMD13	3.835
AD	PSEN1-WT	TNPO3	3.018	HD	HTT506-Q145	HSPA8	3.839
AD	PSEN1-WT	DNAJB11	3.029	HD	HTT506-Q145	ACTR3	3.839
AD	PSEN1-WT	DDOST	3.074	HD	HTT506-Q145	PLEC1	3.918
AD	PSEN1-WT	TMEM43	3.160	HD	HTT506-Q145	COMMD3	3.931
AD	PSEN1-WT	PSMA5	3.174	HD	HTT506-Q145	PSMA7	4.108
AD	PSEN1-WT	PSMA7	3.185	HD	HTT506-Q145	PPP1CA	4.162
AD	PSEN1-WT	RPN2	3.203	HD	HTT506-Q145	OGT	4.174
AD	PSEN1-WT	PSMA4	3.211	HD	HTT506-Q145	SKP1	4.177
AD	PSEN1-WT	HSPA5	3.235	HD	HTT506-Q145	PPGB	4.221
AD	PSEN1-WT	PSMB5	3.305	HD	HTT506-Q145	PSMD2	4.255
AD	PSEN1-WT	CDKN2A	3.319	HD	HTT506-Q145	EEF1B2	4.391
AD	PSEN1-WT	FAF2	3.319	HD	HTT506-Q145	PSMD14	4.591
AD	PSEN1-WT	BCAP31	3.364	HD	HTT506-Q145	UFD1L	4.631
AD	PSEN1-WT	PSMB1	3.380	HD	HTT506-Q145	DYNLL1	4.640
AD	PSEN1-WT	HSPA8	3.466	HD	HTT506-Q145	SEC13	4.660
AD	PSEN1-WT	PSMB2	3.469	HD	HTT506-Q145	RANBP1	4.672

AD	PSEN1-WT	TTC35	3.488	HD	HTT506-Q145	DNAJA2	4.687
AD	PSEN1-WT	RPN1	3.534	HD	HTT506-Q145	COPS3	4.709
AD	PSEN1-WT	COX4NB	3.603	HD	HTT506-Q145	NEFL	4.750
AD	PSEN1-WT	FADS2	3.619	HD	HTT506-Q145	GLB1	4.775
AD	PSEN1-WT	DHCR24	3.673	HD	HTT506-Q145	PSMD7	5.068
AD	PSEN1-WT	FAM62A	3.782	HD	HTT506-Q145	WDR82	5.069
AD	PSEN1-WT	KIAA0090	3.815	HD	HTT506-Q145	PPP6C	5.170
AD	PSEN1-WT	BAT3	3.840	HD	HTT506-Q145	DNAJA1	5.176
AD	PSEN1-WT	DNAJB12	3.945	HD	HTT506-Q145	CALM1	5.209
AD	PSEN1-WT	SKP1	4.183	HD	HTT506-Q145	ACTA1	5.280
AD	PSEN1-WT	UBC	4.329	HD	HTT506-Q145	CARM1	5.294
AD	PSEN1-WT	DNAJA1	4.401	HD	HTT506-Q145	NRBP1	5.349
AD	PSEN1-WT	SOAT1	4.587	HD	HTT506-Q145	PSMD1	5.385
AD	PSEN1-WT	MLF1	4.592	HD	HTT506-Q145	ACTBL2	5.438
AD	PSEN1-WT	CYP51A1	5.155	HD	HTT506-Q145	STRAP	5.453
AD	PSEN1-WT	DNAJC7	5.357	HD	HTT506-Q145	ACTG1	5.482
AD	PSEN1-WT	MAGEB2	5.419	HD	HTT506-Q145	EIF3G	5.530
AD	PSEN1-WT	HSPB1	5.506	HD	HTT506-Q145	PRRC1	5.640
AD	PSEN1-WT	SRPRB	5.780	HD	HTT506-Q145	PSMA5	5.652
AD	PSEN1-WT	BAG2	7.495	HD	HTT506-Q145	EIF4E2	5.720
AD	PSEN1-A431E	FAF2	2.091	HD	HTT506-Q145	RAE1	5.743
AD	PSEN1-A431E	RHBDL7	2.109	HD	HTT506-Q145	EEF1G	5.767
AD	PSEN1-A431E	TMEM43	2.112	HD	HTT506-Q145	VCP	5.793
AD	PSEN1-A431E	PSMA5	2.124	HD	HTT506-Q145	CNOT10	6.035
AD	PSEN1-A431E	DDX20	2.127	HD	HTT506-Q145	EEF1D	6.038
AD	PSEN1-A431E	GLB1	2.135	HD	HTT506-Q145	CETN2	6.210
AD	PSEN1-A431E	CHMP1A	2.150	HD	HTT506-Q145	NEFM	6.398
AD	PSEN1-A431E	PSMC3	2.167	HD	HTT506-Q145	G3BP1	6.644
AD	PSEN1-A431E	STT3A	2.176	HD	HTT506-Q145	WDR68	6.666
AD	PSEN1-A431E	MLEC	2.176	HD	HTT506-Q145	ATXN2L	6.683
AD	PSEN1-A431E	PSMA6	2.225	HD	HTT506-Q145	CNOT7	6.785
AD	PSEN1-A431E	HSPA8	2.296	HD	HTT506-Q145	EIF3I	6.786
AD	PSEN1-A431E	TMEM33	2.381	HD	HTT506-Q145	PABPC4	7.036
AD	PSEN1-A431E	PSMB1	2.442	HD	HTT506-Q145	LSM12	7.252
AD	PSEN1-A431E	PSMB2	2.442	HD	HTT506-Q145	PABPC1	7.272
AD	PSEN1-A431E	PSMA4	2.536	HD	HTT506-Q145	VIM	7.482
AD	PSEN1-A431E	KIAA0090	2.586	HD	HTT506-Q145	UBL4A	7.492
AD	PSEN1-A431E	SOAT1	2.671	HD	HTT506-Q145	HSPB1	8.387
AD	PSEN1-A431E	TTC35	2.673	HD	HTT506-Q145	BAG2	8.500
AD	PSEN1-A431E	DEGS1	2.728	HD	HTT506-Q145	CNOT3	8.587
AD	PSEN1-A431E	UBC	2.799	HD	HTT506-Q145	CNOT2	INF
AD	PSEN1-A431E	PSMA2	2.812	HD	HTT506-Q145	CNOT8	INF
AD	PSEN1-A431E	FADS2	2.885	HD	HTT506-Q145	COMMD4	INF
AD	PSEN1-A431E	DHCR24	2.927	HD	HTT506-Q145	HAUS2	INF

AD	PSEN1-A431E	PSMA7	2.934
AD	PSEN1-A431E	COX4NB	3.048
AD	PSEN1-A431E	HSPA5	3.050
AD	PSEN1-A431E	DNAJA1	3.103
AD	PSEN1-A431E	SAR1A	3.194
AD	PSEN1-A431E	SKP1	3.194
AD	PSEN1-A431E	DNAJC7	3.462
AD	PSEN1-A431E	MAGEB2	3.709
AD	PSEN1-A431E	BAT3	3.929
AD	PSEN1-A431E	SRPRB	4.292
AD	PSEN1-A431E	CYP51A1	4.554
AD	PSEN1-A431E	SCD	4.579
AD	PSEN1-A431E	HSPB1	4.665
AD	PSEN1-A431E	RDH11	4.939
AD	PSEN1-A431E	BAG2	6.406
AD	APP-WT	VGF	2.601
AD	APP-WT	PARP1	4.911
AD	APP-WT	LRPPRC	3.854
AD	APP-WT	CBX1	2.897
AD	APP-WT	CBX5	2.542
AD	APP-WT	CBX3	4.415
AD	APP-WT	PDIA6	4.052
AD	APP-WT	PDIA4	3.337
AD	APP-WT	PDIA3	4.037
AD	APP-K670N/M671L	PDIA3	2.825
AD	APP-K670N/M671L	VGF	2.090
AD	APP-K670N/M671L	LRPPRC	1.509
AD	APP-K670N/M671L	CBX1	2.509
AD	APP-K670N/M671L	CBX5	1.546
AD	APP-K670N/M671L	CBX3	2.981
AD	APP-V717I	LRPPRC	1.346
AD	APP-V717I	CBX1	3.839
AD	APP-V717I	CBX5	4.179
AD	APP-V717I	CBX3	4.890

HD	HTT506-Q145	HAUS3	INF
HD	HTT506-Q145	HAUS4	INF
HD	HTT506-Q145	HAUS5	INF
HD	HTT506-Q145	HSPB11	INF
HD	HTT506-Q145	KDM5B	INF
HD	HTT506-Q145	WDR45	INF
HD	HTT-Ex1-Q79	RPL13	2.372
HD	HTT-Ex1-Q79	ST13	2.778
HD	HTT-Ex1-Q79	UBC	2.956
HD	HTT-Ex1-Q79	HSPB1	2.993
HD	HTT-Ex1-Q79	BAG2	3.112
HD	HTT-Ex1-Q79	HSPA8	3.229
HD	HTT-Ex1-Q79	DNAJA1	3.910
HD	HTT-Ex1-Q79	RBM25	4.804

Supplementary Table VII.2 | Identified differential PPIs from q-AP-MS screen
Listed are gene names of identified differential interactors from the q-AP-MS screen for each preferential bait variant, respectively (for specificity assessment cf. III.1). *Log_2FC* reflects the absolute logarithmized H/L ratio fold changes from the combined forward and reverse experiment of the direct wild-type versus disease-associated variant pull-down experiments. (e.g. CSNK2A1 binds preferentially to Htt506-Q23 compared to Htt506-Q145, observed absolute log_2FC from both forward and reverse experiments was 2.002). In case several mutants were screened (applies for APP and SNCA screens), the preferential variants are indicated.

Bait variant	Prey	Log_2FC	Bait variant	Prey	Log_2FC
pref. HTT506-Q23	CSNK2A1	2.002	pref. ATXN1-Q30	KDM1	1.019
pref. HTT506-Q23	KPNB1	3.424	pref. ATXN1-Q30	PRDX4	1.038
pref. HTT506-Q23	UBC	3.446	pref. ATXN1-Q30	TBL1X	1.262
pref. HTT506-Q23	IPO9	4.486	pref. ATXN1-Q30	SQSTM1	1.279
pref. HTT506-Q23	DHX30	4.977	pref. ATXN1-Q30	HDAC3	1.320
pref. HTT506-Q23	IPO7	5.138	pref. ATXN1-Q30	EIF4E2	1.434
pref. HTT506-Q23	IPO4	5.149	pref. ATXN1-Q30	CDK2	1.740
pref. HTT506-Q145	RANGAP1	1.139	pref. ATXN1-Q30	CHORDC1	1.774
pref. HTT506-Q145	DDB1	1.367	pref. ATXN1-Q30	HEY2	2.193
pref. HTT506-Q145	ACLY	1.385	pref. ATXN1-Q30	CIC	2.844
pref. HTT506-Q145	ILF2	1.517	pref. ATXN1-Q82	ZNF207	1.074
pref. HTT506-Q145	FLOT1	1.539	pref. PSEN1-WT	DDOST	0.990
pref. HTT506-Q145	EPPK1	1.567	pref. PSEN1-WT	BCAP31	1.035
pref. HTT506-Q145	AP2B1	1.593	pref. PSEN1-WT	SLC1A5	1.080
pref. HTT506-Q145	MATR3	1.611	pref. PSEN1-WT	RPN1	1.145
pref. HTT506-Q145	HSPA8	1.637	pref. PSEN1-WT	SCD	1.301
pref. HTT506-Q145	PSMD6	1.668	pref. PSEN1-WT	DHCR24	1.370
pref. HTT506-Q145	COMMD3	1.767	pref. PSEN1-WT	SRPRB	1.376
pref. HTT506-Q145	PPIH	1.784	pref. PSEN1-WT	TMED10	1.476
pref. HTT506-Q145	POLR1C	1.793	pref. PSEN1-WT	RDH11	1.554
pref. HTT506-Q145	COPS7B	1.959	pref. PSEN1-WT	CYP51A1	1.570
pref. HTT506-Q145	SUMO2	2.058	pref. PARK2-WT	GSTP1	1.232
pref. HTT506-Q145	IMMT	2.084	pref. PARK2-WT	HNRNPAB	1.244
pref. HTT506-Q145	PLEC1	2.156	pref. PARK2-WT	HSP90AB1	1.324
pref. HTT506-Q145	VCP	2.230	pref. PARK2-WT	CSE1L	1.364
pref. HTT506-Q145	GEMIN7	2.279	pref. PARK2-WT	YWHAZ	1.470
pref. HTT506-Q145	LSM5	2.296	pref. PARK2-WT	CFL1	1.556
pref. HTT506-Q145	PSMD1	2.343	pref. PARK2-WT	MDH2	1.619
pref. HTT506-Q145	NRBP1	2.352	pref. PARK2-WT	ALDOA	1.648
pref. HTT506-Q145	WDR61	2.365	pref. PARK2-WT	PKM2	1.957
pref. HTT506-Q145	EIF3B	2.379	pref. PARK2-WT	EIF5A	2.054
pref. HTT506-Q145	OGT	2.383	pref. PARK2-WT	ACTG1	2.227
pref. HTT506-Q145	HGS	2.407	pref. PARK2-WT	PRDX2	2.464
pref. HTT506-Q145	PSMD7	2.461	pref. PARK2-WT	PPIA	2.474
pref. HTT506-Q145	PSMD14	2.546	pref. PARK2-WT	PGK1	2.661
pref. HTT506-Q145	PPGB	2.556	pref. PARK2-WT	PFN1	2.663

PREF. HTT506-Q145	UFD1L	2.643	PREF. PARK2-WT	LDHB	2.696
PREF. HTT506-Q145	KDM1	2.645	PREF. PARK2-WT	LDHA	2.836
PREF. HTT506-Q145	PPP1CA	2.696	PREF. PARK2-WT	HSPD1	3.119
PREF. HTT506-Q145	HNRNPM	2.710	PREF. PARK2-WT	NCL	3.388
PREF. HTT506-Q145	COMMD1	2.808	PREF. PARK2-WT	NPM1	3.416
PREF. HTT506-Q145	EEF1B2	2.817	PREF. PARK2-WT	HNRNPA2B1	3.504
PREF. HTT506-Q145	CALM1	3.092	PREF. APP-WT OVER APP-K670N/M671L	CBX3	3.023
PREF. HTT506-Q145	PPP6C	3.224	PREF. APP-WT OVER APP-K670N/M671L	CBX5	3.880
PREF. HTT506-Q145	NEFL	3.256	PREF. APP-WT OVER APP-K670N/M671L	PARP1	3.893
PREF. HTT506-Q145	EIF4E2	3.408	PREF. APP-K670N/M671L OVER APP-WT	LRPPRC	1.442*
PREF. HTT506-Q145	RAD23B	3.436	PREF. SNCA-A30P OVER SNCA-A53T	YWHAE	1.037
PREF. HTT506-Q145	STRAP	3.445	PREF. SNCA-A30P OVER SNCA-A53T	HSPD1	1.584
PREF. HTT506-Q145	ATXN2L	3.450	PREF. SNCA-A53T OVER SNCA-A30P	ILF2	1.294
PREF. HTT506-Q145	COPS3	3.514	PREF. SNCA-A53T OVER SNCA-A30P	ILF3	1.417
PREF. HTT506-Q145	WDR68	3.529	PREF. SNCA-E46K OVER SNCA-A53T	HSPD1	1.320
PREF. HTT506-Q145	UBL4A	3.634	PREF. SNCA-WT OVER SNCA-A30P	LRPPRC	3.683
PREF. HTT506-Q145	DYNLL1	3.699	PREF. SNCA-WT OVER SNCA-A53T	YWHAE	1.687
PREF. HTT506-Q145	DNAJA2	3.767	PREF. SNCA-WT OVER SNCA-A53T	UBA1	2.915
PREF. HTT506-Q145	NEFM	3.859	PREF. SNCA-WT OVER SNCA-A53T	LRPPRC	2.937
PREF. HTT506-Q145	VIM	3.919	PREF. SNCA-WT OVER SNCA-A53T	HSPD1	4.692
PREF. HTT506-Q145	CNOT10	3.929	PREF. SNCA-WT OVER SNCA-E46K	ILF2	1.969
PREF. HTT506-Q145	EIF3G	3.966	PREF. SNCA-WT OVER SNCA-E46K	ILF3	2.112
PREF. HTT506-Q145	DNAJA1	3.977	PREF. SNCA-WT OVER SNCA-E46K	LRPPRC	3.867
PREF. HTT506-Q145	WDR82	4.213	PREF. SNCA-WT OVER SNCA-E46K	NCL	5.138
PREF. HTT506-Q145	CETN2	4.286			
PREF. HTT506-Q145	EEF1D	4.341			
PREF. HTT506-Q145	EEF1G	4.358			
PREF. HTT506-Q145	BAG2	4.360	* $\log_2$FC from the forward experiment only, no LRPPRC peptides could be quantified in the corresponding reverse experiment		
PREF. HTT506-Q145	EIF3I	4.462			
PREF. HTT506-Q145	RAE1	4.492			
PREF. HTT506-Q145	TCEB2	4.533			
PREF. HTT506-Q145	PRRC1	4.572			
PREF. HTT506-Q145	CNOT7	5.003			
PREF. HTT506-Q145	G3BP1	5.357			
PREF. HTT506-Q145	LSM12	5.459			
PREF. HTT506-Q145	CARM1	5.629			
PREF. HTT506-Q145	PABPC1	5.759			
PREF. HTT506-Q145	PABPC4	6.267			
PREF. HTT506-Q145	SEC13	6.290			
PREF. HTT-Ex1-Q79	HSPA8	1.509			
PREF. HTT-Ex1-Q79	HSPB1	2.649			
PREF. HTT-Ex1-Q79	DNAJA1	3.963			
PREF. HTT-Ex1-Q79	BAG2	4.512			
PREF. HTT-Ex1-Q79	ST13	4.624			

Supplementary Table VII.3 | Utilized shRNA fly strains

Modifications by the induction of RNAi in polyQ and tau models were categorized as follows: wild type-like phenotype (---); obvious REP suppression (--); subtle REP suppression (-); no change of REP (0); subtle enhancement of REP (+); obvious enhancement of REP (++) and lethal (+++); n.a. = not assessable

* = due to MaxQuant software version issues, initially 7 additional candidates have been analyzed for disease-modifying effects in the fly, although they are not included in the final PPI network. For consistency reasons, they are listed here and depicted in Supplementary FIG. VII.2 as well.

#	VDRC accession number	Human Gene ID	Human Gene Symbol	Fly Gene ID	Fly Gene Symbol	Fly Annotation Symbol	REP effect	Tau effect	control RNAi effect	
1	30280	47	ACLY	36760	ATPCL	CG8322	++	0	0	*
2	35296	9532	BAG2	39679	-	CG7945	++	0	0	
3	21037	9184	BUB3	43490	Bub3	CG7581	++	0	0	
4	41838	983	CDC2	34411	cdc2	CG5363	+	-	+	
5	45127	984	CDC2L1	40292	Pitslre	CG4268	+++	0	+	
6	22300	26973	CHORDC1	42874	CHORD	CG6198	++	0	0	
7	27858	10399	GNB2L1	34070	Rack1	CG7111	++	0	0	*
8	35513.5	8841	HDAC3	44446	Hdac3	CG2128	+	0	0	
9	30561	23493	HEY2	35764	Hey	CG11194	++	0	0	
10	14882	3309	HSPA5	32133	Hsc70-3	CG4147	+++	+++	+++	
11	45596	3312	HSPA8	39542	Hsc70-1	CG8937	++	+	0	
12	45121.5	3608	ILF2	41529	-	CG5641	+	0	0	*
13	25218	23028	KDM1	40217	Hdm	CG17149	+++	0	0	
14	13697	9442	MED27	40696	MED27	CG1245	+/-	0	0	
15	45280	11051	NUDT21	39083	-	CG3689	+++	0	0	*
16	43254	10549	PRDX4	39083	Jafrac2	CG1274	+++	0	0	
17	16104	5686	PSMA5	53577	Prosalpha5	CG10938	+++	+++	+++	*
18	34801	5689	PSMB1	39855	Pros26	CG4097	+++	+++	+++	
19	22214	65263	PYCRL	42106	Ptp61F	CG5840	n.a.	0	0	
20	13426	7536	SF1	43912	SF1	CG5836	0	0	0	
21	20943	10946	SF3A3	40678	noi	CG2925	0	+	0	*
22	28975	6500	SKP1	36298	skpB	CG8881	+	0	0	
23	51149	9789	SPCS2	32095	Spase25	CG1751	+	0	0	*
24	1414	60559	SPCS3	42885	Spase22-23	CG5677	+++	0	0	
25	40862	6907	TBL1X	33212	ebi	CG4063	-	0	0	
26	24177	11338	U2AF2	32602	U2af50	CG9998	+++	0	0	
27	15884	7531	YWHAE	42186	14-3-3ε	CG31196	n.a.	n.a.	n.a.	
28	48724	7534	YWHAZ	36059	14-3-3ζ	CG17870	++	0	0	

VIII Acknowlegdements

"...you need more than luck to navigate successfully through a thousand sieves in succession, one sieve under the other." (Richard Dawkins, River out of Eden, 1995). The concept of a PhD thesis, besides its scientific progress, entails the development of self-reliance and training of independent thinking. Although demonstration of these particular conceptual skills is indispensable, the magnificent help and input from numerous people have greatly contributed to this present PhD thesis. Hence, I would like to thank all the people who assisted me to achieve this major project and helped me weathering through my years as a PhD student.

First and foremost I would like to thank my supervisor Matthias Selbach for giving me the opportunity to work on this fascinating assignment. The exceptionally combination of proteomics and NDD research in the present project is most certainly unique in its inherent design and perfectly suited my personal scientific interests. I am grateful for Matthias' scientific guidance, his enthusiasm for this venture and his promotional kind to get the best out of the project, helping me to develop my scientific skills and abilities. I am much obliged to Thomas Sommer for accepting the official supervision of my doctorate thesis at the Humboldt University of Berlin. Furthermore, I am indebted to all my colleagues and members of the Selbach lab over the last four years: Flo, Björn, Olivia, Christian, This, Marie, Jimmy, Erik, Sharbani, Anna-Laura, Murat and of course our lab mascot Murphy. I greatly benefited from all your scientific input during endless progress reports and daily lab issues, grateful candy donations, motivational sport activities in our office room a.k.a. sauna, musical inspiration in the lab through our sound system, droll entertaining videos and red flag battles [sic!] and of course from our late-night 'meetings' in various bars and clubs spread over Berlin. A special thank-you goes to Christian for introducing me over and over again and in all peace of mind to the fascinating world of practical mass spectrometry handling with all its technical refinements and yet mysterious error messages. Thanks to our amazing toys / crotchety lab children Ernie, Bert, Tiffy, Bibo and Kermit. I never ever thought working with screw wrenches and hex keys would be part of my doctoral work. Neither will I forget the greasy work while performing an oil change on a 700.000 € machine.

Thanks a million to Petra, Sabine and Sonja for all the organization and bureaucratic caretaking, you made my life much easier. I am much obliged to all of my collaborators, who made this whole project even better through their great contributions: Hannes Vossfeldt and Aaron Voigt for all the fly breeding, crossing and phenotype visualization plus the joint boozy nights in Göttingen and Berlin's Saphire bar; Matthias Heinig, Kathrin Saar and Norbert Hübner for the cumbrous GWAS cohort data acquisition and the PPI/GWAS matching; Emanuel Wyler and

Markus Landthaler for qRT-PCRs and joint efforts on LRPPRC function; Vanessa Schmidt and Thomas Willnow for help with the Aβ-ELISA; Martin Schaefer for providing early access to the HIPPIE database and initial parsing; Katja Muehlenberg and Erich Wanker for cloning instrumentality during the very early steps of this project and continuous fruitful discussions on the follow-ups; and finally to many members of the NeuroNet consortium, who taught me deeper insights into the field of neurodegeneration through all the discussions and meetings especially in the beginning of my thesis work. I acknowledge the kind gift of the Ataxin-1 disease fly model strain by the Juan Botas lab. Many thanks also to the office of the Helmholtz Graduate School 'Molecular Cell Biology' for the continuous support throughout the whole PhD thesis via travel & training grants and for all the further training possibilities on-campus. Kudos to Anup for all the MDC black market trades and for the chitchat all over the place.

I am also very grateful to Nadine, who supported me substantially for a long period of the thesis and made the valuable connection to the fly guys in Aachen. This thesis is devoted to you, may your soul rest in peace.

Finally, I would like to thank all my fellow scientific friends from Berlin and Heidelberg for sharing stories on success and failure of daily lab routines, making the job a bit easier and taking it with a pinch of salt. Deepest thanks to all my oldest and closest friends from Karlsruhe, making me feel at home every time and everywhere we met across Europe. I especially enjoyed the time you peeps visited me / lived here in Berlin, it was just fantastic!

I owe the most deepest thanks to my parents and my whole family for unwavering support in each and every situation & continuous confidence in me and my vocational aims and interest. Thank you K.A.Y. particularly for providing a place of tranquility far from home. All of you helped me in an unbelievable way to go through with this very important part of my life.

IX Selbständigkeitserklärung

Ich versichere hiermit, dass ich die von mir vorgelegte Dissertation selbständig angefertigt, die benutzten Quellen und Hilfsmittel vollständig angegeben und die Stellen der Arbeit - einschließlich Abbildungen und Tabellen -, die anderen Werken im Wortlaut oder dem Sinn nach entnommen sind, in jedem Einzelfall als Entlehnung kenntlich gemacht habe; dass diese Dissertation noch keiner anderen Fakultät oder Universität zur Prüfung vorgelegt habe; dass sie - abgesehen von weiter oben angegebenen Teilpublikationen - noch nicht veröffentlicht worden ist, sowie, dass ich eine solche Veröffentlichung vor Abschluss des Promotionsverfahrens nicht vornehmen werde.

Die Bestimmungen der Promotionsordnung der Mathematisch-Naturwissenschaftlichen Fakultät I der Humboldt-Universität zu Berlin sind mir bekannt.

Die von mir vorgelegte Dissertation ist von Prof. Dr. Matthias Selbach und Prof. Dr. Thomas Sommer betreut worden.

Berlin, den 04.02.2013

Fabian Hosp